JUL 06 2004 STA:15 (65)

ENGINEERING DATA TRANSMITTAL

1. EDT 820933

1A. Page 1 of 1

2. To: (Receiving Organization) Distribution	3. From: (Originating Organization) Fluor Government Group
4. Related EDT No.: N/A	7. Purchase Order No.: N/A
5. Proj./Prog./Dept./Div.: Integrated Disposal Facility	6. Design Authority/Resp Engr./Design Agent: F.M. Mann
9. Equip./Component No.: N/A	10. System/Bldg./Facility: N/A
8. Originator Remarks: Far-Field Hydrology Data Package, 2005 IDF Performance Assessment	12. Major Assembly Dwg. No.: N/A
	13. Permit/Permit Application No.: N/A
11. Receiver Remarks:	11A. Design Basis Document? ☐ Yes ☒ No
	14. Required Response Date: June 30, 2004

15. DATA TRANSMITTED

(A) Item No.	(B) Document/Drawing No.	(C) Sheet No.	(D) Rev. No.	(E) Title or Description of Data Transmitted	(F) Approval Desig-nator	(G) Reason for Trans-mittal	(H) Origi-nator Dispo-sition	(I) Recei-er Dispo-sition
1	RPP-20621	-	0	Far-Field Hydrolgy Data Package For The Hanford	N/A	1	1	1
				Disposal Facility Performance Assessment				

16. KEY

Approval Designator (F)	Reason for Transmittal (G)	Disposition (H) & (I)
See TFC-ESHQ-Q-INSP-C-05	1. Approval 3. Post-Review 2. Review	1. Approved 3. Reviewed no comment 5. Disapproved 2. Approved w/comment 4. Reviewed w/comment

17. SIGNATURE/DISTRIBUTION

(G) Reason	(H) Disp.	(J) Name	(K) Signature	(L) Date	(M) MSIN	(G) Reason	(H) Disp.	(J) Name	(K) Signature	(L) Date	(M) MSI
4	4	Design Auth.				1	1	R Khaleel	R Khaleel	06/21/04	E6-17
1	1	Resp. Engr. FM Mann	FM Mann	6/21/04	E6-35						
1	1	Resp. Mgr. JG Field	JG Field	6/21/04	H6-62						
5	5	QA									
		Safety									
		Env.									
		Design Agent									
3	3										
1	1	GL Parsons	GL Parsons	7-1-04	H6-19						

18. JG Field 6/21/04
Signature of EDT Originator Date

19. DOE APPROVAL (if required)
Ctrl. No.

20. JG Field 6/21/04
Design Auth./Resp. Engr./Resp. Mgr. Date

BD-7400-172.2 (08/0

DISTRIBUTION SHEET

To	From	Page 1 of 2
Distribution	R. Khaleel	Date June 21, 2004
Project Title/Work Order		EDT No. 820933
Far-Field Hydrology Data Package for the Integrated Disposal Facility Performance Assessment		ECN No.

Name	MSIN	Text With All Attach.	Text Only	Attach./ Appendix Only	EDT/ECN Only
R. Yasek (1 hard copy) DOE ORP	H6-60	x			
Carol Babel (1 hard copy) DOE ORP	H6-60	x			
Phil Lamont (1 hard copy) DOE ORP	H6-60	x			
R.W. Lober (1 hard copy) DOE ORP	H6-60	x			
J. Field (1 hard copy) CH2M HILL HANF	H6-62	x			
Kris Colosi (1 hard copy) CH2M HILL HANF	H6-19	x			
Greg Parsons (1 hard copy) CH2M HILL HANF	H6-19	x			
M. Connelly (1 hard copy) CH2M HILL HANF	E6-35	x			
F. Anderson (1 hard copy) CH2M HILL HANF	E6-35	x			
F.M. Mann (1 hard copy) CH2M HILL HANF	E6-35	x			
A.J. Knepp (1 hard copy) CH2M HILL HANF	H6-03	x			
A. Amonette - files (1 hard copy)	E6-35	x			
FLUOR GOVERNMENT GROUP					
R. Khaleel (5 hard copies)	E6-17	x			
R.J. Puigh (1 hard copy)	E6-17	x			
S. Finfrock (1 hard copy)	E6-17	x			
FLUOR HANFORD, INC.					
M.I. Wood (1 hard copy)	H8-44	x			
B. Ford (1 hard copy)	E6-35	x			
PACIFIC NORTHWEST NATIONAL LABORATORY					
C.T. Kincaid (1 hard copy)	E6-35	x			
F. Zhang (1 hard copy)	K9-33	x			
M. Fayer (1 hard copy)	K9-33	x			
P.D. Meyer (1 hard copy)	BPO	x			
P. McGrail (1 hard copy)	K6-81	x			
D. Bacon (1 hard copy)	K9-33	x			
G. Last (1 hard copy)	K6-81	x			
S. Reidel (1 hard copy)	K6-81	x			
R.J. Serne (1 hard copy)	P7-22	x			
Tom Fogwell (1 hard copy) DURATEK	E6-35	x			
Hanford Technical Library (1 hard copy)	P8-55	x			
Central Files	B1-07	x			

Far-Field Hydrology Data Package for the Integrated Disposal Facility Performance Assessment

R. Khaleel

Richland, WA 99352
U.S. Department of Energy Contract DE-AC27-99RL14047

EDT/ECN: 820933 UC:
Cost Center: Charge Code: 191 N.F
B&R Code: Total Pages: ~~194~~ 7-6-04

Key Words: Far-Field, Hydrology, Flow/transport modeling, Integrated Disposal Facility, Performance Assessment

Abstract: This report provides far-field hydrology data for flow/transport modeling for the Integrated Disposal Facility Performance Assessment

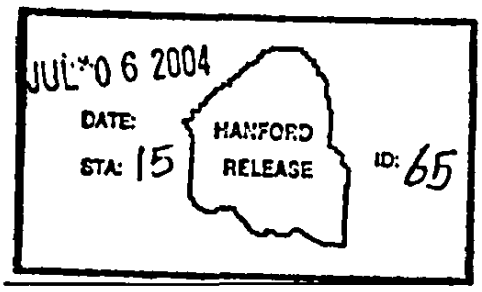

Nancy A. Fouad 7-6-04
Release Approval Date

Release Stamp

Approved For Public Release

RPP-20621
Revision 0

FAR-FIELD HYDROLOGY DATA PACKAGE

FOR THE

INTEGRATED DISPOSAL FACILITY PERFORMANCE ASSESSMENT

R. Khaleel
Fluor Government Group, Inc.

Prepared for
CH2M HILL Hanford Group, Inc.

Date Published
June 2004

CH2MHILL
Hanford Group, Inc.

Post Office Box 1500
Richland, Washington

Prepared for the U.S. Department of Energy
Office of River Protection

Contract # DE-AC27-99RL14047, Modification M030

Approved for Public Release; Further Dissemination Unlimited

This page intentionally left blank.

EXECUTIVE SUMMARY

A number of data packages are being assembled as part of 2005 Integrated Disposal Facility (IDF) Performance Assessment (PA). In this data package report the far-field hydrology data needed to perform vadose zone flow and transport modeling for the IDF PA is presented as well as the laboratory measurements of the physical and hydraulic properties for soil samples at the disposal site. In addition, the results of the application of stochastic theory to small-scale measurements are discussed. The effective (upscaled) parameter estimates are derived for saturated hydraulic conductivity, soil moisture retention and unsaturated hydraulic conductivity, bulk density, unretarded macrodispersivity and sorption-enhanced macrodispersivity. These parameters will serve as input to VAM3DF, a variably saturated vadose zone flow and transport code; VAM3DF will generate 'mean' solutions for the pressure head and contaminant concentration.

The stratigraphy at the disposal site is dominated by two distinctly different sediment sequences. The upper part of the vadose zone is characterized by a sandy sequence, whereas the lower part is characterized primarily by a gravel sequence. At saturation, compared to the gravel-dominated sequence, the sand-dominated sequence is described by a smaller log-conductivity variance. However, compared to the gravel-dominated sequence, the log-unsaturated conductivity variance for the sand-dominated sequence is higher. Consequently, the macroscopic anisotropy relations for the sandy and gravelly sediments are different. The differences in the characteristics of the two sediment sequences also result in different macrodispersivity estimates. Overall, compared to sandy soils, gravelly soils are characterized by a much smaller saturated water content, higher bulk density, higher log-conductivity variance, smaller log-unsaturated conductivity variance, a much smaller macroscopic anisotropy, and smaller macrodispersivities.

A methodology is presented to estimate uncertainties in model predictions. For far-field hydrology, three sources contribute to uncertainty estimates: (a) variations in model configurations, (b) uncertainties in the calculated mean solution for concentration, and (c) uncertainties around the calculated mean solution for concentration. The following approach will be used to evaluate these uncertainties. First, uncertainty will be defined for the 'mean' solutions for concentration distribution at the water table (as a function of position and time). The combined contribution to uncertainty in the mean solution due to model configuration and effective parameter (i.e., unsaturated hydraulic conductivity and macrodispersivity) variations will be investigated. A methodology developed by Kapoor and Gelhar (1994a, b) will then be used to estimate the uncertainty around the mean solution.

Model configurations will include variations in stratigraphy and clastic dike networks. Base case and uncertainty in stratigraphy and clastic dike network models will be provided in the geology data package. Selected VAM3DF runs will be performed to estimate the impact of these uncertainties on the resultant contaminant distribution at the water table. The uncertainty attributed to isotropy and sloped layering on calculated mean solutions will also be estimated.

Bounding estimates for concentrations at the water table will be provided through a choice of parameters and model configurations judged to provide a reasonable bounding case representation of the system.

This page intentionally left blank.

TABLE OF CONTENTS

LIST OF TABLES

LIST OF FIGURES

LIST OF APPENDICES

This page intentionally left blank.

LIST OF TERMS

IDF	Integrated Disposal Facility
ILAW	Immobilized Low-Activity Tank Waste
PA	Performance Assessment

This page intentionally left blank.

1.0 INTRODUCTION

The *Integrated Disposal Facility* (IDF) *Performance Assessment* (PA), hereinafter referred to as the IDF PA, examines the long-term environmental and human health effects associated with the planned disposal of the mixed wastes, low-level solid wastes, and the vitrified low-level fraction of the waste presently contained in Hanford Site high-level waste tanks. The objectives of the performance assessment are to provide a reasonable expectation that the disposal of the waste will be protective of the general public, groundwater resources, air resources, inadvertent intruder and surface water resources. A number of data packages are being assembled as part of 2005 IDF PA. This data package deals only with the far-field hydrology data needed to perform vadose zone flow and transport modeling for the IDF PA and is an update of *Far-Field Hydrology Data Package for the Immobilized Low-Activity Tank Waste Performance Assessment* (Khaleel 1999).

Figure 1 illustrates the overall computational strategy for the PA. The near-field environment is defined as the domain through the disposal trench to some distance below the floor of the trench. A coupled unsaturated flow, chemical reactions, and contaminant transport simulator (STORM) will be used within the near-field (Bacon and McGrail 1997). The plume exiting the region near the trench is expected to be of high ionic strength and pH, and will migrate down into the near-field vadose zone for some distance. However, at some distance from the disposal trench, geochemical conditions will approach those more typical of the Hanford vadose zone and for which simplifying assumptions (such as linear sorption, negligible precipitation/dissolution, no changes in hydraulic properties, and no density effects) can be used. This region is defined as the far-field environment and can be simulated using standard, nonreactive flow and transport codes. For the IDF PA, computations in the far-field domain will be done by VAM3DF (Huyakorn and Panday 1995), a variably saturated flow and transport code. The primary reason for switching from the near-field simulator to VAM3DF is to apply a less complicated code for the far-field, and therefore a faster turnaround for the numerical simulations. The radionuclide flux exiting the far-field domain to the unconfined aquifer will be provided by VAM3DF and will be used as a boundary condition for the unconfined aquifer flow and transport simulator. The final step in the methodology (using the impact assessment integrator) is to compute the impacts, if any, from ingestion, inhalation, and external radiation to humans who become exposed to the contaminants by withdrawing water from the aquifer.

1.1 SCOPE OF THIS DATA PACKAGE

The scope for the far-field hydrology data package for the IDF disposal site includes the following information:

- Data on laboratory measurements for soil moisture retention, saturated and unsaturated hydraulic conductivity, and bulk density for sediment samples from the IDF site (Section 2.0).

Note: The International System of Units is used in this report. To convert feet to meters (m), multiply by 3.28. To convert millimeters to inches (in.), multiply by 3.94×10^{-2}.

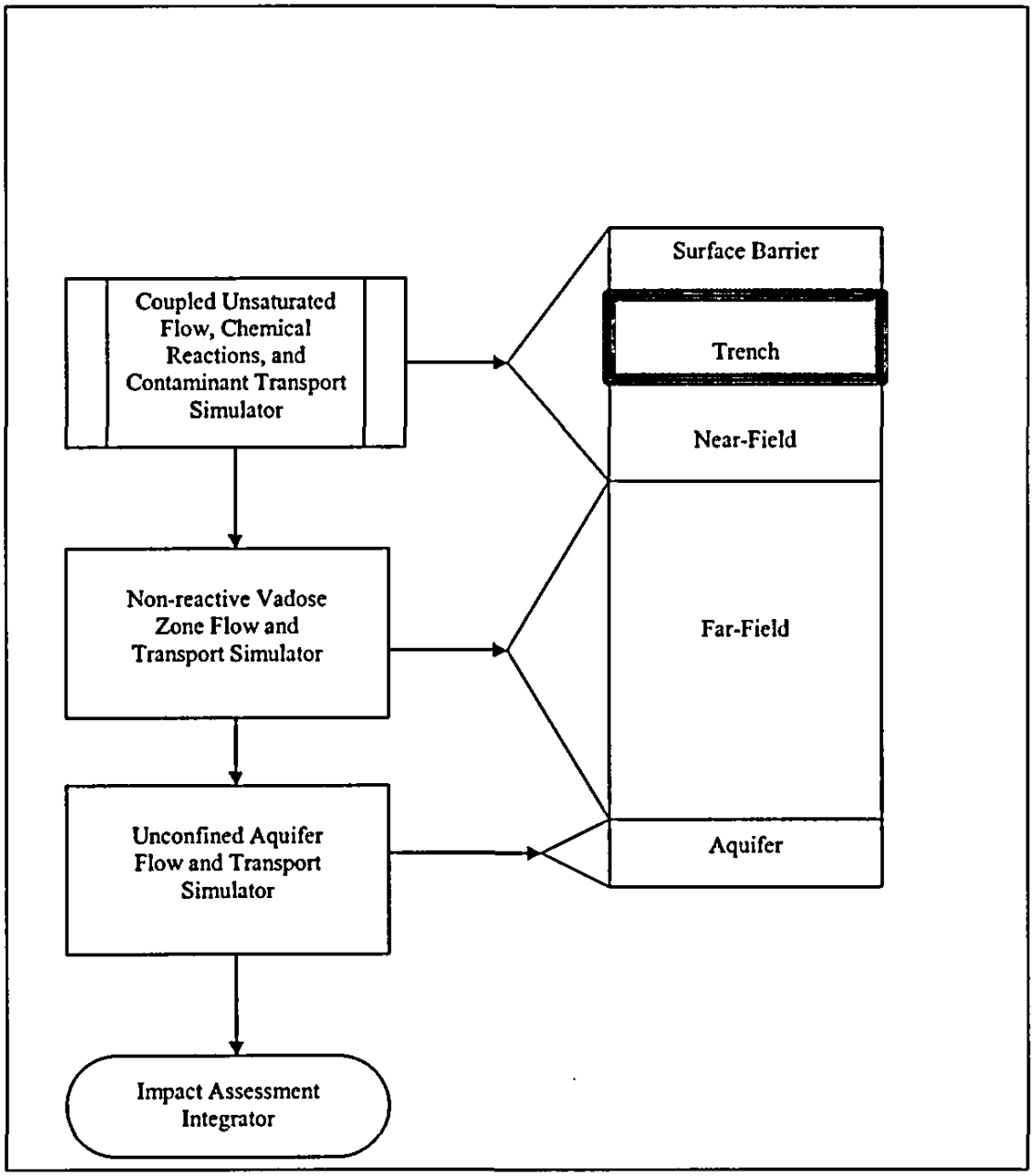

Figure 1. Modeling Strategy for Assessing IDF Disposal System Impacts (after McGrail et al. 1998)

- Effective (upscaled) moisture retention, saturated and unsaturated hydraulic conductivity, bulk density, diffusivity, and macrodispersivity estimates for geologic formations in the far-field vadose zone (Section 3.0). This section also presents the equations used to estimate unsaturated hydraulic conductivity.
- Sorption-enhanced macrodispersivity estimates for selected radionuclide species (Section 3.0).
- Moisture retention, saturated and unsaturated hydraulic conductivity, bulk density, and macrodispersivity estimates for clastic dike infilling materials (Section 4.0).
- Bounding scenarios on model configurations and uncertainty estimates about the calculated mean concentration and around mean concentration (Section 4.0).

Appendices A, B, and F contain the physical and hydraulic measurements of FY 1998 borehole cores, ILAW Borehole No. 2 well cores, and FY 1998 clastic dike samples, respectively. The ILAW Borehole No. 3 Hydraulic Properties Multistep Test Results are presented in Appendix C. Appendix D contains the laboratory data on the physical and hydraulic properties for 100 Area samples, and Appendix E presents the hydraulic parameters of the upper Hanford formation. Finally, Appendix G presents some quality assurance/quality control considerations used in this report.

1.2 BASIC ASSUMPTIONS

For the integrated disposal facility with a capillary barrier and a surface barrier, the vadose zone water contents beneath the facility are expected to approach the natural moisture regime for arid soils. Field moisture contents are expected to be less than 10% (by volume); matric potentials of the order of -1000 cm and recharge rates of the order of 0.1 cm/yr. Under such arid conditions, the features and processes identified in the scope carry significant importance for the PA calculations. For example, the layered heterogeneous soils in 200 Areas are expected to show bulk anisotropic behavior, with the hydraulic conductivity parallel to the layers being larger than that normal to the layers. Furthermore, the degree of anisotropy increases rapidly with increasing tension or decreasing moisture content, becoming large in dry soils of the kind expected beneath the disposal facility. Also, the infiltrating water diverted around the trenches by the capillary barrier can potentially move beneath the vaults, creating moist conditions and enhancing contaminant movement to the water table. In addition, recent theoretical work and field experiments (e.g., Gelhar 1993; Garabedian et al. 1991) have shown that spreading of contaminants undergoing heterogeneous linear equilibrium sorption can be significantly larger than that of the non-sorbing tracer. Dispersivity enhancement can cause early arrival at the water table before the contaminants undergoing heterogeneous sorption have had an opportunity to decay. Also, clastic dikes are of concern because they can potentially create preferred pathways.

This page intentionally left blank.

2.0 LABORATORY MEASUREMENTS FOR SOIL HYDRAULIC PROPERTIES

The purpose of this section is to summarize available data on laboratory measurements for moisture retention, saturated and unsaturated hydraulic conductivity for sediment samples from the IDF site. A description of the site geology is provided in *Geologic Data Package for 2005 Integrated Disposal Facility Waste Performance Assessment* (Reidel 2004).

2.1 IDF SITE SEDIMENT SAMPLES

As part of site characterization activity for the IDF site, sediment samples were obtained in fiscal years 1998, 2001 and 2002 via a borehole drilling and sampling program that obtained about 50 samples from three boreholes. The Hanford formation sandy sequence is about 200 ft thick and is the dominant facies at the site. The lower gravelly sequence is about 70 ft thick. For the purposes of this data package, no distinction is made on gravel-dominated sequences of the lower Hanford formation and the upper Ringold Formation. The sediments from both of these formations have similar physical and hydraulic properties and are characterized essentially as sandy gravel, with a significant gravel fraction (Khaleel and Freeman 1995a, b).

Details on sampling, laboratory procedures, and analysis of samples from three boreholes are included as Appendices A, B and C. The following summary is based on details provided in the appendices. As described in Section 2.1.1, for the gravel-dominated sequence, data on hydraulic properties from elsewhere on the Hanford Site were used as surrogates.

The procedures used to analyze the borehole samples are described in detail in the appendices. Briefly, the multistep and steady state methods were used to obtain moisture retention and unsaturated conductivity data. Both methods were performed on the same core using the same sensor locations. In addition to cumulative outflow, the multistep method, which is an improvement over the one-step method of Kool et al. (1985a, b), provides water content-matric potential (θ-ψ) pairs. These data were used in conjunction with a numerical inversion procedure (Eching and Hopmans 1993) to determine the optimal set of van Genuchten model (van Genuchten 1980) parameters. The steady-state method, described by Klute and Dirksen (1986), provides water content-matric potential-unsaturated conductivity (θ-ψ-K) triplets; the method was primarily used as a check on the multistep method.

Tables 1 through 4 provide the van Genuchten model parameters determined using the numerical inversion procedure and data from the multistep test. The pore-size distribution parameter ℓ (Mualem 1976) was kept fixed at 0.5. The fitted moisture retention curves and unsaturated conductivity curves for all 44 samples for the sandy sequence from the three boreholes are shown in Figure 2. Note that not all ten FY02 samples are included in Table 3 and Figure 2. Some of FY02 samples were actually clastic dike samples; others showed extreme variability that was not present in FY98 and FY01 samples.

2.1.1 100 Area Sediment Samples

As discussed earlier, no site-specific data on soil moisture characteristics are available at the disposal sites for sediments in the gravel-dominated sequence. However, as part of the Environmental Restoration Project, moisture retention and unsaturated conductivity data for sandy gravel sediments are available elsewhere (100 Area along the Columbia River) on the Hanford Site. Fifteen samples having a large gravel fraction were chosen. These samples ranged in gravel content from 43 to 75 percent and were used as surrogates to represent the hydraulic properties for the gravel-dominated sequence.

Standard laboratory and Westinghouse Hanford Company quality assurance procedures were used to analyze these gravelly samples. The moisture retention data for the fine fraction (< 2 mm) and for the drainage cycle of up to -1,000 cm of pressure head were measured using "Tempe" pressure cells; the rest of the drainage data up to -15,000 cm was measured using the pressure plate extraction method (Klute 1986). Saturated hydraulic conductivities for the bulk samples (including gravels) were measured in the laboratory using a constant-head permeameter. A unit gradient method (Klute and Dirksen 1986; Khaleel et al. 1995; Khaleel and Relyea 2001; Khaleel and Heller 2003) was used to measure unsaturated hydraulic conductivities for the bulk samples. The laboratory measured data on the < 2mm size fraction were corrected for the gravel fraction (Gardner 1986; Khaleel and Relyea 1997). No correction was needed for the saturated and unsaturated conductivities since these were measured on the bulk sample.

The van Genuchten parameters were obtained via the RETC code (van Genuchten et al. 1991) and a simultaneous fit of both laboratory-measured moisture retention and unsaturated conductivity data; all five unknown parameters θ_r, θ_s, α, n, and K_s, with m=1-1/n (van Genuchten 1980), were fitted to the data. The pore size distribution factor, ℓ (Mualem 1976) was kept fixed at 0.5 during the simultaneous fitting. The laboratory data, following gravel-correction of the moisture retention data, are included in Appendix B for the 15 samples. Appendix B serves as the input data file for RETC. The fitted moisture retention curves and unsaturated conductivity curves for the 15 samples for the gravel sequence are shown in Figure 3. Note that, unlike the borehole samples, the 100 Area samples were fitted for θ_r, θ_s, α, n, and K_s.

It should be recognized that the gravelly samples were used as surrogates for the predominantly open framework gravelly formation at the IDF site. However, unlike the open framework gravels, the gravelly samples contain a significant fine fraction and their unsaturated conductivities are not much different from those for the sandy media (Khaleel and Relyea 2001; Khaleel and Heller 2003). Therefore, while the moisture retention curves for the gravelly samples exhibit the expected behavior, the unsaturated conductivity values for the two soil types are not much different. However, for the simulated recharge rates at the IDF site, and because of drainage of open framework gravels, the average moisture content and, thus, the unsaturated conductivity for the sandy sequence are expected to be higher than for the gravelly sequence.

Table 1. Van Genuchten Parameters (Based on the Multistep Method) and Saturated Hydraulic Conductivity Data for 20 FY98 Borehole Samples from the Sandy Sequence (after Fayer et al. 1998)

Sample	θ_s (cm^3/cm^3)	θ_r (cm^3/cm^3)	α (1/cm)	n (-)	Saturated Hydraulic Conductivity (cm/s)
7A	0.377	0.0404	0.0290	1.825	1.04E-03
10A	0.413	0.0279	0.1161	1.784	2.95E-03
12A	0.363	0.0309	0.0650	1.755	2.15E-03
14A	0.416	0.0324	0.0445	1.728	1.99E-03
15A	0.380	0.0254	0.0487	1.844	2.09E-03
16A	0.420	0.0228	0.0682	1.710	9.57E-03
17A	0.423	0.0382	0.0689	1.899	1.99E-03
19A	0.444	0.0279	0.2010	1.542	4.31E-03
20A	0.419	0.0321	0.0305	2.081	2.54E-03
21A	0.403	0.0276	0.0545	1.926	2.94E-03
22A	0.352	0.0252	0.1078	1.585	5.06E-03
23A	0.371	0.0411	0.0079	1.553	2.65E-04
24A	0.321	0.0413	0.0130	1.684	5.69E-04
25A	0.345	0.0267	0.0842	2.158	5.40E-03
27A	0.377	0.0354	0.0830	1.532	8.14E-03
29A	0.359	0.0317	0.0784	1.732	3.75E-03
31A	0.418	0.0444	0.0058	2.012	8.21E-04
32A	0.359	0.0401	0.0931	1.703	6.71E-03
34A	0.316	0.0324	0.0819	2.398	1.32E-02
35A	0.299	0.0428	0.0897	2.160	1.06E-02

Table 2. Van Genuchten Parameters (Based on the Multistep Method) and Saturated Hydraulic Conductivity for 21 FY01 Borehole Samples from the Sandy Sequence (after Oostrom et al. 2002)

Sample	θ_s (cm^3/cm^3)	θ_r (cm^3/cm^3)	α (1/cm)	n (-)	Saturated Hydraulic Conductivity (cm/s)
45L	0.385	0.008	0.1039	1.737	3.24E-2
45U	0.385	0.005	0.088	1.664	3.24E-2
50L	0.420	0.025	0.073	1.710	1.75E-3
50U	0.420	0.013	0.045	1.667	1.75E-3
80L	0.359	0.031	0.0403	2.368	1.05E-3
80U	0.359	0.033	0.0313	2.572	1.05E-3
85L	0.406	0.023	0.1074	1.697	3.84E-2
85U	0.406	0.027	0.0847	1.595	3.84E-2
110L	0.412	0.039	0.0362	2.328	5.16E-4
110U	0.412	0.046	0.0268	3.182	5.16E-4
130L	0.358	0.032	0.0940	2.003	1.97E-2
130U	0.358	0.036	0.0674	1.934	1.97E-2
150L	0.431	0.015	0.0992	1.547	7.48E-3
150U	0.431	0.024	0.0703	1.514	7.48E-3
200L	0.410	0.002	0.0995	2.162	4.93E-2
215L	0.370	0.028	0.0448	1.918	2.24E-3
215U	0.370	0.023	0.0333	1.815	2.24E-3
230L	0.309	0.040	0.0472	1.658	3.56E-3
230U	0.309	0.038	0.0400	1.658	3.56E-3
251L	0.427	0.032	0.084	1.845	1.43E-2
261L	0.390	0.045	0.0191	2.485	5.54E-4

Table 3. Van Genuchten Parameters (Based on the Multistep Method) and Saturated Hydraulic Conductivity for Three FY02 Borehole Samples from the Sandy Sequence (after Fayer et al. 2003)

Sample	θ_s (cm^3/cm^3)	θ_r (cm^3/cm^3)	α (1/cm)	n (-)	Saturated Hydraulic Conductivity (cm/s)
C3826-171	0.382	0.0226	0.0390	1.84	7.96E-03
C3827-63.5	0.444	0.0	0.0914	1.50	2.23E-02
C3827-221	0.361	0.0220	0.0660	1.77	7.30E-03

Table 4. Van Genuchten Parameters and Fitted Saturated Hydraulic Conductivity Data for 15 Sandy Gravel Samples

Sample	Operable Unit	Well Number	Depth (m)	Percent Gravel	θ_s (cm^3/cm^3)	θ_r (cm^3/cm^3)	α (1/cm)	n (-)	Fitted K_s (cm/s)
2-1307	100-HR-3	199-D5-14	18.90	43	0.236	0.0089	0.0130	1.447	1.29E-04
2-1308	100-HR-3	199-D5-14	30.64	58	0.120	0.0208	0.0126	1.628	6.97E-05
2-1318	100-HR-3	199-D8-54A	15.54	60	0.124	0.0108	0.0081	1.496	1.67E-04
2-2663	100-BC-5	199-B2-12	8.20	61	0. 135	0.0179	0.0067	1.527	6.73E-05
2-2664	100-BC-5	199-B2-12	24.84	73	0.125	0.0136	0.0152	1.516	1.12E-04
2-2666	100-BC-5	199-B4-9	21.49	71	0.138	0.00	0.0087	1.284	1.02E-04
2-2667	100-BC-5	199-B4-9	23.93	75	0.094	0.00	0.0104	1.296	1.40E-04
3-0570	100-KR-1	116-KE-4A	3.50	60	0.141	0.00	0.0869	1.195	2.06E-02
3-0577	100-FR-3	199-F5-43B	7.16	66	0.107	0.00	0.0166	1. 359	2.49E-04
3-0686	100-FR-1	116-F-14	6.49	55	0.184	0.00	0.0123	1.600	5.93E-04
3-1702	100-DR-2	199-D5-30	9.78	68	0.103	0.00	0.0491	1.260	1.30E-03
4-1086	100-K	199-K-110A	12.77	65	0.137	0.00	0.1513	1.189	5.83E-02
4-1090	100-K	199-K-111A	8.20	50	0.152	0.0159	0.0159	1.619	4.05E-04
4-1118	100-K	199-K-109A	10.30	66	0.163	0.00	0.2481	1.183	3.89E-02
4-1120	100-K	199-K-109A	18.90	63	0.131	0.0070	0.0138	1.501	2.85E-04

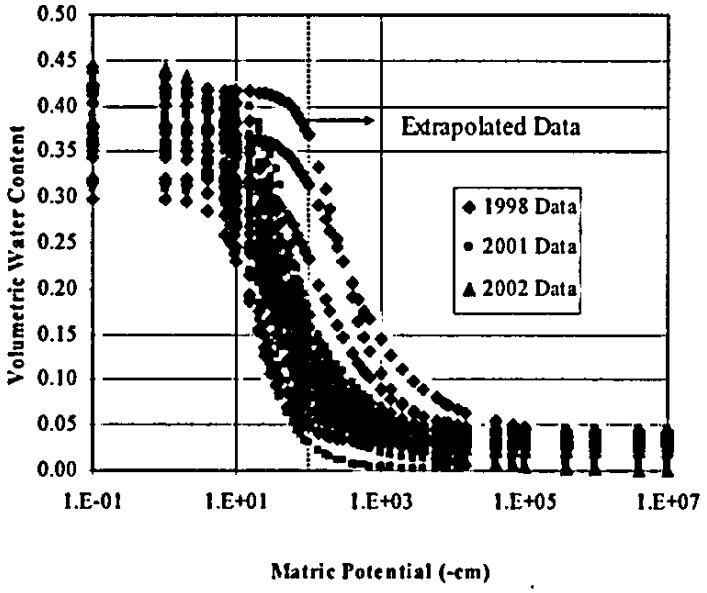

(a)

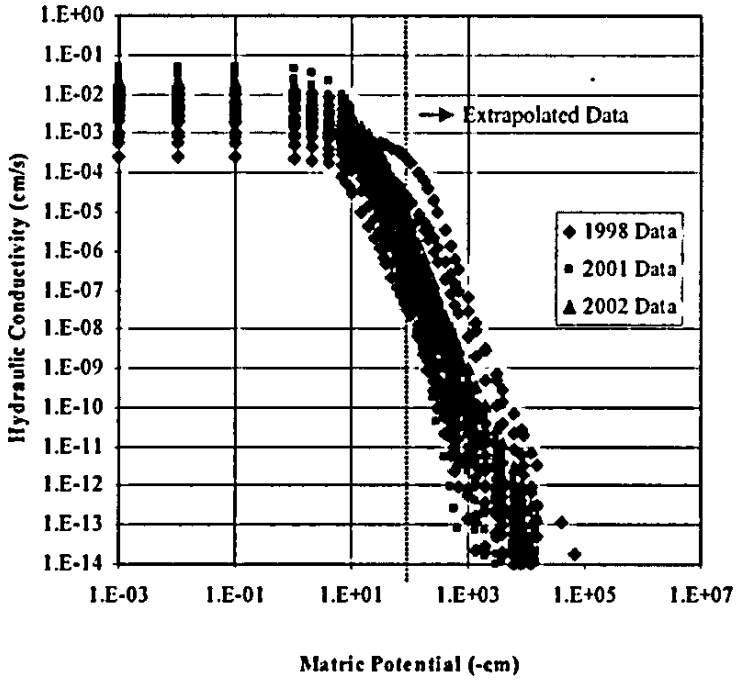

(b)

Figure 2. Fitted (a) Moisture Retention and (b) Unsaturated Conductivity Curves for 44 Samples from Three Boreholes for the Sand-Dominated Sequence. *The symbols represent fitted curves for different samples, not experimental data.*

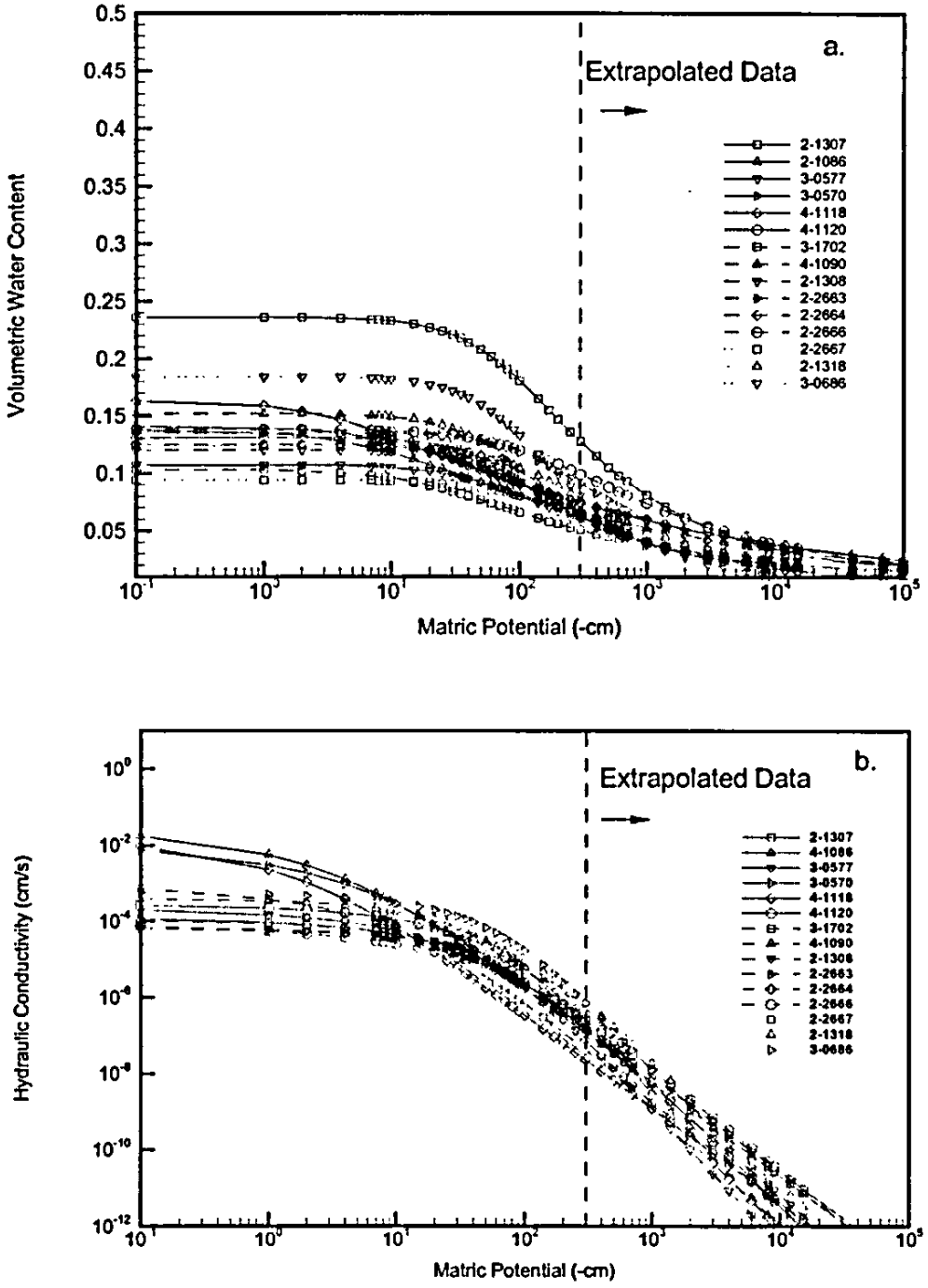

Figure 3. Fitted (a) Moisture Retention and (b) Unsaturated Conductivity Curves for 15 Samples for the Gravel-Dominated Sequence. *The symbols represent fitted curves for different samples, not experimental data.*

This page intentionally left blank.

3.0 EFFECTIVE (UPSCALED) FLOW AND TRANSPORT PROPERTIES

Data on hydraulic properties, described in the preceding section, were obtained via laboratory tests on core samples (scales of the order of cm). However, numerical models of fluid flow and contaminant transport in the unsaturated zone require specifying hydraulic properties for each discrete grid block that is often of the order of meters. Therefore, the scale of the grid blocks is usually much larger than the scale at which the unsaturated properties were measured. The process of defining large-scale properties for the numerical grid blocks based on small, measurement-scale point measurements is called upscaling (Khaleel et al. 2002; Rockhold et al. 1999).

This section provides effective (upscaled) values of flow and transport parameters for the far-field vadose zone. Specific flow parameters include moisture retention, saturated and unsaturated hydraulic conductivity. Transport parameters include bulk density, diffusivity, and macrodispersivity. Sorption coefficients are included as part of another data package and will not be discussed here. Note that the upscaling process applies to spatial variability of hydraulic and transport properties for a heterogeneous vadose zone; large-scale heterogeneities such as clastic dikes are discussed in Section 4.0.

3.1 EFFECTIVE (UPSCALED) FLOW PARAMETERS

Any attempt at upscaling is confronted with the issue of spatial variability of hydraulic properties due to small-scale soil heterogeneities. The presence of spatial variability in hydraulic properties of Hanford soils has been well documented (e.g., Schaap et al. 2003; Khaleel and Freeman 1995a). A fundamental issue is then how best to incorporate the effects of natural heterogeneity in modeling. A traditional approach is to use deterministic models and attempt to incorporate the overall heterogeneity of the system, such as layering, while neglecting the small-scale heterogeneity. The considerable spatial variability of Hanford soils makes complete characterization of the hydraulic properties at the field scale an almost impossible task, as an enormous amount of data is required for proper representation of the actual media heterogeneities.

An alternative approach is to define an equivalent homogeneous medium with average, effective (upscaled) hydraulic properties that are related to the local small-scale heterogeneities and thereby predict the mean flow and transport behavior of the field-scale, larger media. However, to represent a heterogeneous medium by its homogeneous equivalent, we need to estimate the effective hydraulic properties that represent this equivalent homogeneous medium. A straightforward approach would be to use statistical averages (arithmetic or geometric) of the local soil hydraulic properties, but such simple estimates may not always be able to properly describe the complicated nonlinear behavior in heterogeneous soils.

3.1.1 Stochastic Upscaling

For saturated media, an averaging of the heterogeneities in geologic media at a smaller scale leads to an effective hydraulic conductivity value at the larger (macroscopic) scale, with the lateral hydraulic conductivity being much larger than the vertical conductivity (Freeze and Cherry 1979). For unsaturated media, theoretical (e.g., Mualem 1984, Yeh et al. 1985a, b, c; Bear et al. 1987; Mantoglou and Gelhar 1987; Green and Freyberg 1995) and experimental analyses (e.g., Stephens and Heerman 1988; Yeh and Harvey 1990; McCord et al. 1991) of field-scale unsaturated flow indicates that in stratified sediments, the effective hydraulic conductivity tensor is anisotropic with a tension-dependent (or moisture-dependent) degree of anisotropy. The anisotropy ratio of horizontal hydraulic conductivity to vertical hydraulic conductivity increases with decreasing moisture content. Variable, moisture-dependent anisotropy in unsaturated soils is therefore an effective, large-scale (macroscopic) flow property which results from media heterogeneities at a smaller scale, and provides a framework for upscaling laboratory-scale measurements to the effective (upscaled) properties for the large-scale vadose zone. An alternate approach to stochastic upscaling has recently been advanced by Zhang et al. (2003).

3.1.2 Field Observations

Field observations in the vicinity of the IDF site do indeed provide evidence of saturation-dependent anisotropy and lateral migration. A test facility comprising an injection well at the center and a radial array of 32 monitoring wells was constructed in 1980 south of the Plutonium Uranium Reduction Extraction Facility (PUREX) in the 200 East Area. The facility was used in late 1980 and early 1981 to conduct an infiltration and multiple tracer (i.e., chloride, nitrate, barium, rubidium, strontium-85 (Sr-85) and cesium-134 (Cs-134) test, in which 45,000 L of liquid (in 11 increments) were injected at a depth of 4.7 m over a period of 133 days (Sisson and Lu 1984). Three-dimensional water content profiles in layered, coarse sediments were monitored to a depth of 18 m by down-hole neutron probe measurements. The initial water contents were measured at 30-cm increments over the 30- to 1800-cm depths in all 32 observation wells. In situ gamma-energy analysis data were collected to determine the distribution of radioactive tracers. The unique three-dimensional nature of the experiment and the measured water content profiles provide evidence of tension-dependent anisotropy. The field data clearly show lateral spreading that occurred during injection. The horizontal wetting patterns dominated the experiment. In fact, numerical modeling results (Sisson and Lu 1984), based on the assumption of a uniform and isotropic model, showed a much deeper penetration of the moisture profile than that occurring in the field (Sisson and Lu 1984). The degree of spreading was remarkable considering the apparent uniform lithology at the site.

3.1.3 Composite Macroscopic Relationships

The fitted moisture retention curves (Figures 2a and 3a) show spatial variability, although the degree of variation at a given tension is more modest than that of hydraulic conductivity (Figures 2b and 3b). Based on data in Tables 1 through 4, composite parameters for the moisture retention relations were determined. For both sandy and gravelly soils, the composite van Genuchten parameters were obtained via RETC (van Genuchten et al. 1991) and a simultaneous

fit of both moisture retention and unsaturated conductivity predictions; all four unknown parameters θ_r, θ_s, α, and n with m=1-1/n (van Genuchten 1980) were fitted to the data. The pore size distribution factor ℓ was kept constant at 0.5 during the simultaneous fitting. The saturated conductivity, K_s, was also kept constant as geometric mean of the sample estimates.

The fitted composite van Genuchten-Mualem parameters for the sandy and gravelly sequences are shown in Table 5. Equivalent horizontal and vertical hydraulic conductivities are derived using Polmann macroscopic anisotropy relations (see Section 3.1.3.2) and the composite van Genuchten-Mualem parameter estimates (Table 5).

Table 5. Composite van Genuchten-Mualem Parameters for the Sand- and Gravel-Dominated Sequences

Formation	Number of samples	θ_s	θ_r	α (1/cm)	n	ℓ	Fitted K_s (cm/s)
Sandy	44	0.394	0.049	0.0631	2.047	0.5	4.15E-03
Gravelly	15	0.138	0.010	0.021	1.374	0.5	5.60E-04

3.1.3.1 Stochastic Model for Macroscopic Anisotropy

As discussed earlier, variable, tension-dependent anisotropy provides a framework for upscaling small-scale measurements to the effective (upscaled) properties for the large-scale vadose zone. A stochastic model is used to evaluate tension-dependent anisotropy for sediments at the IDF site.

Yeh et al. (1985b) analyzed steady unsaturated flow through heterogeneous porous media using a stochastic model; parameters such as hydraulic conductivity are treated as random variables rather than as deterministic quantities. The Gardner (1958) relationship was used by Yeh et al. to describe unsaturated hydraulic conductivity (K) as a function of saturated hydraulic conductivity (K_s) and tension (ψ), i.e.,

$$K(\psi) = K_s \exp(-\beta\psi) \qquad (1)$$

where β is a fitting parameter. Equation (1) can be re-written as

$$\ln K(\psi) = \ln K_s - \beta\psi \qquad (2)$$

Equation (2) is referred to as the log-linear model, since lnK is linearly related to ψ through the constant slope β. However, such a constant slope is often inadequate in describing $\ln K(\psi)$ over ranges of tension of practical interest for field applications. As an alternative, the slope β can be approximated locally by straight lines over a fixed range of tension. The "$\ln K_s$" term in equation (2) can then be derived by extrapolating the local slopes back to zero tension.

Using a linear correlation model between the log-conductivity zero-tension intercept and β, Polmann (1990) presents a generalized model that accounts for the cross-correlation of the local soil property (i.e., $\ln K_s$ and β) residual fluctuations. Compared to uncorrelated $\ln K_s$ and β model, partial correlation of the properties is shown to have a significant impact on the magnitude of the effective parameters derived from the stochastic theory. The Polmann (1990) equations for deriving the effective parameters are as follows:

$$
\begin{aligned}
&< LnK >=< LnK_s > -A < \psi > -\sigma^2_{LnKs}\lambda[p - p^2 < \psi > -\zeta^2 < \psi >]/(1 + A\lambda) \\
&\sigma^2_{LnK} = \sigma^2_{LnKs}[(1 - p < \psi >)^2 + \zeta^2 < \psi >^2]/(1 + A\lambda) \\
&K_h^{eq} = \exp[< LnK > +(\sigma^2_{LnK}/2)] \\
&K_v^{eq} = \exp[< LnK > -(\sigma^2_{LnK}/2)]
\end{aligned}
\qquad (3)
$$

where σ^2_{LnK} = variance of log unsaturated conductivity (which depends on mean tension),

<ψ> = mean tension,

σ^2_{LnKs} = variance of $\ln K_s$

<$\ln K_s$>=mean of $\ln K_s$,

p = slope of the β versus $\ln K_s$ regression line,

$\zeta = \sigma_\delta/\sigma_{\ln Ks}$,

σ_δ = standard deviation of the residuals in the β versus $\ln K_s$ regression,

A = mean slope, β, for $\ln K_s$ vs. ψ,

λ = vertical correlation lengths for $\ln K_s$ (assumed to be same as that of β),

K_h^{eq} = equivalent unsaturated horizontal conductivity, and

K_v^{eq} = equivalent unsaturated vertical conductivity.

3.1.3.2 Macroscopic Anisotropy Relations

Note that values listed in Table 5 are the composite van Genuchten-Mualem parameters for the sandy and gravelly sequences at the IDF site. Equation (3) is used only to assign the variable Polmann anisotropy (i.e., the ratio of equivalent unsaturated horizontal conductivity to equivalent unsaturated vertical conductivity) as a function of saturation. The van Genuchten-Mualem parameters in Table 5 are then used to assign the actual unsaturated hydraulic conductivity estimates. Note that the fitted K_s values in Table 5 represent the vertical components.

Results of the application of equation (3) for variable anisotropy are presented below. The same 44 samples (Tables 1 through 3) of the sandy sequence were used to obtain parameters <$\ln Ks$>, $\sigma^2_{LnK_s}$, p, ζ, and A. The slope and pseduo $\ln K_s$ estimates, discussed in the preceding section, were evaluated for the moisture regime of interest (i.e., tension range of 150 cm to 200 cm for the sandy sequence and 300 cm to 400 cm for the gravelly sequence). Based on a unit gradient model, the preceding tension regime is consistent with the assumed recharge rate for the numerical simulations. The macroscopic anisotropy noted in Figures 5 and 6 applies to the preceding expected tension regime. It should be noted also that no experimental data are

available for unsaturated conductivities in the tension range of interest; β and $\ln K_s$ estimates were based on the fitted van Genuchten-Mualem curves.

An estimate of the correlation length, λ, is needed for anisotropy calculations. Most of the measurements in the vicinity of the IDF site have been obtained at sampling intervals that are too coarse to yield a reasonable estimate for the correlation length. However, one data set is available (Fayer et al. 1993) that provides saturated conductivity estimates at about 30 cm intervals for a depth of 18 m within the Hanford formation; the site is located about 1/2 mile east of the IDF site. Figure 4 shows the experimental variogram and the fitted spherical variogram model for saturated conductivities. The fitted spherical variogram suggests a correlation length, λ, of about 50 cm; i.e., the distance at which the variogram drops to [1-(1/e)] times the sill (Figure 4). The correlation length, λ, for both $\ln K_s$ and β were assumed to be equal.

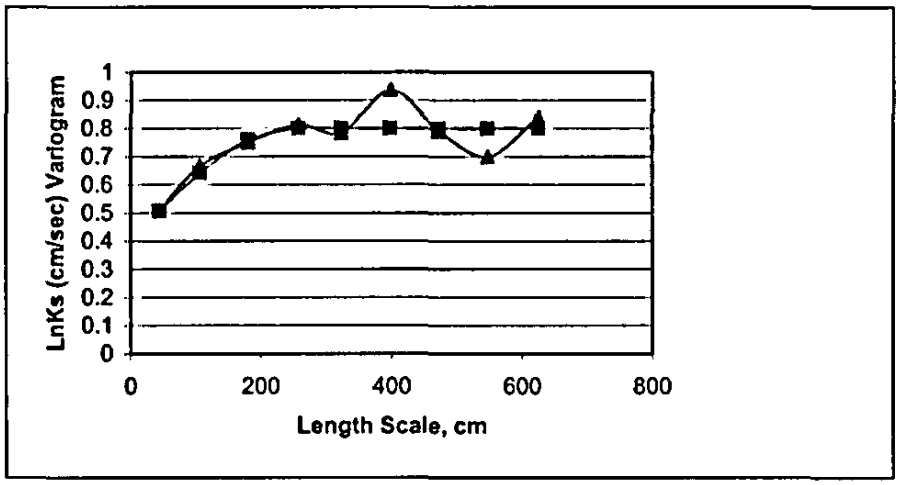

Figure 4. Experimental (triangles) and Fitted Theoretical (squares) Variogram for $\ln K_s$

The Polmann parameters for both sandy and gravel-dominated sequences are shown in Table 6. Note that, compared to the sandy soils, mean slope, A, $\langle \ln Ks \rangle$, $\sigma^2_{\ln K_s}$, and ζ values for the gravelly soils are significantly lower; σ_β^2 for the gravelly samples was also almost two orders of magnitude lower. Because of these different characteristics, the macroscopic anisotropy relations for the sandy and gravelly sediments are quite different. Figures 5 and 6 illustrate the macroscopic anisotropy relations for the two sediments. The anisotropy for the gravelly soils is much less compared to that for sandy soils. In fact, for the tension range of interest for IDF PA modeling, the anisotropy ratio is about two. Note that, for gravelly soils, no data were available for a variogram analysis. However, a smaller λ value (30 cm) is used (Table 6) because of a much higher variance of $\ln K_s$ for the gravelly soils than for the sandy soils.

Table 6. Macroscopic Anisotropy Parameters for the Sand- and Gravel-Dominated Sequences

Formation	Number of samples	$\langle LnK_s \rangle$	$\sigma^2_{LnK_s}$	p	ζ	λ (cm)	A
Sandy	44	-12.4	2.77	-8.1E-4	3.01E-3	50	0.0234
Gravelly	15	-13.3	1.37	3.7E-4	7.89E-4	30	0.0081

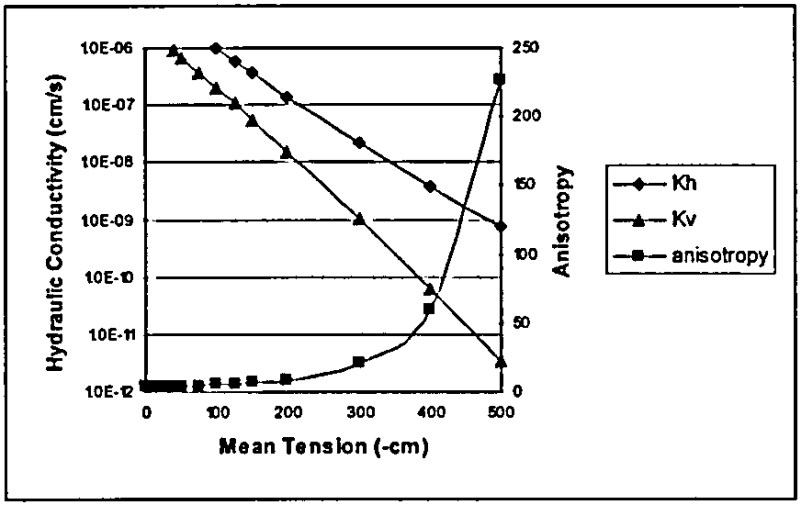

Figure 5. Calculated Macroscopic Anisotropy (Equation 3) as a Function of Mean Tension for the Sand-Dominated Sequence

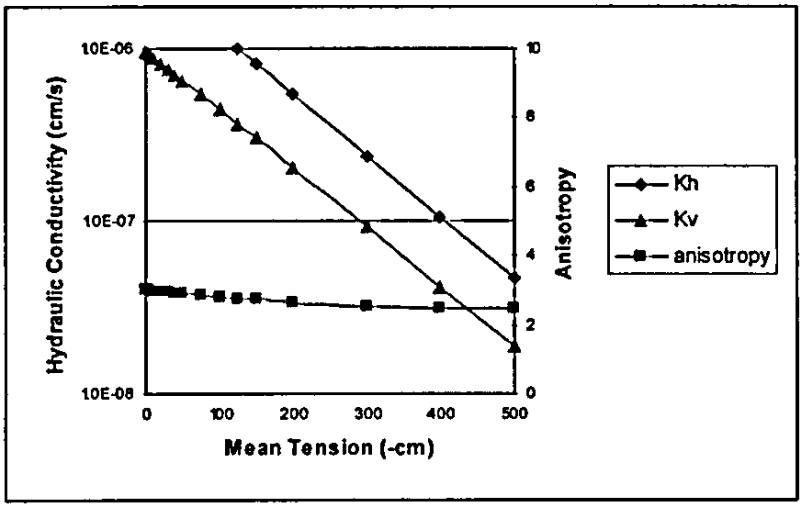

Figure 6. Calculated Macroscopic Anisotropy (Equation 3) as a Function of Mean Tension for the Gravel-Dominated Sequence

3.2 EFFECTIVE TRANSPORT PARAMETERS

Base case effective transport parameter (bulk density, diffusivity, and dispersivity) estimates are presented in this section. Because of natural variability, the transport parameters are all spatially variable. The purpose is again, similar to the flow parameters, to evaluate the effect of such variability on the large-scale transport process.

3.2.1 Bulk Density and Distribution Coefficient

Both bulk density (ρ_b) and distribution coefficient (K_d) estimates are needed to calculate retardation factors for different species. The effective, large-scale estimate for the product [$\rho_b K_d$] is the average of the product of small-scale laboratory measurements for bulk density and K_d (Gelhar 1993). The laboratory measurements for ρ_b are shown in Table 7 for the sandy (a) and the gravel-dominated (b) sequences, whereas the K_d measurements for cesium, strontium, uranium and selenium are available in *Radionuclide Distribution Coefficients for Sediments Collected from Borehole 299-E17-21* (Kaplan et al. 1998). The K_d values were corrected for the gravel fraction. The bulk density measurements in Table 7a and b also account for the presence of any gravel fraction. Table 8 provides the effective, large-scale estimates.

3.2.2 Diffusivity

It is assumed that the effective, large-scale diffusion coefficients for both sandy and gravel-dominated sequences at the IDF site are a function of volumetric moisture content, θ. VAM3DF uses the Millington-Quirk (1961) empirical relation:

$$D_e(\theta) = D_0 \frac{\theta^{10/3}}{\theta_s^2} \qquad (4)$$

where $D_e(\theta)$ is the effective diffusion coefficient of an ionic species, and D_0 is the effective diffusion coefficient for the same species in free water. The molecular diffusion coefficient for all species in pore water is assumed to be 2.5×10^{-5} cm^2/sec (Kincaid et al.1995).

Table 7. Laboratory Measurements of Bulk Density for the (a) Sandy and (b) Gravelly Sediments

(a) Sandy Sediments			(b) Gravelly Sediments	
Samples for the sand-dominated sequence	Bulk Density (g/cm^3)		Samples for the gravel-dominated sequence	Bulk Density (g/cm^3)
7A	1.70		2-1307	2.15
10A	1.62		2-1308	2.13
12A	1.74		2-1318	2.16
14A	1.58		2-2663	2.38
15A	1.69		2-2664	2.25
16A	1.58		2-2666	2.10
17A	1.57		2-2667	2.16
19A	1.52		3-0570	2.12
20A	1.58		3-0577	2.32
21A	1.62		3-0686	2.17
22A	1.78		3-1702	2.33
23A	1.72		4-1086	2.26
24A	1.85		4-1090	2.21
25A	1.80		4-1118	2.12
27A	1.71		4-1120	2.06
29A	1.76		-	-
31A	1.60		-	-
32A	1.78		-	-
34A	1.92		-	-
35A	1.98		-	-

Table 8. Effective Parameter Estimates, $E[\rho_b K_d]$, for the Product of Bulk Density (g/cm^3) and K_d (cm^3/g) at the IDF Disposal Site

Species	$E[\rho_b K_d]$	
	Sand-dominated sequence	Gravel-dominated sequence
Cs	3473	1700
Sr	25.20	12.20
U	1.05	0.51
Se	11.32	5.56

3.2.3 Dispersivity

An extended review is provided in the following sections on the rationale of choice for vadose zone dispersivity estimates. Readers who are familiar with the state-of-the-art can proceed directly to Section 3.2.3.4.

A variety of factors such as the size of the flow domain, the flow regime (saturated versus unsaturated flow), field heterogeneities, and the contaminant species (retarded versus nonretarded) need to be recognized in estimating dispersivities. The objective of this section is to provide appropriate guidance on the choice of vadose zone dispersivity estimates for use in the IDF PA.

It should be noted that laboratory data would be of little use in estimating field-scale dispersivities. While well-designed, large-scale tracer experiments would provide useful information, limited field data are available at this time. Therefore, the dispersivity estimates needed for modeling are essentially based on literature values and the available stochastic equations.

Literature data suggest that much more information is available on dispersion in saturated media than in unsaturated media. Therefore, first the available data on dispersivities in saturated media are summarized (Gelhar et al. 1992). Second, available data on vadose zone dispersivities are presented, including results of small-scale tracer experiments in the vicinity of the IDF site in 200 East Area. Third, the stochastic framework used in obtaining dispersivity estimates is reviewed, and estimates are provided for use in the IDF PA.

3.2.3.1 Saturated Media Dispersivities For Field Sites

A critical review of dispersivity observations from 59 different field sites was performed by Gelhar et al. (1992). In this review, extensive tabulations of information were included on aquifer type, hydraulic properties, flow configuration, type of monitoring network, tracer, method of data interpretation, overall scale of observation and longitudinal, horizontal transverse and vertical transverse dispersivities from original sources. The information was then used to classify the dispersivity data into three reliability classes: low, intermediate, and high. Overall, the data indicate a trend of systematic increase of the longitudinal dispersivity with observation scale, but the trend is much less apparent when the reliability of data (Figure 7) is considered. The longitudinal dispersivity ranged from 10^{-1} to 10^{5} m, but the largest scale for high reliability data was only 250 m. When the data are classified according to porous versus fractured media, no significant differences were apparent between these aquifer types. At a given scale, the longitudinal dispersivity values were found to range over 2 to 3 orders of magnitude and the higher reliability data approached the lower portion of this range. The high reliability dispersivity data ranged from a low of about 0.6 m at a scale of 15 m to about 1 m at a scale of 250 m; some data are on the order of 2 to 3.5 m at a scale of 30 m (Figure 7). It is not appropriate to represent the longitudinal dispersivity data by a single universal line. The variations in dispersivity reflect the influence of differing degrees of aquifer heterogeneity at different sites. The data on transverse dispersivities are more limited but clearly indicate that vertical transverse dispersivities are typically an order of magnitude smaller than horizontal transverse dispersivities (Gelhar et al. 1992). Reanalysis of data from several of the field sites showed that improved interpretations most often lead to smaller dispersivities (Gelhar et al.

1992). Overall, Gelhar et al. concluded that longitudinal dispersivities in the lower part of the indicated range are more likely to be realistic for field situations. This suggests that, for conservative species, a longitudinal dispersivity of the order of a meter is a reasonable estimate for saturated media domains that are a couple of hundred meters in scale. Note that the estimates are for saturated media and conservative species. As discussed later, dispersivity estimates are enhanced due to heterogeneous sorption in both saturated and unsaturated media.

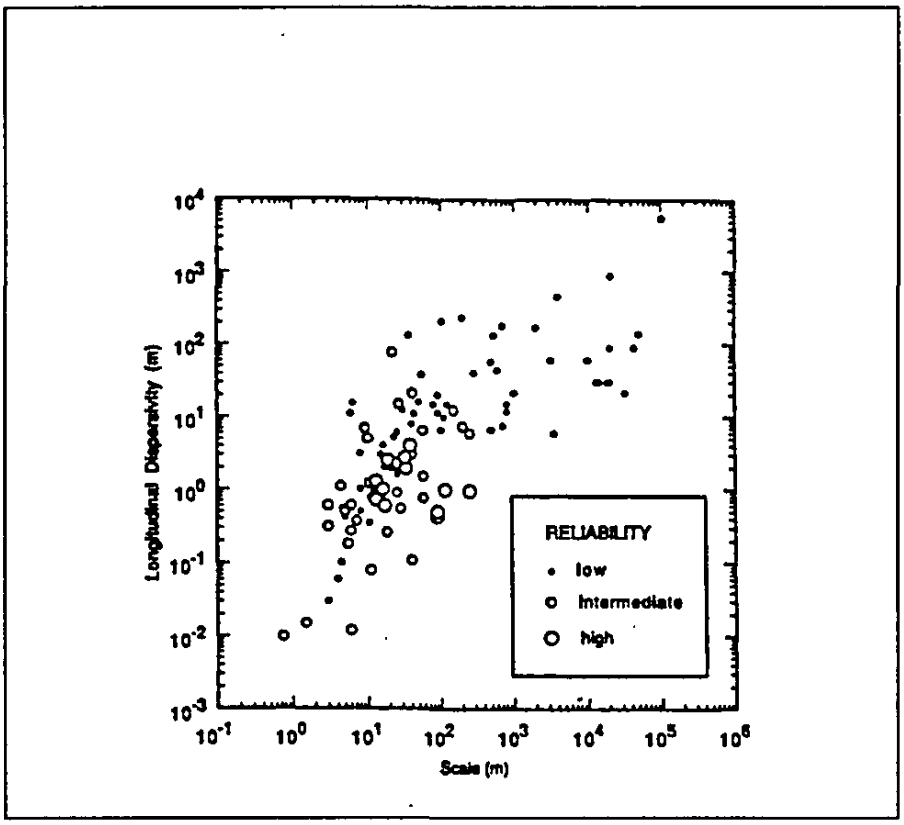

Figure 7. Longitudinal Macrodispersivity in Saturated Media as a Function of Overall Problem Scale with Data Classified by Reliability (after Gelhar et al. 1992)

3.2.3.2 Vadose Zone Dispersivities For Dry Desert Environments

As discussed earlier in Section 1.1, for an engineered waste disposal facility with a capillary barrier and a surface barrier on top, the vadose zone water contents beneath the disposal facility are expected to approach the natural moisture regime for arid soils. Although exceptional precipitation events may cause transient high water contents near the soil surface, the source of the infiltration is not likely to be sustained at great depths within the vadose zone.

This inference is supported by the results of artificial tracer experiments on much shorter time scales. For example, two massively instrumented solute transport experiments were performed in desert soils near Las Cruces, New Mexico (Wierenga et al. 1991; Hills et al. 1991). Drip emitters were used to irrigate a plot adjoining a deep trench in a heterogeneous soil possessing

well in excess of one order of magnitude standard deviation in saturated hydraulic conductivity. Monitoring of the trench face showed a spatially uniform progression of the wetting front and did not reveal indications of preferential flow (Wierenga et al. 1991). Hills et al. (1991) found that a dispersivity of 5 cm provided reasonably realistic simulations of tritium (^3H) and bromide (Br) tracer distributions.

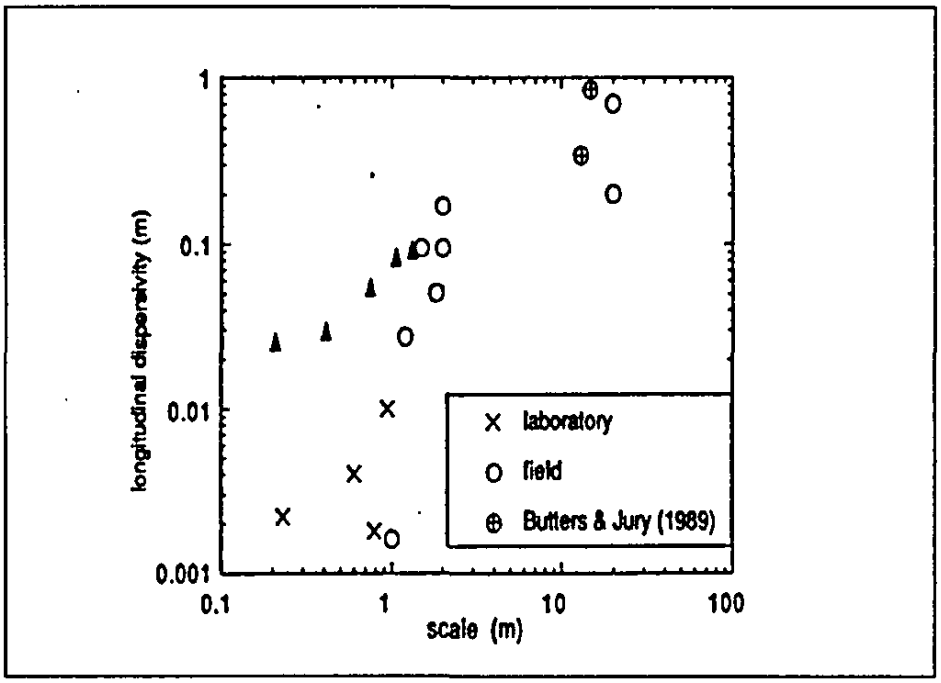

Figure 8. Longitudinal Macrodispersivity in Unsaturated Media as a Function of Overall Problem Scale (after Gelhar 1993). *[Note that the triangles are data from Ward et al. 1998[1]]*

For unsaturated flow, long-term environmental tracer studies at several arid southwestern sites indicate dispersivities of less than 10 cm. Phillips et al. (1988) assessed the degree of mixing in desert soils using the conventional advection-dispersion modeling, yielding a dispersion coefficient of 50 cm^2/yr. This compares with the calculated effective diffusion coefficient of 25 cm^2/yr. A similar study by Scanlon (1992) at another southwestern arid site obtained a dispersion coefficient of about 14 cm^2/yr. These, then, lead to effective dispersivities of about 7 and 4 cm, at the two arid sites, and Peclet numbers (displacement divided by dispersivity) of 23 and 17.

Ward et al. (1998)[1] obtained dispersivity estimates via field measurements at a location close to the IDF site, using potassium chloride (KCl) as a tracer. Analysis of the data provided dispersivities that ranged from 1.3 to 7.8 cm for travel distances ranging from 25 to 125 cm (Appendix E, Table 2, p. E-15). Dispersivity increased with depth to about 0.75 m, after which it

[1] Ward, A.L., R.E. Clayton, and J.S. Ritter. 1998. Determination of in situ hydraulic parameters of the upper Hanford formation. Letter Report to Fluor Daniel Northwest, Inc. December, 1998. Pacific Northwest National Laboratory. Richland, WA.

essentially became constant. Although these estimates are for the Hanford formation, the transport distance within the vadose zone is indeed of limited extent. Nevertheless, results based on the limited data are consistent with the concept of a scale-dependent dispersivity. Thus, although no data exist on large-scale dispersivities near the IDF site, it is expected that they will be larger than those based on the small-scale tracer experiment of Ward et al. (1998).

Based on a survey of literature, Gelhar (1993) presented the longitudinal vadose zone dispersivities as a function of the scale of the experiment, as shown in Figure 8. The figure shows a lack of data for scales larger than 2 m. Nevertheless, similar to saturated flow, Figure 8 shows an increase of dispersivity with an increase in scale. Also, shown in Figure 8 are results from the Ward et al. experiment; their data are in close agreement with others.

3.2.3.3 Stochastic Models and Macrodispersivities for Large-Scale Media

Field-scale dispersivities are referred to as macrodispersivities. The heterogeneities that exist at various length scales result in a scale dependence of macrodispersivities. Stochastic models have been developed which relate the macrodispersive spreading to the spatial variability of saturated hydraulic conductivity field in a saturated porous media (e.g., Gelhar and Axness 1983; Dagan 1984). The Gelhar and Axness (1983) model provides the asymptotic estimates of macrodispersivity, while the Dagan (1984) model describes the preasymptotic estimates of macrodispersivities for the near-source, early-time period. The Dagan (1984) model predicts that under steady state flow with a uniform mean hydraulic gradient, the ensemble longitudinal macrodispersivity increases with time and displacement distance as the solute first enters the flow domain. A constant, asymptotic value (i.e., Fickian behavior) is eventually reached after the solute travels a few tens of correlation scales of the hydraulic conductivity field.

For prediction of contaminant transport during early time or for short travel distances, simulating effects of scale-dependence on macrodispersion is a consideration. The dispersivities increase with time (or equivalently with distance) until they tend to converge on their unique asymptotic (large time) values. The second-moment evolution curve or the time-dependent, preasymptotic macrodispersivities are of particular interest, since it can take a long time (e.g., years or decades) for the asymptotic Fickian approximation to take hold. However, the early time scale dependence is of little consequence in simulations involving long times or large mean travel distances such as those for IDF PA. For these predictions over large travel distances or large times, the use of a constant (asymptotic) dispersivity is considered to be adequate. An estimate of the maximum or asymptotic value of macrodispersivity for saturated media can be based on the Gelhar and Axness (1983) stochastic solution:

$$A_L = \sigma^2_{LnK_s} \lambda \qquad (5)$$

where λ is the vertical correlation scale (i.e., average distance over which conductivities are correlated) for log saturated hydraulic conductivity.

In addition to the size of flow domain and vadose zone soil heterogeneities, dispersivities are expected to be a function of soil moisture content (or matric potential). Macrodispersivities are expected to increase with a decrease in saturation (e.g., Polmann 1990; Gelhar et al. 1994). Russo (1993) suggests that vadose zone macrodispersivities can be defined in a manner similar

to saturated media estimates. This is based on his finding that the product of the variance and the correlation scale of log conductivity for both saturated and unsaturated media are of similar magnitude. In other words, an increase in the variance of log conductivity (and, concurrently, in the velocity variance) as moisture content decreases is compensated in part by a decrease in the correlation scale of log conductivity (and, concurrently, in the correlation scale of the longitudinal component of the velocity). Such an approximation (a) assumes use of Gardner's (1958) equation to describe unsaturated conductivity as a function of matric potential, and (b) holds as long as the correlation scale of β in Gardner's equation is relatively small compared with that of the log saturated conductivity.

3.2.3.4 Macrodispersivity Estimates For Non-Reactive Species

The Gelhar and Axness equation can be used to estimate asymptotic values of macrodispersivity. However, to account for effects of unsaturated flow, a modified version is used:

$$A_L(<\psi>) = \sigma^2_{LnK}\lambda \qquad (6)$$

where the longitudinal macrodispersivity depends on the mean tension $<\psi>$. To apply equation (6), an estimate of the vertical correlation scale for unsaturated conductivity is needed. As discussed earlier, a correlation length of the order of about 50 cm was obtained for the sandy formation. However, compared to the saturated K's, an increase in the variance of log conductivity is expected to be compensated in part by a decrease in the correlation scale of log unsaturated conductivity. A correlation length of 30 cm is assumed for both sandy and gravelly formations. Table 9 provides the log unsaturated conductivity variances (at a recharge rate of about 0.1 cm/yr) and the estimated longitudinal (A_L) and transverse (A_T) macrodispersivities for the two formations. The transverse dispersivities are estimated as $1/10^{th}$ of the longitudinal values (Gelhar et al. 1992). Gelhar (1993) presented results of stochastic analysis of macrodispersion in unsaturated media by Mantoglou and Gelhar (1985). The large-scale macrodispersivity estimates in Table 9 are of similar magnitude to those reported in Gelhar (1993) for Panoche and Maddock soil types.

Table 9. Non-reactive Macrodispersivity Estimates for Soils at the IDF Disposal Site for an Approximate Recharge Rate of 0.1 cm/yr

Formation	σ^2_{LnK}	Correlation length, λ (cm)	A_L (cm)	A_T (cm)
Sandy	5.51	30	~200	20
Gravelly	0.96	30	~30	3

3.2.3.5 Heterogeneous Sorption Enhanced Macrodispersivities

As expected, the net effect of sorption is to retard the velocity of the contaminant in the soil. Because sorption for specific contaminants may be a function of soil properties, as the soil properties experience spatial variability, the sorption also varies (Gelhar 1993; Talbott and Gelhar 1994). The variation directly affects the velocity of the contaminant, which, in turn, enhances the spreading of the plume. The enhanced spreading is defined by a larger reactive longitudinal macrodispersivity, different from the non-reactive longitudinal macrodispersivity, as discussed in the preceding section. The increased plume spreading due to heterogeneous sorption (over and above the result for no sorption) is defined as the macrodispersivity enhancement. Stochastic theory and field data on contaminant plumes suggest that the effect of macrodispersivity enhancement only occurs in the longitudinal direction. The transverse macrodispersivity is unaffected by sorption variability (Garabedian et al. 1991). The results presented in this section support the use of species-dependent enhanced longitudinal macrodispersivities in the IDF PA modeling.

The radioisotopes considered are cesium-137, strontium-90, uranium, and selenium (Cs-137, Sr-90, U, and Se, respectively). The objective is to evaluate differences in macrodispersivity enhancement due to a long-lived mobile radionuclide (e.g., U) and a short-lived relatively immobile radionuclide (e.g., Sr-90). During the laboratory analysis, measurements of K_d for each species were obtained on the same soil samples, as were measurements of unsaturated hydraulic conductivity.

Based on laboratory measurements of unsaturated conductivity, K (Fayer et al. 1998) and K_d (Kaplan et al. 1998) for the same 20 samples for the Hanford sandy sequence, a direct correlation of K and K_d was derived for Cs-137, Sr-90, U, and Se. Stochastic theory developed by Gelhar (1993) was evaluated to determine the importance of varying longitudinal macrodispersivity by contaminant species on the basis of sorption heterogeneity and correlation with hydraulic conductivity. An enhancement of macrodispersivity can have significant effects on the expected contaminant predictions for numerical models.

In order to understand clearly the importance of heterogeneous, spatially variable sorption, a number of parameters were defined. The variable K_d may be prescribed by a mean (K_d) and a standard deviation (σ_{Kd}). Further, a retardation factor, R, was related to K_d by the following:

$$R = 1 + \frac{\rho_b K_d}{\theta} \qquad (7)$$

where R may be described statistically by an effective retardation, $\overline{R}$ = E[R], and its standard deviation, σ_R.

By analyzing the mean and standard deviation of a sample data set of a measured soil property, and by showing a relationship between the soil property and R, $\overline{R}$ and σ_R were calculated as a function of the soil property data set.

The net result of the variation in the retardation and the relationship between the retardation and LnK is to increase the longitudinal macrodispersivity of the sorbed species according to the following equation given by Talbott and Gelhar (1994):

$$A_{11} = A_0\left\{\left[1+\gamma\frac{\sigma_R}{R\sigma_{LnK}}\sqrt{\zeta}\right]^2+(1-\zeta)\frac{\sigma_R^2\lambda_n}{\overline{R}^2\sigma_{LnK}^2\lambda_1}\gamma^2\right\} \qquad (8)$$

where A_0 is the non-reactive longitudinal macrodispersivity, λ_1 is the horizontal correlation scale, $\lambda_n=\lambda_1$, and γ is defined as the ratio of harmonic to geometric mean for unsaturated K.

Equation (8) is identical to that in Talbott and Gelhar (1994), except that the appropriate variables are evaluated for unsaturated conditions. Equation (8) assumes random K_d but constant bulk density and moisture content. However, using the more general case (Gelhar 1993, p. 256) when all three (i.e., K_d , bulk density, and moisture content) vary, it was found that the contribution to equation (8) from variations of bulk density and moisture content were negligibly small, compared to variations of K_d.

The result of stochastic analysis for macrodispersivity enhancement for the Hanford sandy sequence for the four contaminants is shown in Table10. Note that the unsaturated K's were evaluated at -100 cm via the fitted van Genuchten-Mualem relation. As expected, the log conductivity variance, σ^2_{LnK} at a matric potential of -100 cm is much higher (~5.5) compared to the σ^2_{LnKs} (~1.0) for the same 20 samples at saturation. The macrodispersivity enhancement, A_{11}/A_o ranges from about 1.06 for Se to about 2.12 for U. Figure 9a-d shows the LnK versus R relation for the four species for the sandy sequence.

Table 10. Macrodispersivity Enhancement (Equation 8) for the Sandy Sequence at the IDF Site [ρ_b in g/cm^3 and K_d in cm^3/g]

Species	$\overline{K_d}$	$\sigma_{K_d}/\overline{K_d}$	$\overline{R}$	$\sigma_R/\overline{R}$	$\overline{\rho_b}$	$\overline{\theta}$	σ^2_{LnK}	γ	ζ	λ_n/λ_1	A_{11}/A_o
Cs-137	2055	0.29	31002	0.50	1.71	0.138	5.51	0.22	0.52	1	1.07
Sr-90	14.7	0.11	241	0.62	1.71	0.138	5.51	0.22	0.45	1	1.08
U	0.62	0.20	11.1	0.52	1.71	0.138	5.51	0.22	0.53	1	2.12
Se	6.73	0.28	98.5	0.28	1.71	0.138	5.51	0.22	0.68	1	1.06

The LnK versus R relation for the four species for the gravelly sequence are shown in Figure 10. The result of stochastic analysis for macrodispersivity enhancement for the Hanford gravelly sequence is shown in Table 11. Again, the unsaturated K's were evaluated at -100 cm via the

fitted van Genuchten-Mualem relation for the 15 gravelly samples. No data are available on the measurements of sorption coefficients for the gravel-dominated sequence. Based on the information for the sandy samples, all gravelly samples were first assigned the same average sorption coefficient for their respective species. This resulted in the coefficient of variation (i.e., $\sigma_{K_d}/\overline{K_d}$, see column 3 in Table 11) to be identically zero for all four species. The bulk (gravel and fine fraction) retardation coefficients are then based on a correction of the actual surface area available for sorption, based on the individual gravel fraction for the 15 samples. Unlike for the sandy sequence, the log conductivity variance, σ^2_{LnK} at a matric potential of -100 cm is much lower (~0.96) compared to the σ^2_{LnKs} (~5.31) for the same 15 samples at saturation. The macrodispersivity enhancement, A_{11}/A_o varies over a very narrow range — from about 1.05 for U to about 1.07 for Cs-137.

Table 11. Macrodispersivity Enhancement (Equation 8) for the Gravelly Sequence at the IDF site
[ρ_b in g/cm^3 and K_d in cm^3/g]

Species	$\overline{K_d}$	$\sigma_{K_d}/\overline{K_d}$	$\overline{R}$	$\sigma_R/\overline{R}$	$\overline{\rho_b}$	$\overline{\theta}$	σ^2_{LnK}	γ	ζ	λ_n/λ_1	A_{11}/A_o
Cs-137	2055	0	17148	0.21	2.19	0.10	0.96	0.62	0.033	1	1.07
Sr-90	14.7	0	124	0.20	2.19	0.10	0.96	0.62	0.033	1	1.06
U	0.62	0	6.13	0.17	2.19	0.10	0.96	0.62	0.033	1	1.05
Se	6.73	0	57.12	0.20	2.19	0.10	0.96	0.62	0.033	1	1.06

3.2.3.6 Numerical Considerations

A complicating factor in numerical modeling of contaminant transport in porous media is that both finite-difference and finite-element solutions are affected by "numerical dispersion," which refers to artificial dispersion caused by errors associated with discretization of the flow domain. To minimize such errors, the grid should be designed so that the Peclet number (P_e = grid distance/dispersivity) is less than or equal to one, although acceptable solutions can be obtained with P_e as high as 10 (Huyakorn and Pinder 1983). With low dispersivities within the vadose zone, the Peclet number criterion results in grid spacings that are not very practical to implement. This is why numerical modelers often resort to higher values of dispersivity. An alternative is to consider use of "upwinding" option (Huyakorn and Pinder 1983) to control numerical dispersion.

Another consideration is simulation time interval so that the Courant number (C_r = pore velocity*time interval/grid spacing) is less than or equal to one. That is, the time step should be selected so that the chosen time interval is less than the value obtained by the ratio of grid spacing to pore velocity. Thus, the time step should be selected so that it is less than the time it takes for the solute to move one grid spacing. Note that, for a three-dimensional problem, the P_e and C_r criteria are applicable to transport in all three directions.

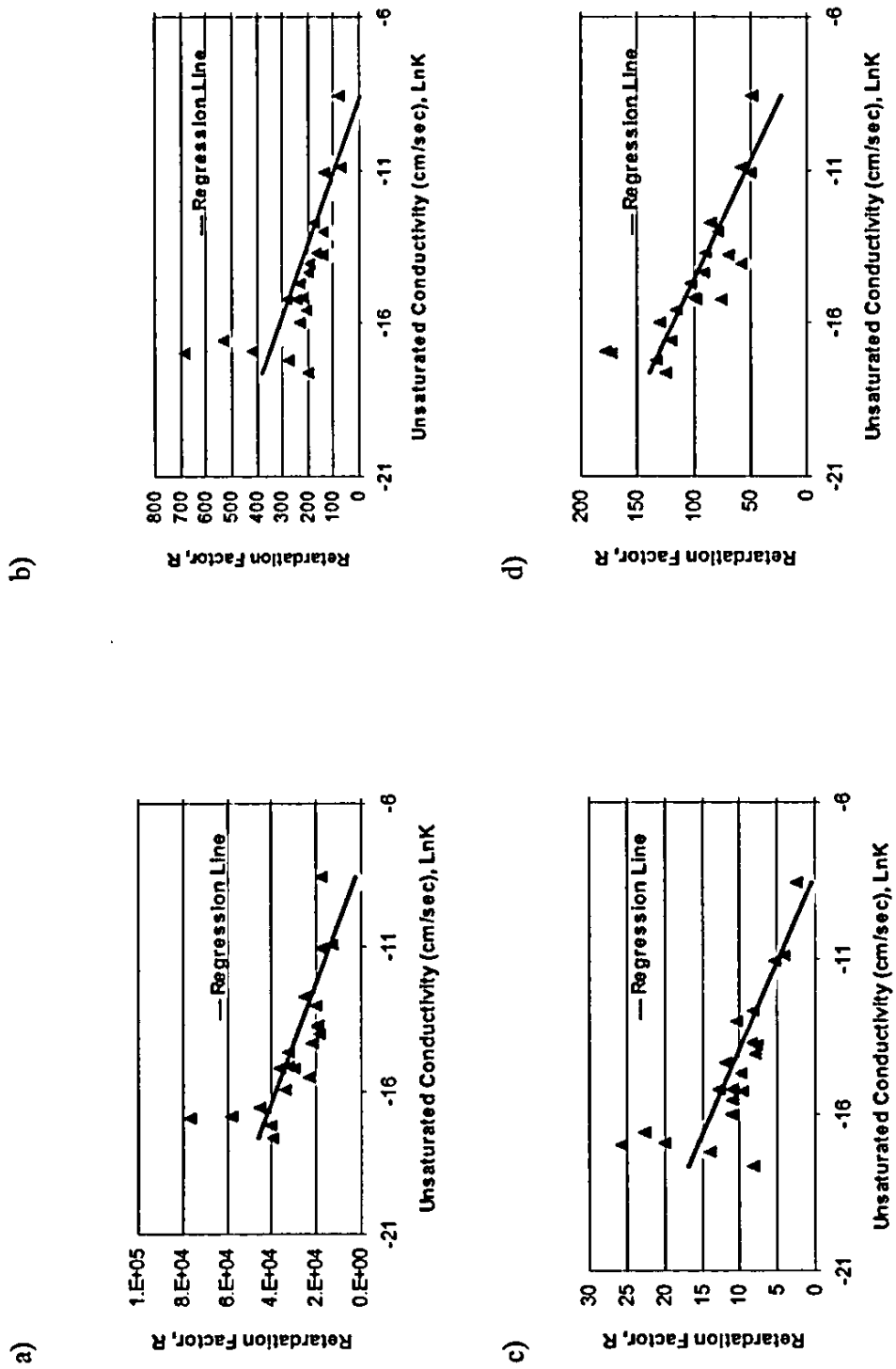

Figure 9. LnK versus R for (a) Cesium-137, (b) Strontium-90, (c) Uranium, and (d) Selenium for the Sand-Dominated Sequence

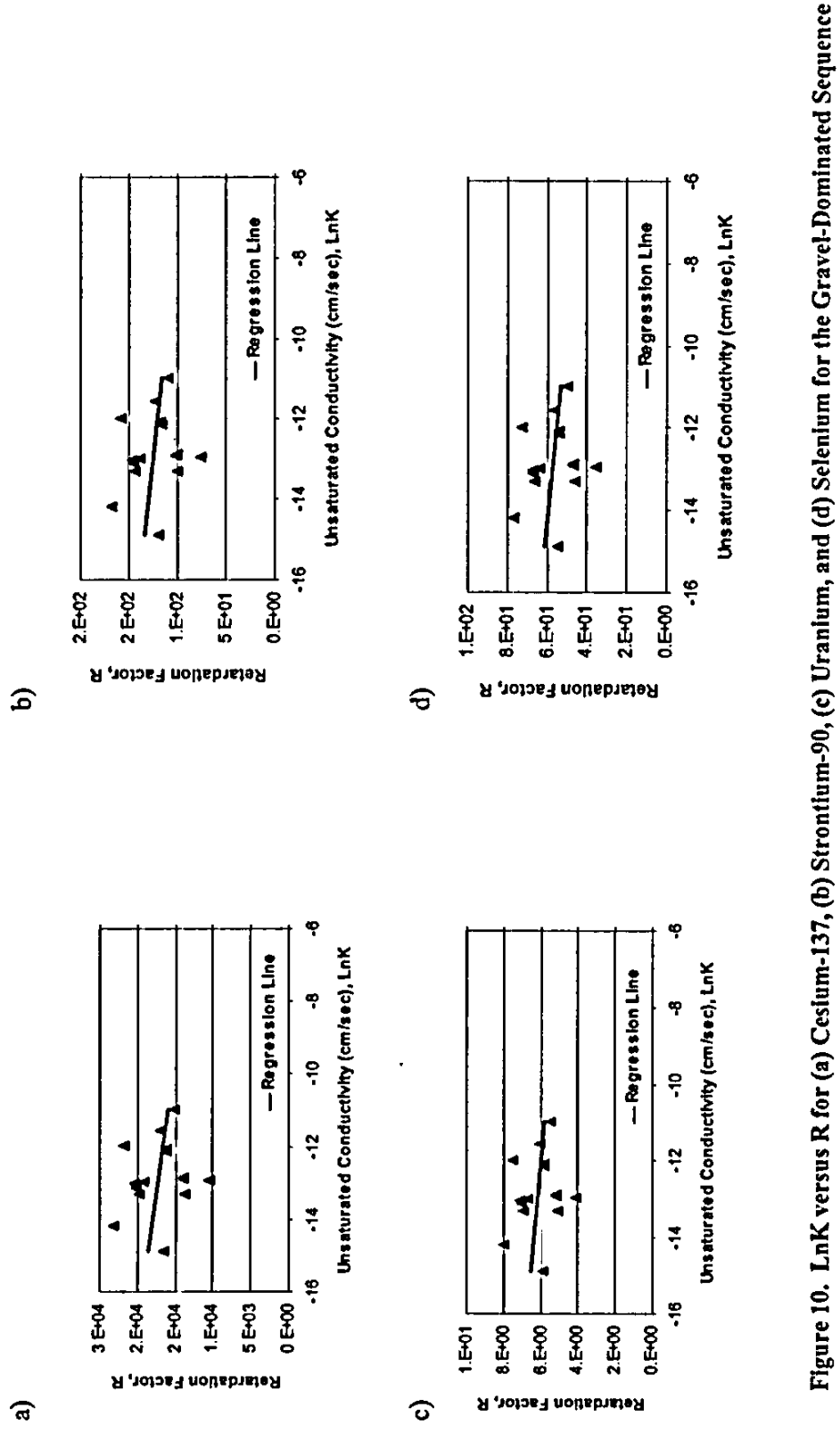

Figure 10. LnK versus R for (a) Cesium-137, (b) Strontium-90, (c) Uranium, and (d) Selenium for the Gravel-Dominated Sequence

4.0 UNCERTAINTIES IN MODEL PREDICTIONS

As discussed in the preceding sections, the application of stochastic theory resulted in effective (upscaled) parameter estimates for saturated hydraulic conductivity, soil moisture retention and unsaturated hydraulic conductivity, bulk density, unretarded macrodispersivity and sorption-enhanced macrodispersivity. These parameters serve as input to VAM3DF (Huyakorn and Panday 1995), a variably saturated flow and transport code; VAM3DF will generate 'mean' solutions for the pressure head and contaminant concentration.

The breakthrough curve due to vitrified tank waste contaminants released from the disposal facility is expected to appear as a "step" function at the water table, with the shape of the rise of the step function primarily governed by vadose zone heterogeneity, macrodispersivity, sorption, and radionuclide decay. Because of the long release time for the contaminants from the disposal facility, compared to the travel time through the vadose zone, it is reasonable to approximate the contaminant release as a step input function. Note that in addition to the step function release, other release mechanisms such as pulse release and diffusional release can also be addressed as part of the uncertainty analysis.

Three sources contribute to uncertainty calculations: (a) variations in model configurations, (b) uncertainties *in* the calculated mean concentration distribution at the water table, and (c) uncertainties *around* the calculated mean concentration distribution at the water table. Figure 11 illustrates the expected concentration distribution at the water table. The sigmoid-shaped mean concentration distribution (Figure 11) is calculated by VAM3DF, based on a particular conceptual model configuration and sensitivities to effective input parameters. However, the mean solution should be viewed as being an average of many 'realizations'. In other words, the expected peak concentration is not necessarily the calculated mean concentration (Figure 11). There is variation among different realizations, because of vadose zone heterogeneities, for example. The variance (σ_C^2) about the mean characterizes such variation *around* a particular mean solution. While the uncertainties *in* the mean solution are calculated directly by VAM3DF, uncertainties *around* the calculated mean solution will be estimated based on available stochastic solutions, as described later.

4.1 MODEL CONFIGURATIONS

4.1.1 Variations in Stratigraphy

At this time, a basic layered geologic model is being postulated for VAM3DF base case calculations. Such a model is based on the most recent geologic information available on the stratigraphy at the IDF site (Reidel 2004). Dips and inclines (as identified in the geology data package) of the various strata will be considered as part of variations of base case model configuration. Such variations of the basic stratigraphic cross-section are part of the geology data package.

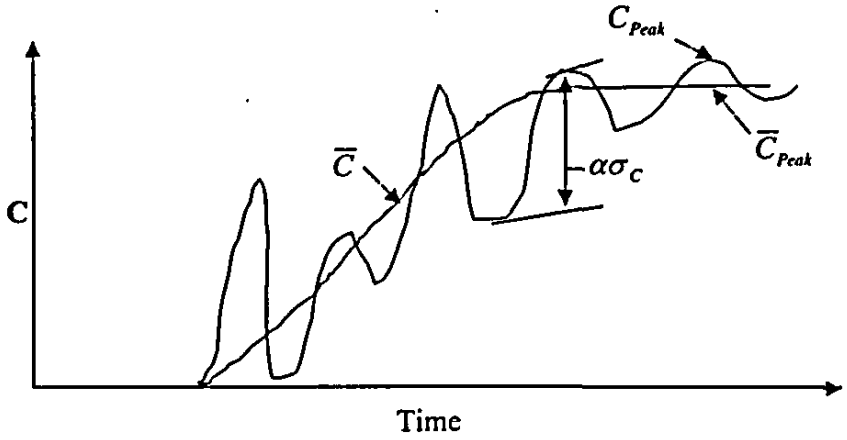

Figure 11. Schematic of Concentration (C) Distribution at the Water Table

[$\overline{C}$=calculated mean concentration, $\overline{C}_{Peak}$=calculated mean peak concentration, C_{Peak} = peak concentration, σ_C=standard deviation of variation around the calculated mean solution, $\alpha\sigma_C$=multiple of variation around the calculated mean solution for a particular model configuration and input effective parameters.]

4.1.2 Clastic dikes

Clastic dikes are ubiquitous sedimentary structures observed in outcrops and trenches that expose the Hanford formation in the 200 Areas. Their distribution, orientation, and other important characteristics are provided in the *Field Investigation Report for Waste Management Area S-SX* (Knepp 2002). The dikes are believed to represent dewatering structures that developed during compaction and settling of cataclysmic flood deposits during or soon after floodwaters drained from the Pasco Basin, approximately 13,000 years ago. The true nature and extent of clastic dikes are difficult to determine, because the dikes are rarely detected or observed in vertically oriented boreholes. Often they form a polygonal pattern where they intersect the ground surface.

An extensive atlas developed by Fecht et al. (1999) addresses a subset of dikes (i.e., clastic injection dikes) that have been formed as a result of sediments in fissures. Clastic injection dikes are fissures which may total a meter or more in thickness. These dikes are typically filled with poor to well-sorted sand, but may also contain silt, clay, and gravel. These dikes are of particular interest to the IDF PA because they occur as near-vertical planar bodies filled with multiple layers of unconsolidated sediments. Thin clay/silt linings separate the margins of most dikes and internal layers within dikes (Murray et al. 2003).

One particular scenario that will be considered to provide a bounding estimate is the presence of a near-vertical clastic dike directly below the trench and extending through the Hanford formation. The width of the dike will be based on information provided in Knepp (2002).

Data on physical and hydraulic parameters are needed for clastic dike infilling materials to model their effects on flow and contaminant transport. Such physical and hydrologic properties (e.g.,

bulk density, particle-size distribution, moisture retention, saturated and unsaturated hydraulic conductivities) for clastic dike infilling materials are included in Fayer and Ritter (1999)[2]. A summary of the physical and hydraulic parameters is given in Table 12. As suggested in Table 12, the measured properties represent fine material.

Table 12. Van Genuchten Parameters (Based on the Multistep Method), Saturated Hydraulic Conductivity, and Bulk Density for Seven Clastic Dike Samples (after Fayer and Ritter 1999)[2]

Sample	θ_s (cm^3/cm^3)	θ_r (cm^3/cm^3)	α (1/cm)	n (-)	Saturated Hydraulic Conductivity (cm/s)	Bulk Density (g/cm^3)
1	0.424	0.063	0.0839	1.33	5.97E-04	1.57
2A	0.446	0.019	0.0762	1.98	4.70E-03	1.50
2B	0.443	0.023	0.0741	1.84	3.14E-03	1.51
3A	0.424	0.025	0.0143	2.49	3.41E-03	1.46
3B	0.448	0.050	0.0593	1.54	1.14E-03	1.52
4A	0.454	0.030	0.0092	1.97	1.84E-03	1.49
4B	0.425	0.021	0.0823	2.09	5.43E-03	1.57

4.1.3 Isotropy

The base case simulations will consider a layer-cake stratigraphy and tension-dependent anisotropy. This is expected to result in more of lateral than vertical migration of contaminants. A variation of the base case will consider an isotropic case. This is expected to result in enhanced vertical migration, compared to the base case.

4.1.4 Sloped Layering

Another case that will be considered has to do with the combined effects of variation in stratigraphy and anisotropy. For unsaturated flow, the degree of anisotropy depends not only on the variability of soil hydraulic properties, but also on the orientation of the soil layers relative to the mean hydraulic gradient. The tension-dependent anisotropy relationships will be re-evaluated for dips and inclines identified (in geology data package) for variations in base case stratigraphy, and their effects examined via VAM3DF simulations.

[2] Fayer M.J. and J.S. Ritter. 1999. Physical and hydraulic measurements of FY 1998 clastic dike samples. Letter Report to Fluor Daniel Northwest, Inc. March, 1999. Pacific Northwest National Laboratory. Richland, WA.

4.2 UNCERTAINTIES IN THE MEAN SOLUTION DUE TO VARIATIONS OF EFFECTIVE PARAMETER ESTIMATES

As mentioned earlier, uncertainties in the mean solution are due to variations in conceptual model configuration and sensitivities to effective input parameters. Variations in conceptual model configuration have been discussed in the preceding section. Sensitivities to effective input parameter variations are discussed in this section.

The sensitivity of the model predictions to uncertainties in the effective parameters will be considered for two important parameters, i.e., unsaturated conductivity and macrodispersivity. Sensitivity of these two effective parameters and their estimated effects on the mean solution are discussed below. Note that variations in saturated conductivity will not be considered, since the moisture regime within the far-field vadose zone for the disposal sites is not expected to be at or near saturation. It should also be noted that recharge and variations in recharge estimates are another source of uncertainty. However, sensitivities to recharge estimates will be propagated via changes in effective parameter estimates for unsaturated conductivity and macrodispersivity.

The stratigraphy at the IDF disposal site is dominated by two distinctly different sediment sequences. The upper part of the vadose zone is characterized by a sandy sequence, whereas the lower part is characterized primarily by a gravel sequence. At saturation, compared to the gravel-dominated sequence, the sand-dominated sequence is described by a smaller log-conductivity variance. However, compared to the gravel-dominated sequence, the log-unsaturated conductivity variance for the sand-dominated sequence is higher. The variations in unsaturated conductivities for both sandy and gravelly sequences were discussed in detail earlier (see Section 3.0). Variability in unsaturated conductivities leads to macroscopic anisotropy relations for the sandy and gravelly sediments that are quite different. Consequently, VAM3DF simulations incorporating variations in macroscopic anisotropy relations will produce different mean concentration distributions at the water table.

A much more important parameter that will affect mean concentration distribution, for a given model configuration, is macrodispersivity. Typically in modeling transport, the same unretarded dispersivity value is assumed for all transported (retarded and unretarded) species. VAM3DF simulations will consider, for the transported species, comparisons of enhanced longitudinal macrodispersivity with that of a nonretarded macrodispersivity. The variability in these estimates, along with professional judgment (e.g., an increase or decrease of 25% of estimated macrodispersivities), will be used to quantify uncertainties in the mean solution.

Note that each VAM3DF-calculated mean solution incorporates effects due to model configuration variations and sensitivities to effective input parameter variations. The goal will be to limit the number of VAM3DF runs. Nevertheless, once the mean solutions are obtained for various VAM3DF runs, they can be used to obtain variance estimates for the mean solutions, and therefore characterize the uncertainty in the mean solutions.

4.3 UNCERTAINTIES AROUND THE MEAN SOLUTION

As described earlier, since the effective concentration predictions represent a mean solution, fluctuations about this mean, due to heterogeneity, are another source of uncertainty. The variations in concentrations around the mean concentration can be characterized through a stochastic evaluation of the concentration variance. It will be assumed that the developed theory for the nonretarded species is applicable to the case with spatially variable sorption, provided that the enhanced macrodispersivity is used for the sorbing species. The concentration variance tends to be large in regions close to the source where concentration gradients are large. Using stochastic approaches described by Kapoor and Gelhar (1994a, b), the coefficient of variation of concentration will be estimated at the water table. Detailed equations are presented in Kapoor and Gelhar, but briefly, the concentration variance is directly proportional to the mean concentration gradient for the VAM3DF-calculated mean concentration distribution at the water table and the longitudinal macrodispersivity, and inversely proportional to the local dispersivity values.

4.4 BOUNDING ESTIMATES

Note that the cumulative effect of uncertainties is not additive. Rather, bounding scenarios will be based on combinations of various reasonable bounding case conditions. For example, a bounding scenario may be postulated as the one having isotropic material properties for both sand- and gravel-dominated sequences, high recharge, clastic dike, and minimum values of macrodispersivity. In other words, bounding estimates will be dictated by selected model configuration and effective parameter estimates that produce a higher mean concentration at the water table.

This page intentionally left blank.

5.0 REFERENCES

Bacon, D.J. and B.P. McGrail. 1997. "Source Term Analysis for Hanford Low-Activity Tank Waste Using the STORM Code: A Coupled Unsaturated Flow and Transport Model." *In Symposium on Science and Technology for Disposal of Radioactive Tank Wastes*, ed. N.J. Lombardo and W.W. Schulz. Plenum Publishing. Las Vegas, NV.

Bear, J., C. Braester and P.C. Menier. 1987. "Effective and relative permeabilities of anisotropic porous media." *Transport in Porous Media* 2: 301-316.

Dagan, G. 1984. "Solute transport in heterogeneous porous formations." *J. Fluid Mech.* 145:151-157.

Eching S.O. and J.W. Hopmans. 1993. "Optimization of hydraulic functions from transient outflow and soil water pressure data." *Soil Sci. Soc. Am. J.* 57:1167-1175.

Fayer, M.J., J. B. Sisson, W. A. Jordan, A. H. Lu, and P. R. Heller. 1993. *Subsurface Injection of Radioactive Tracers: Field Experiment for Model Validation Testing.* NUREG/CR-5996. U. S. Nuclear Regulatory Commission. Washington, D.C.

Fayer, M.J., M. Oostrom, and K. Waters-Husted. 2003. *ILAW Borehole No. 3 Multistep Test Results.* March 15, 2003 Letter Report from M.J. Fayer to F.M. Mann. Pacific Northwest National Laboratory, Richland, WA.

Fayer, M.J., A.L. Ward, J.S. Ritter, and R.E. Clayton. 1998. *Physical and Hydraulic Measurements of FY 1998 Borehole Cores.* September 10, 1998 Letter Report from M.J. Fayer to F.M. Mann. Pacific Northwest National Laboratory. Richland, WA.

Fecht, K.R., K.A. Lindsey, B.N. Bjornstad, D.G. Horton, G.V. Last, and S.P. Reidel. 1999. *Clastic Injection Dikes of the Pasco Basin and Vicinity.* BHI-01103 Rev. 0., Bechtel Hanford Inc. Richland, WA, July 1999.

Freeze, R.A. and J.A. Cherry. 1979. *Groundwater.* Prentice-Hall, Inc., Englewood Cliffs, NJ.

Garabedian, S.P., D.R. LeBlanc, L.W. Gelhar, and M.A. Celia, "Large-scale Natural-gradient Tracer Test in Sand and Gravel, Cape Cod, Massachusetts: 2, Analysis of Tracer Moments for a Nonreactive Tracer." *Water Resources Research*, 27(5), 911-924, 1991.

Gardner, W.H. 1986. "Water Content." *In Methods of Soils Analysis, Part I*, edited by A. Klute, pp. 493-544. Amer. Soc. of Agron. Madison, WI.

Gardner, W.R. 1958. "Some steady-state solutions of the unsaturated moisture flow equation with applications to evaporation from a water table." *Soil Sci.* 85:228-232.

Gelhar, L.W., M.A. Celia and D. McLaughlin. 1994. *Modeling Field Scale Unsaturated Flow and Transport Processes*. NUREG/CR-5965. Nuclear Regulatory Commission, Washington, D.C.

Gelhar, L.W., C. Welty, and K.R. Rehfeldt. 1992. "A critical review of data on field-scale dispersion in aquifers." *Water Resour. Res.* 28:1955-1974.

Gelhar, L.W. 1993. *Stochastic Subsurface Hydrology*, Prentice Hall, New York.

Gelhar, L.W. and C.L. Axness. 1983. "Three-dimensional analysis of macrodispersion in a stratified aquifer." *Water Resour. Res.* 19:161-180.

Green, T.R. and D.L. Freyberg. 1995. "State-dependent anisotropy:comparisons of quasi-analytical solutions with stochastic results for steady gravity drainage." *Water Resour. Res.* 31:2201-2212.

Hills, R.G., P.J. Wierenga, D.B. Hudson, and M.R. Kirkland. 1991. "The second Las Cruces Trench experiment: experimental results and two-dimensional flow predictions." *Water Resour. Res.* 27:2707-2718.

Huyakorn, P.S. and S. Panday. 1995. *VAM3DF - A Variably Saturated Analysis Model in Three Dimensions for the Data Fusion System*. HydroGeoLogic, Inc. Herndon, VA.

Huyakorn, P.S. and G.F. Pinder. 1983. *Computational Methods in Subsurface Flow*. Academic Press, NY.

Kaplan, D.I., K.E. Parker and I.V. Kutynakov. 1998. *Radionuclide Distribution Coefficients for Sediments Collected from Borehole 299-E17-21*. PNNL-11966, Pacific Northwest National Laboratory, Richland, WA.

Kapoor, V. and L.W. Gelhar. 1994a. "Transport in three-dimensionally heterogeneous aquifers 1. Dynamics of concentration fluctuations." *Water Resour. Res.* 30:1775-1788.

Kapoor, V. and L.W. Gelhar. 1994b. "Transport in three-dimensionally heterogeneous aquifers 2. Predictions and observations of concentration fluctuations." *Water Resour. Res.* 30:1789-1801.

Khaleel, R. 1999. *Far-Field Hydrology Data Package for Immobilized Low-Activity Tank Waste Performance Assessment*, HNF-4769, Rev. 1, Fluor Daniel Northwest, Inc., Richland, Washington.

Khaleel, R. and J.F. Relyea. 1997. "Correcting laboratory-measured moisture retention data for gravels." *Water Resour. Res.* 33:1875-1878.

Khaleel, R., J.F. Relyea and J.L. Conca. 1995. "Evaluation of van Genuchten-Mualem relationships to estimate unsaturated conductivity at low water contents." *Water Resour. Res.* 31:2659-2668.

Khaleel, R. and E.J. Freeman. 1995a. *Variability and Scaling of Hydraulic Properties for 200 Area Soils, Hanford Site.* WHC-EP-0883, Westinghouse Hanford Company, Richland, Washington.

Khaleel, R. and E.J. Freeman. 1995b. *A Compilation of Hydrologic Properties for Low-Level Tank Waste Disposal Facility Performance Assessment.* WHC-SD-WM-RPT-165, Rev. 0, Westinghouse Hanford Company, Richland, Washington.

Khaleel, R., T.-C.J. Yeh, and Z. Lu, 2002a, "Upscaled flow and transport properties for heterogeneous unsaturated media." *Water Resources Research*, Vol. 38, No. 5, 10.1029/2000WR000072.

Khaleel, R., and P.R. Heller, "On the hydraulic properties of coarse-textured sediments at intermediate water contents." *Water Resour. Res., 39*(9), 1233, doi:10.1029/2003WR002387, 2003.

Khaleel, R. and J.F. Relyea. 2001. "Variability of Gardner's α for coarse-textured sediments." *Water Resour. Res.* 37(6):1567-1575.

Kincaid, C.T., J.W. Shade, G.A. Whyatt, M.G. Piepho, K. Rhoads, J.A. Voogd, J.H. Westsik, Jr., M. D. Freshley, K. A. Blanchard, B. G. Lauzon. 1995. *Performance Assessment of Grouted Double-Shell Tank Waste Disposal at Hanford*, WHC-SD-WM-EE-004, Rev. 1, Westinghouse Hanford Company, Richland, WA.

Knepp, A.J. 2002. *Field Investigation Report for Waste Management Area S-SX*, RPP-7884, Rev. 0, CH2M HILL Hanford Group, Inc., Richland, Washington.

Klute, A. 1986. "Water Retention: Laboratory Methods." *In Methods of Soils Analysis, Part I,* edited by A. Klute, pp. 635-660. Amer. Soc. of Agron. Madison, WI.

Klute, A. and C. Dirksen. 1986. "Hydraulic Conductivity and Diffusivity: Laboratory methods." *In Methods of Soils Analysis, Part I,* edited by A. Klute, pp. 687-734. Amer. Soc. of Agron. Madison, WI.

Kool, J.B, J.C. Parker, and M.T. van Genuchten. 1985a. "Determining soil hydraulic properties from one-step outflow experiments by parameter estimation, I, Theory and numerical studies." *Soil Sci. Soc. Am. J.* 49:1348-1354.

Kool, J.B., J.C. Parker, and M.T. van Genuchten. 1985b. "Determining soil hydraulic properties from one-step outflow experiments by parameter estimation, II, Experimental studies." *Soil Sci. Soc. Am. J.* 49:1354-1359.

Mann, F.M., R.P. Puigh, II, P.D. Rittmann, N.W. Kline, J.A. Voogd, Y. Chen, C.R. Eiholzer, C.T. Kincaid, B.P. McGrail, A.H. Lu, G.F. Williamson, N.R. Brown and. P.E. LaMont. 1998. *Hanford Immobilized Low-Activity Tank Waste Performance Assessment.* DOE/RL-97-69, Rev.0, U.S. Department of Energy, Richland, WA.

Mantoglou, A. and L.W. Gelhar. 1987. "Stochastic modeling of large-scale transient unsaturated flow." *Water Resour. Res.* 23:37-46. .

Mantoglou, A. and L.W. Gelhar. 1985. "Large scale models of transient unsaturated flow and contaminant transport using stochastic methods." Ralph M. Parsons Laboratory Tech. Rpt. 299. Massachusetts Institute of Technology, Cambridge, MA.

McCord, J.T., D.B. Stephens and J.L. Wilson. 1991. "Hysteresis and state-dependent anisotropy in modelling unsaturated hillslope hydrologic processes." *Water Resour. Res.* 27:1501-1518.

McGrail, B.P., W.L. Ebert, D.H. Bacon, and D.M. Strachan. 1998. *A Strategy to Conduct an Analysis of the Long-Term Performance of Low-Activity Waste Glass in a Shallow Subsurface Disposal System at Hanford.* PNNL-11834, Pacific Northwest National Laboratory, Richland, WA.

Millington, R.J. and J.P. Quirk. 1961. "Permeability of Porous Solids." *Trans. Faraday Soc.* 57:1200-1207.

Mualem, Y. 1984. "Anisotropy of unsaturated soils." *Soil Sci. Soc. Am. J.* 48:505-509.

Mualem, Y. 1976. "A new model for predicting the hydraulic conductivity of unsaturated porous media." *Water Resour. Res.* 12:513-522.

Murray, C.J., A.L. Ward, and J.L. Wilson, III. 2003. *Influence of Clastic Dikes on Vertical Migration of Contaminants in the Vadose Zone at Hanford.* PNNL-14224, Pacific Northwest National Laboratory, Richland, WA.

Oostrom, M., K. Waters-Husted, J.S. Ritter, and M.J. Fayer. 2002. *Physical and Hydraulic Measurements of ILAW Borehole No. 2 Well 299-E24-21 [C3177] Cores.* March 17, 2001 Letter Report from M. J. Fayer to F. M. Mann. Pacific Northwest National Laboratory, Richland, WA.

Phillips, F., J. Mattick, T. Duval, D. Elmore, and P. Kubik. 1988. "Chlorine 36 and tritium from nuclear weapons fallout as tracers for long-term liquid and vapor movement in desert soils." *Water Resour. Res.* 24:1877-1891.

Polmann, D.J. 1990. *Application of Stochastic Methods to Transient Flow and Transport in Heterogeneous Unsaturated Soils.* Ph.D. Thesis. Massachusetts Institute of Technology, Cambridge, MA.

Reidel, S.P. 2004. *Geologic Data Package for 2005 Integrated Disposal Facility Waste Performance Assessment.* PNNL-14586, Pacific Northwest National Laboratory, Richland, WA.

Rockhold, M.L., C.J. Murray, and M.J. Fayer. 1999. "Conditional simulation and upscaling of soil hydraulic properties." In *Characterization and Measurement of the Hydraulic Properties of Unsaturated Porous Media*, Vol. 2, ed. M. Th. van Genuchten, F. J. Leij, and L. Wu, pp. 1391-1401. University of California Press, Riverside, CA.

Russo, D. 1993. "Stochastic modeling of macrodispersion for solute transport in a heterogeneous unsaturated porous formation." *Water Resour. Res.* 29:383-397.

Scanlon, B.R. 1992. "Evaluation of liquid and vapor water flow in desert soils based on chlorine 36 and tritium tracers and nonisothermal flow simulations." *Water Resour. Res.* 28:285-297.

Schaap, M. G., P.J. Shouse, and P.D. Meyer. 2003. *Laboratory Measurements of the Unsaturated Hydraulic Properties at the Vadose Zone Transport Field Study Site.* PNNL-14284, Pacific Northwest National Laboratory, Richland, WA.

Sisson, J.B. and A.H. Lu. 1984. *Field Calibration of Computer Models for Application to Buried Liquid Discharges: A Status Report.* RHO-ST-46P. Rockwell Hanford Operations, Richland, WA.

Stephens, D.B. and S. Heermann. 1988. "Dependence of anisotropy on saturation in a stratified sand." *Water Resour. Res.* 24:770-778.

Talbott, M.E. and L.W. Gelhar, *Performance Assessment of a Hypothetical Low-Level Waste Facility: Groundwater Flow and Transport Simulation*, NUREG/CR-6114 Vol. 3, U.S. Nuclear Regulatory Commission, Washington, D.C., 1994.

van Genuchten, M. Th. 1980. "A closed-form solution for predicting the conductivity of unsaturated soils." *Soil Sci. Soc. Am. J.* 44:892-898.

van Genuchten, M. Th., F.J. Leij, and S.R. Yates. 1991. *The RETC code for quantifying the hydraulic functions of unsaturated soils.* U.S. E.P.A., EPA/600/2-91/065.

Ward, A.L., R.E. Clayton, and J.S. Ritter. 1998. Determination of in situ hydraulic parameters of the upper Hanford formation. Letter Report to Fluor Daniel Northwest, Inc. December, 1998. Pacific Northwest National Laboratory. Richland, WA.

Wierenga, P.J., R.G. Hills, and D.B. Hudson. 1991. "The Las Cruces Trench site: Characterization, experimental results, and one-dimensional flow predictions." *Water Resour. Res.* 27:2695-2706.

Yeh, T.-C. J. and D.J. Harvey. 1990. "Effective unsaturated hydraulic conductivity of layered sands." *Water Resour. Res.* 26:1271-1279.

Yeh, T.-C. J., L.W. Gelhar and A.L. Gutjahr. 1985a. "Stochastic analysis of unsaturated flow in heterogeneous soils, 1. statistically isotropic media." *Water Resour. Res.* 21:447-456.

Yeh, T.-C. J., L.W. Gelhar and A.L. Gutjahr. 1985b. "Stochastic analysis of unsaturated flow in heterogeneous soils, 2. statistically anisotropic media with variable α." *Water Resour. Res.* 21:457-464.

Yeh, T.-C. J., L.W. Gelhar and A.L. Gutjahr. 1985c. "Stochastic analysis of unsaturated flow in heterogeneous media, 3. observations and applications." *Water Resour. Res.* 21:465-471.

Zhang, Z.F., A.L. Ward, and G.W. Gee. 2003. "A Tensorial Connectivity–Tortuosity Concept to Describe the Unsaturated Hydraulic Properties of Anisotropic Soils." *Vadose Zone Journal* 2(3):313-321.

Zhang. Z.F., A.L. Ward, and G.W. Gee. 2002. *Estimating Field-Scale Hydraulic Parameters of Heterogeneous Soils Using A Combination of Parameter Scaling and Inverse Methods.* PNNL-14109, Pacific Northwest National Laboratory, Richland, WA.

APPENDIX A

PHYSICAL AND HYDRAULIC MEASUREMENTS OF FY1998 BOREHOLE CORES

This page intentionally left blank.

Physical and Hydraulic Measurements of FY 1998 Borehole Cores

MJ Fayer, AL Ward, JS Ritter, and RE Clayton
10 September 1998

Introduction

Pacific Northwest National Laboratory (PNNL) assists the Lockheed Martin Hanford Company (LMHC) in designing and assessing the performance of disposal facilities for radioactive wastes stored in single and double shell tanks at the Hanford Site. The preferred method of disposing of the portion that is classified as immobilized low-activity waste (ILAW) is to vitrify the waste and place the product in a near-surface, shallow-land burial facility. The current plans are that some of the ILAW will be placed in the existing vaults (built by the former Grout Project); the majority will be placed in the ILAW Disposal Site, to be located southwest of the PUREX Plant. The LMHC project to assess the performance of these two disposal facilities is known as the Hanford ILAW Performance Assessment (PA) Activity, hereafter called the ILAW PA.

Regulatory and public acceptance of ILAW disposal at Hanford depends on demonstrating that public health and the environment are adequately protected. This goal is achieved by predicting contaminant migration from the facility and using the predictions to calculate the impacts to public health and the environment. To predict contaminant migration requires estimates of the physical and hydraulic properties of sediments within the vadose zone beneath and around the disposal facility. These properties include water retention and hydraulic conductivity of the major sediment types as well as descriptions of their spatial variability. In addition to supporting the PA, these data and parameters can be used to support remediation and closure activities at sites such as tank farms and specific retention basins that have similar geology.

As part of site characterization activity for the ILAW disposal facility, sediment samples were obtained in fiscal year 1998 via a borehole drilling and sampling program (Reidel and Reynolds 1998). A work plan was also prepared that provides details on the measurement and analysis of the hydraulic properties for the ILAW borehole sediment samples (Khaleel 1998)[1].

As part of the work plan, a PNNL task was initiated, entitled "Hydraulic Property Lab Tests for ILAW Samples." The objective of this task is to provide the measured data for various geologic formations and soil types at the disposal sites (LMHC 1997; Reidel and Reynolds 1998). These data will provide the basis for upscaling of laboratory data to field estimates (Khaleel 1998), which will be used to predict the movement of contaminants from the disposal

[1] Khaleel R, January 1998. "Work plan for measurement and analysis of hydraulic properties for clastic dikes and the ILAW Borehole No. 1 sediment samples," Fluor Daniel Northwest, Inc., P.O. Box 1050, Richland, Washington.

facility to the groundwater. The objective of this letter report is to document the physical and hydraulic properties for the first characterization borehole.

Properties

Physical and hydraulic properties are required for each of the major geologic materials identified by Reidel and Reynolds (1998), namely, the Hanford sandy sequence, the Hanford lower gravel, and the Ringold Unit E. Multiple measurements of these properties are required to give some estimate of the degree of variability within each geologic material. The properties, which are required (directly or indirectly) by the models used for the ILAW PA, are:

Particle Size Distribution. Particle size distribution (PSD) refers to the fractions of the various particle-size classes (e.g., the fraction of particles with diameters between 1 and 2 mm).

Particle Density (ρ_p). Particle density is the mass of the sediment or construction material particles per unit volume of the same sediment or material. This property is used to relate the bulk density to the porosity.

Bulk Density (ρ_b). Bulk density is the mass of oven-dry material per unit bulk volume. The unit bulk volume is the combined volume of material, water, and air prior to oven drying.

Porosity (ϕ). Porosity is the volume of voids per unit bulk volume.

Water Retention. Water retention refers to the retention of water by the sediment at various matric potentials. Mathematical functions are fit to the retention data and the resulting parameters are used directly in computer models for predicting water and contaminant movement. Numerous functions are available, but the van Genuchten function is most commonly used:

$$\theta = \theta_r + (\theta_s - \theta_r)\left[(1 + (\alpha h)^n\right]^{-m}$$

where θ_s = saturated water content (cm^3/cm^3)
θ_r = residual water content (cm^3/cm^3)
h = matric potential (-cm)
α, n, m = empirical fitting parameters (α units are 1/cm; n and m are dimensionless)

Typically, m is approximated as $m = 1 - 1/n$

Saturated Hydraulic Conductivity (K_s). Saturated hydraulic conductivity is the proportionality constant in the Darcy equation that relates the flux density to a unit potential gradient.

Unsaturated Hydraulic Conductivity [$K = f(\theta, \psi)$]. Unsaturated hydraulic conductivity is the proportionality factor in the Richards equation that relates the flux density to a unit potential gradient at a specific water content. Because the water content varies in the unsaturated zone, the unsaturated conductivity varies also.

Mathematical functions are used to represent the unsaturated conductivity data; these functions are typically estimated using the water retention functions and saturated conductivity. When measured unsaturated conductivity values are available, the conductivity and retention data can be fit to optimize both the retention and conductivity functions. Several functions are available, but the Mualem conductivity function is most commonly used (in conjunction with the van Genuchten retention function, assuming $m = 1 - 1/n$):

$$K = K_s \frac{\left\{1-(\alpha h)^{n-1}\left[1+(\alpha h)^n\right]^{-m}\right\}^{\ell}}{\left[1+(\alpha h)^n\right]^{m}}$$

The K_s value and the pore interaction term (ℓ) are the only requirements for this model. The parameter ℓ is typically assigned a value of 0.5.

Borehole Cores

The FY 1998 borehole was drilled in the spring of 1998 (Reidel et al. 1998). A total of 45 cores were collected in liners. Thirty of the 45 liners had a 8.26-cm (3.25-inch) internal diameter and came from depths between 45 and 175 ft. The remaining fifteen liners had a 9.53-cm (3.75-inch) internal diameter and came from depths between 175 and 242 ft. All of the sediment from the depth interval from 0 to 45 ft went to the tracer task for tracer-specific analyses. The decision was made that undisturbed cores from this interval were not necessary for hydraulic property measurements because these sediments will not exist in their current state once the disposal facility is built. No vadose zone cores were collected below 242 ft. because this zone was open framework gravel (i.e., gravel that supports itself with little to no finer grained material) and could not be sampled with the method used.

PNNL was requested to analyze twenty of the FY 98 borehole cores for hydraulic and physical properties. Each of the 45 liners was inspected to verify whether a 15-cm (6-inch) long undisturbed section could be obtained. Thirteen liners did not meet this requirement because they were either incompletely filled, the sediments were disturbed, or the liner material was damaged. These liners will be stored for possible future testing. Of the remaining 32 acceptable liners, twenty liners were chosen for testing by the FDNW principal investigator for the ILAW PA far-field hydrology task, in consultation with the PNNL principal investigator. These twenty liners were chosen on the basis of providing somewhat evenly spaced coverage of the sampled vadose zone. Table 1 lists the sample numbers, depths, and diameters. Figure 1 shows the location of the liners relative to the geologic cross-section derived from the borehole data.

Table 1. Liner samples analyzed for the first characterization borehole

Sample ID	Total Depth Interval ft	Internal Diameter in.	Depth Interval of Intact Core ft
B8500-07A	45.9 to 47.9	3.25	46.3 to 46.8
B8500-10A	57.8 to 59.8	3.25	58.0 to 58.5
B8500-12A	69.4 to 70.95	3.25	69.8 to 70.3
B8500-14A	80.3 to 82.8	3.25	80.8 to 81.3
B8500-15A	90.5 to 93.0	3.25	90.8 to 91.3
B8500-16A	100.5 to 103.0	3.25	102.0 to 102.5
B8500-17A	109.8 to 112.2	3.25	111.3 to 111.8
B8500-19A	121.0 to 123.5	3.25	122.6 to 123.1
B8500-20A	129.7 to 132.0	3.25	131.1 to 131.6
B8500-21A	141.5 to 144.0	3.25	141.8 to 142.3
B8500-22A	151.9 to 154.4	3.25	153.7 to 154.2
B8500-23A	160.4 to 162.9	3.25	162.1 to 162.6
B8500-24A	180.7 to 182.7	3.75	181.9 to 182.4
B8500-25A	189.7 to 191.7	3.75	190.9 to 191.4
B8500-27A	199.3 to 201.3	3.75	200.5 to 200.9
B8500-29A	209.4 to 211.4	3.75	210.6 to 211.1
B8500-31A	219.6 to 221.6	3.75	220.9 to 221.3
B8500-32A	226.1 to 228.1	3.75	227.4 to 227.9
B8500-34A	236.1 to 238.1	3.75	237.2 to 237.7
B8500-35A	239.5 to 241.5	3.75	240.7 to 241.2

Figure 1. Geologic cross section of the disposal site based on the borehole samples (after Reidel et al. 1998).

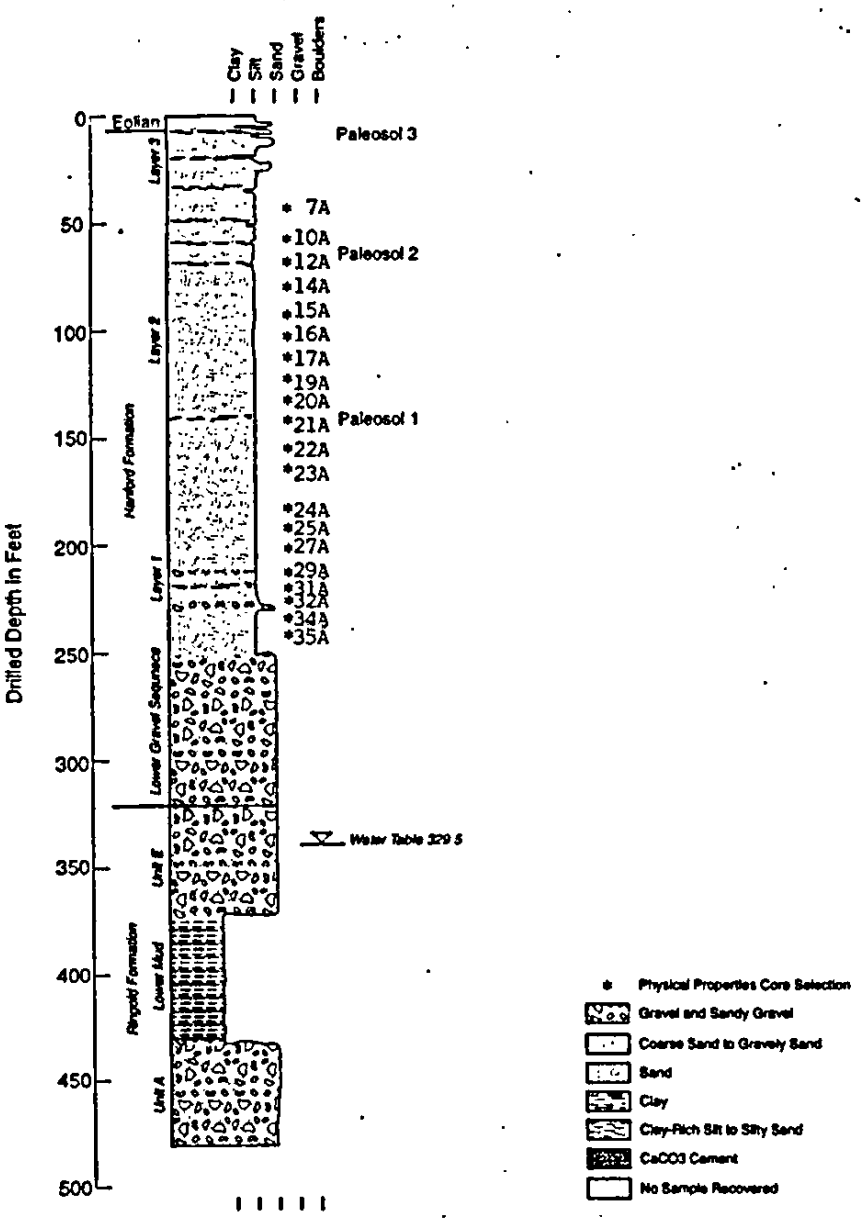

Methods

Two types of subsamples were removed from each liner. One subsample was an intact portion of the liner that retained its undisturbed nature. This intact core was used for the unsaturated conductivity tests and for determining bulk density and porosity. The depth intervals of these intact cores are listed in Table 1. A second subsample was taken from a 4 to 5 inch portion of the liner next to the intact core. This loose material, which ranged from 850 to 1200 g, was placed in a sealed bag and mixed thoroughly. It was used for the tests of particle size distribution, particle density, initial water content, and water retention using pressure plates and vapor adsorption, as well as the sorption tests that were conducted by another task under this project.

Intact Core Preparation

Each 0.6-m-long liner was inspected to identify portions that displayed no visible disturbance such as cracking or mixing. Within the undisturbed portion, a 15-cm length was chosen for the unsaturated conductivity test. The liner was marked where the base plate would go. A band saw was used to cut most of the way through the liner, then a thin metal plate was advanced into the cut as the blade proceeded around the liner for the final cut. This technique kept sediment loss to a minimum. When completely cut, the sample was placed vertically upside down and the bottom end cap was attached[2]. The sample was then placed horizontally, marked, and cut in the same manner as before. The sample was then placed vertically upright and the upper end cap was attached. The entire assembly was weighed. The total internal volume of the 3.25-in diameter cores was 803 cm^3; it was 1,069 cm^3 for the 3.75-in diameter core.

Two holes were drilled horizontally into the liner and tapped to yield threads for the tensiometer assemblies. The holes were positioned 1.5 cm from each end plate. Each tensiometer was 0.62 cm in diameter and 6.4 cm long, which allowed the tensiometers to penetrate about 75% of the core diameter. The sediment was fairly soft so each tensiometer was pushed directly into the sample without removing any material.

Two additional holes were drilled horizontally into the liners to accommodate the time-domain reflectometry (TDR) probes. The holes were offset 90 degrees laterally from the tensiometers and about 1 cm from the plane of the tensiometers and towards the core center. Because of the thinness of the liner, plexiglass blocks were glued to the outside of the liner in the TDR location to provide enough material to tap and provide threads for the TDR assemblies. The TDR rods were 0.23 cm in diameter and 8 cm long, which allowed the TDR rods to penetrate about 95% of the core diameter. Like the tensiometers, the TDR rods were pushed directly into the samples without removing material.

Figure 2 shows the final assembly with tensiometers, TDR rods, end plates, and two ports on either end plates to facility liquid and gas addition or removal from the core. Each assembly was tested at 0.5 bar positive pressure to identify leaks prior to conducting the conductivity tests.

---

[2] End caps were purchased from Soil Measurements Systems of Tucson, Arizona. Each end cap contained a rubber gasket and rubber O-ring to ensure a tight seal with the core liner.

Figure 2. Conductivity testing cell

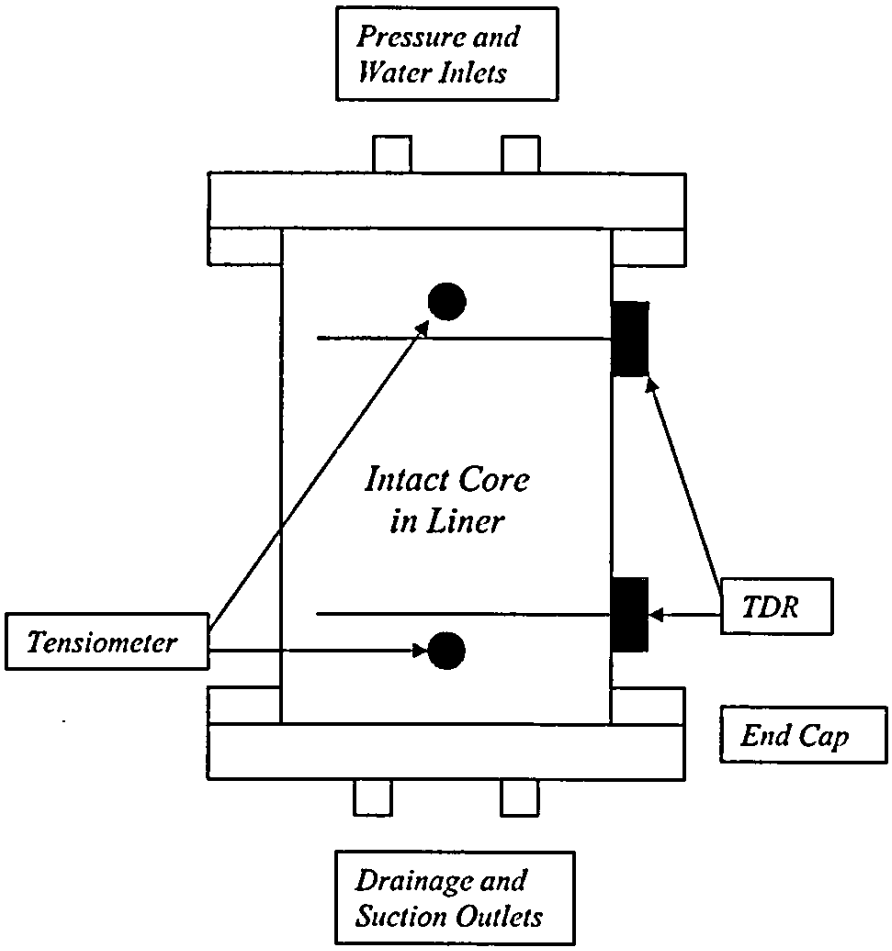

Leaks were eliminated using Teflon™ tape, vacuum grease, and Silly Putty™. After leak testing, a vacuum was applied to one of the upper ports of each assembly. The entire assembly was then wetted from below using a solution comprising tap water and 5 g thymol per 20 L of water for control of bacterial growth. Wetting in this manner placed the samples on the primary drainage path.

Procedures

Table 2 lists the procedures used to analyze the samples. Additional details for each procedure are discussed below.

Particle Density. Two replicates of the particle density test were performed using 30 g of the loose subsample for each test using the pycnometer method (Blake and Hartge 1986a).

Initial Water Content. Two replicate measurements of the initial water content were made using the loose subsample for each test using the method of Gardner (1986).

Particle Size Distribution. The PSD test was performed using 40 g of the loose subsample for each test using the methods ASTM 1985 and Gee and Bauder (1986).

Bulk Density. A single measurement of bulk density was made using the intact core. Following the conductivity test, the sediment in the core was oven dried and weighed. Dividing this weight by the volume of the core yielded the bulk density, as per the method of Blake and Hartge (1986b).

Porosity. A single estimate of porosity was made using the bulk density of intact core and the average particle density. The formula used was $\phi = 1 - \rho_b / \rho_s$ (Freeze and Cherry 1979).

Water Retention. Water retention data were obtained using the pressure-plate extraction and vapor equilibrium methods described by Klute (1986). Additional measurements were obtained during the unsaturated conductivity tests.

Saturated Hydraulic Conductivity. Saturated hydraulic conductivity was measured on the intact core prior to the unsaturated conductivity tests using the method of Klute and Dirksen (1986). The measurement of saturated conductivity was conducted several times to verify that a steady value of conductivity was achieved.

Unsaturated Hydraulic Conductivity. The multistep and steady state methods were used to measure unsaturated conductivity. Both methods were performed on the same core using the same sensor locations. The multistep method, which is an improvement of the one-step method of Kool et al. (1985 a,b), provides θ-ψ pairs and cumulative outflow. These data were used in conjunction with the MULSTP program (Eching and Hopmans 1993) to determine the optimal set of hydraulic parameters. MULSTP employs a numerical inversion procedure to find the set

---

Teflon is a trademark of E.I. du Pont de Nemours and Company, Wilmington, DE
Silly Putty is a trademark of Binney & Smith Inc., Corporation, DE

Table 2. Procedures for measuring physical and hydraulic properties.

Number	Title	Comment
PNL-MA-567, SA-2	Sieve Procedure	For materials > 50 μm effective diameter
PNL-MA-567, SA-3	Particle-Size Analysis	Hydrometer method for materials < 50 μm effective diameter
PNL-MA-567, SA-4	Constant Head Hydraulic Conductivity (HC)	Laboratory measurement for materials with HC> 10^{-6} cm/s
PNL-MA-567, SA-5	Falling Head--Saturated Hydraulic Conductivity (HC)	Laboratory measurement for materials with HC <10^{-6} cm/s
PNL-MA-567, SA-6	Water Retention Procedure	Laboratory method for core or bulk sample (saturation to air dry)
PNL-MA-567, SA-7	Water Content	Necessary for constant head hydraulic conductivity
PNL-MA-567, SA-8	Clod Density/Bulk Density	Necessary for constant head hydraulic Conductivity
PNL-MA-567, SA-9	Determining Particle Density	Necessary for constant head hydraulic conductivity
Klute (1986)	Water Retention: Laboratory Methods	Pressure plate and vapor adsorption methods
Klute and Dirksen (1986)	Hydraulic Conductivity and Diffusivity: Laboratory Methods	Steady-state flux control method for unsaturated conductivity
Eching and Hopmans (1993)	Unsaturated Hydraulic Properties	Multistep outflow method for unsaturated conductivity and water retention estimation

of parameters that minimizes the differences between simulated variables and those test variables contained in the objective function. For these tests, the objective function contained the cumulative outflow data and the matric potential data. Eching and Hopmans (1993) found that this objective function yielded excellent results when compared to independently measured data. Although this method relies on specific retention and conductivity functions and it does not yield specific values of conductivity, it promises to be quicker than the steady-state method and could represent a cost savings for future sample analyses.

The steady-state method, described by Klute and Dirksen (1986), provides θ-ψ-K triplets, which can be fitted with retention and conductivity functions. The value of this method is that it provides simultaneous triplets that are independent of retention and conductivity models. If the resulting parameter set for these functions is equivalent to the set derived by the multistep method, then the multistep method could be employed more frequently to achieve the same result.

Because several tests must be performed on the same core, the following test sequence was established: saturated conductivity, multistep unsaturated conductivity, and steady state unsaturated conductivity. Following the saturated conductivity test, the cores were re-wetted to saturation and analyzed using the multistep method. Two pressure changes were used: 0.06 and 0.3 bars. Changes in water content and matric potential were monitored with a datalogger every 0.1-h following each pressure change. Outflow was monitored manually at time intervals ranging from 3 minutes to 24 hours. The next change in pressure was initiated only after the most recent change outflow was less than 1% of the cumulative outflow since the last pressure change.

Following the multistep test, the cores were re-wetted to saturation and analyzed using the steady-state method. A Mariotte-type reservoir was used to provide a source of water at a pre-defined matric potential at the upper surface of the samples. Fluxes into each sample were unique and dependent on the unsaturated conductivity of the sample at the imposed matric potential. Concurrent with establishing the matric potential at the top of the sample, the matric potential at the bottom of the sample was set to the same value by lowering the outflow tube. Water content and matric potential were measured continuously. Once the matric potential values within the sample ceased changing, indicating steady flow conditions had been achieved, the matric potential at the top of the sample was lowered to the next value and the outflow tube was lowered a similar amount. After equilibrating with the final and lowest potential, the cores were opened and the bulk density values were determined.

Results

Table 3 shows that particle density varies between 2.71 and 2.82 g/cm^3 for this section of the Hanford formation. The average and median values are both 2.74 g/cm^3, which would indicate a normal distribution. However, the two deepest values are the highest. These two samples, as shown below, have a higher gravel content. Subsequent tests could be used to determine whether the gravel has a particle density that is higher than the finer sediment.

Table 3 also shows that the initial water contents of the loose subsample material ranged from 0.0119 to 0.0382 g/g. The average and median values were similar: 0.020 and 0.0196 g/g, respectively. These water content values are low but not atypical of the Hanford formation. They were measured two to three months after drilling and, during that interval, the liners were stored in a refrigerated container where they could have experienced some evaporative losses. However, the water content values in Table 3 are very similar to values measured by Ellyn Murphy, another ILAW project researcher. Dr. Murphy measured water contents on a small sample from the end of each core immediately after the cores were drilled. Her average water contents were about 10% less than what is shown in Table 3.

Table 4 shows the results for both the sieve and hydrometer methods. In all but two samples, the gravel content was less than 2%. In contrast, samples 34A and 35A had 13 and 25% gravel, respectively. These were the deepest samples that were analyzed (between 236 and 242 ft). As shown in Figure 1, this depth range corresponds to the lower gravel sequence of the Hanford formation. Figure 3 shows all of the data combined to highlight the degree of variability in particle size distribution.

Table 5 shows that the bulk density ranged from 1.52 to 1.98 g/cm^3. The mean and median were identical: 1.70 g/cm^3. The highest densities were associated with the two samples (34A and 35A) that had significant gravel contents. Khaleel and Relyea (1997) found a similar effect from high gravel contents. Table 5 also shows the porosity data, which ranged from 0.299 to 0.444 and had nearly identical mean and median values of 0.377 and 0.374, respectively.

When opened for the bulk density measurements, most of the cores appeared homogenous. However, several cores had noticeable layering. The most dramatic layering

occurred in sample 7A, which had about 7 cm of sand in the upper part of the core and 8 cm of finer-textured sand in the lower part of the sample. It appeared that the upper set of sensors penetrated the coarser material and the lower set penetrated the finer material. Sample 19A had a 1-mm thick, silty-looking layer located about 1 cm from the top of the sample. Layers in two other samples were less distinct and not recorded.

Another feature that we observed when the cores were opened was the presence of a layer of finer and denser material along the walls of roughly half of the liners. We had observed this effect when we were preparing the cores, but it was more obvious when the cores were wet. One possible explanation is that the drilling technique caused migration of fines to the wall, where the heat from drilling caused water to more towards the interior of the sample, thus allowing the fines to consolidate more densely. We estimated the thickness of this zone as no more than 2 mm, which accounts for less than 5% of the sample area. Because of the small area, we expect that this phenomenon did not have a major impact on the measurements reported here, but it should be looked at more closely if another borehole is drilled for samples.

Table 6 shows the pressure plate data for four pressures. As expected, samples that were finer-textured (e.g., 31A) had higher water contents at any given pressure. The mean values at each pressure are all greater than the mean value of the initial water contents reported in Table 3. This result suggests that the *in situ* matric potential values were less than -4,080 cm (4 bar), the lowest pressure tested.

Table 7 shows that the vapor adsorption data covered a significant range of matric potential, from -4,170 cm to as dry as -1,110,000 cm. The associated water contents ranged from 0.056 to 0.0 g/g. This range of water content encompasses the initial water contents reported in Table 4.

Table 8 shows the saturated hydraulic conductivity values for the intact cores. The values range from 2.65E-4 to 1.32E-2 cm/s, with average and median values of 4.30E-3 and 2.94E-3 cm/s, respectively. The two highest values were for the two deepest cores (34A and 35A), which contained the highest gravel content.

Table 9 shows the parameter estimates determined using the MULSTP program and data from the multistep test. Parameters α and n were fitted to matric potential data, drainage data, and a single retention point using a weighting scheme to adjust the importance of each; typical weightings were 1, 1, and 1, respectively. Some samples had weightings of 0.5 and 0 for tension data; these are identified in Table 9. During parameter estimation, θ_s and saturated K were fixed at measured values; θ_r was estimated for tension value of 15,300 cm using linear interpolation between pressure plate reading of 4,080 cm and wettest vapor adsorption value that was still drier than 15,300 cm.

Figure 3 shows how the predictive model, based on MULSTP-derived parameters, simulates the experimental data for matric potential and drainage for the 20 samples. In general, the comparison is good.

Table 10 shows the θ-ψ-K triplets that were generated using the steady state method. The measurements are all at matric potentials above -40 cm. Even so, unsaturated conductivity values were 1 to 2 orders of magnitude less than the saturated values. Because the potentials were so high, the water contents were also relatively high. Water contents were much lower at the end of the multistep test.

Summary

Twenty intact cores from the FY 98 ILAW PA borehole were analyzed for physical and hydraulic properties. These data and parameters will be used to predict the movement of contaminants from the disposal facility to the groundwater. Health and environmental impacts from the contamination will be calculated and the results used to ascertain the suitability of the disposal facility to protect the public and the environment. In addition to supporting the ILAW PA, these data and parameters can be used to support remediation and closure activities at sites such as tank farms and specific retention basins that have similar geology.

The twenty cores reported here were from the geologic unit known as the Hanford formation sandy sequence. The cores showed a fairly uniform set of properties deriving from the high percentage of medium to fine sand in nearly all of the cores. The variability among the twenty cores is within the range reported by Khaleel and Freeman (1995) for the 200 Areas. What is significant and valuable is that the data reported here give a true indication of the parameters and their variability *beneath the ILAW disposal site*. These data are also significant to the ILAW analysis for other reasons. First, a complete set of physical and hydraulic properties was measured on undisturbed cores. The tests included measurements of unsaturated conductivity and water retention in dry sediments. Secondly, a set of geochemical measurements was performed on the core material. Having a complete set of physical, chemical, and hydraulic data on site-specific cores is rare and should facilitate the PA calculations and enhance their credibility.

Two zones in the borehole were finer in texture and had lower saturated conductivity values than the other zones. These zones, or layers, could impact flow and transport calculations and increase lateral spreading. The results in this report will be considered in forming the conceptual model of the site. Additional boreholes planned for FY 1999 and FY 2000 will help to verify whether these and other particular layers are continuous across the disposal site.

A unexpected feature of the ILAW borehole site was the presence of a relatively thick open-framework gravel sequence below 250 ft. No data are available at present on the physical and hydraulic properties of this sequence. However, plans are in place to collect the necessary data for the gravelly sequence as part of the ILAW site characterization via boreholes No. 2 and 3.

Regarding parameter estimation of vadose zone hydraulic properties, several issues were raised by the 1997 external peer-review panel for the ILAW PA (Mann et al. 1998). These include a) use of the standard van Genuchten-Mualem approach with the saturated conductivity as a match point, b) correction for the presence of gravel in sediments, and c) upscaling of laboratory-measured data to block scale values in numerical models. Issues (a) and (b) are being

addressed as part of the analysis and parameter estimation of hydraulic properties for the borehole samples. The upscaling issue is being addressed as part of other FY98 tasks.

Table 3. Particle density and initial water content of material adjacent to the cores

Sample	Particle Density rep 1 (g/cm^3)	Particle Density rep 2 (g/cm^3)	Average Particle Density, g/cm^3	Initial Water Content, rep 1, g/g	Initial Water Content, rep 2, g/g	Average Initial Water Content, g/g
B8500-07A	2.718	2.717	2.72	0.0157	0.0176	0.0166
B8500-10A	2.747	2.745	2.75	0.0153	0.0152	0.0152
B8500-12A	2.740	2.737	2.74	0.0164	0.0174	0.0169
B8500-14A	2.716	2.711	2.71	0.0166	0.0163	0.0165
B8500-15A	2.720	2.722	2.72	0.0119	0.0120	0.0119
B8500-16A	2.728	2.727	2.73	0.0149	0.0148	0.0149
B8500-17A	2.720	2.721	2.72	0.0285	0.0268	0.0276
B8500-19A	2.728	2.731	2.73	0.0196	0.0199	0.0197
B8500-20A	2.720	2.722	2.72	0.0194	0.0203	0.0199
B8500-21A	2.721	2.723	2.72	0.0228	0.0213	0.0220
B8500-22A	2.751	2.750	2.75	0.0139	0.0146	0.0142
B8500-23A	2.731	2.736	2.73	0.0163	0.0162	0.0163
B8500-24A	2.731	2.731	2.73	0.0258	0.0236	0.0247
B8500-25A	2.748	2.745	2.75	0.0199	0.0197	0.0198
B8500-27A	2.747	2.745	2.75	0.0199	0.0189	0.0194
B8500-29A	2.733	2.736	2.74	0.0201	0.0204	0.0203
B8500-31A	2.756	2.750	2.75	0.0395	0.0370	0.0382
B8500-32A	2.753	2.752	2.75	0.0272	0.0275	0.0273
B8500-34A	2.793	2.797	2.80	0.0175	0.0178	0.0176
B8500-35A	2.822	2.822	2.82	0.0189	0.0217	0.0203

Table 4. Particle size distribution of material adjacent to the cores

Sample 7A		Sample 10A		Sample 12A		Sample 14A	
Particle Diameter (µm)	% Less Than Diameter	Particle Diameter (µm)	% Less Than Diameter	Particle Diameter (µm)	% Less Than Diameter	Particle Diameter (µm)	% Less Than Diameter
2000	99.8	2000	100.0	2000	99.3	2000	99.8
1000	99.3	1000	95.6	1000	93.9	1000	96.5
500	94.7	500	52.3	500	68.6	500	76.5
250	74.2	250	33.8	250	36.1	250	34.1
106	41.5	106	24.1	106	17.3	106	15.2
75	30.7	75	19.8	75	13.8	75	12.2
53	24.3	53	14.4	53	11.5	53	10.4
52.0	23.4	53.4	13.7	53.2	11.4	53.7	11.1
30.4	18.0	31.1	10.0	30.9	9.3	31.1	9.1
16.9	12.7	17.1	7.2	17.0	8.1	17.1	6.6
9.8	12.1	9.9	6.5	9.8	8.1	9.9	6.3
6.9	9.8	7.0	5.5	6.9	7.0	7.0	6.3
5.7	8.9	5.7	5.2	5.7	5.8	5.7	5.2
4.9	6.8	5.0	5.0	4.9	5.1	5.0	5.0
1.4	5.2	1.4	2.7	1.4	4.4	1.4	4.5

Sample 15A		Sample 16A		Sample 17A		Sample 19A	
Particle Diameter (µm)	% Less Than Diameter	Particle Diameter (µm)	% Less Than Diameter	Particle Diameter (µm)	% Less Than Diameter	Particle Diameter (µm)	% Less Than Diameter
2000	99.5	2000	98.5	2000	99.7	2000	100.0
1000	90.7	1000	87.5	1000	97.3	1000	99.1
500	58.6	500	56.7	500	87.9	500	95.8
250	29.7	250	29.3	250	60.8	250	73.6
106	17.9	106	18.0	106	33.5	106	33.1
75	14.9	75	15.4	75	27.0	75	21.4
53	13.0	53	13.3	53	22.0	53	15.4
53.4	12.4	53.4	15.9	52.4	19.1	52.6	15.1
31.0	10.0	31.1	12.3	30.7	13.8	30.8	10.2
17.1	7.2	17.2	9.6	16.9	11.3	16.9	8.3
9.9	6.0	10.0	7.2	9.8	8.8	9.8	6.2
7.0	4.8	7.1	6.2	7.0	7.4	7.0	4.9
5.7	4.8	5.8	6.5	5.7	6.4	5.7	4.5
5.0	4.5	5.0	5.3	5.0	5.5	4.9	4.5
1.4	4.8	1.4	2.9	1.4	5.1	1.4	3.2

Table 4. Particle size distribution of material adjacent to the cores (cont.)

Sample 20A		Sample 21A		Sample 22A		Sample 23A	
Particle Diameter (μm)	% Less Than Diameter	Particle Diameter (μm)	% Less Than Diameter	Particle Diameter (μm)	% Less Than Diameter	Particle Diameter (μm)	% Less Than Diameter
2000	99.8	2000	99.6	2000	98.4	2000	100.0
1000	98.3	1000	96.6	1000	88.2	1000	99.9
500	87.1	500	80.7	500	46.5	500	98.2
250	54.2	250	44.5	250	19.3	250	75.5
106	25.3	106	19.5	106	10.6	106	35.6
75	19.0	75	14.7	75	8.7	75	28.1
53	14.8	53	11.6	53	7.3	53	23.5
53.1	14.0	53.4	11.2	54.2	10.5	53.0	23.2
31.0	10.2	30.9	10.8	31.3	9.2	31.0	18.2
17.1	7.6	17.1	7.1	17.3	5.9	17.1	13.4
9.9	6.4	9.9	6.0	10.0	3.6	9.9	11.5
7.0	4.7	7.0	4.3	7.1	3.3	7.1	8.9
5.7	4.0	5.7	3.0	5.8	3.6	5.8	8.4
5.0	4.5	5.0	3.2	5.0	3.3	5.0	8.4
1.4	4.3	1.4	4.1	1.4	1.6	1.4	3.6

Sample 24A		Sample 25A		Sample 27A		Sample 29A	
Particle Diameter (μm)	% Less Than Diameter	Particle Diameter (μm)	% Less Than Diameter	Particle Diameter (μm)	% Less Than Diameter	Particle Diameter (μm)	% Less Than Diameter
2000	99.8	2000	99.7	2000	98.3	2000	98.8
1000	95.8	1000	96.5	1000	89.3	1000	93.7
500	75.0	500	79.5	500	58.9	500	68.5
250	37.3	250	28.6	250	18.9	250	27.8
106	17.0	106	10.1	106	8.3	106	12.5
75	13.4	75	7.5	75	6.6	75	10.1
53	11.0	53	5.9	53	5.5	53	8.9
54.2	13.2	54.2	7.8	54.1	8.4	56.3	5.9
31.5	9.7	31.4	6.4	31.4	6.4	32.7	4.5
17.3	8.5	17.2	5.4	17.2	5.7	18.0	2.6
10.0	7.9	10.0	4.2	10.0	4.4	10.4	1.6
7.1	8.2	7.1	4.7	7.1	4.7	7.4	1.4
5.8	7.3	5.8	4.7	5.8	4.9	6.1	0.5
5.0	7.3	5.0	4.0	5.0	4.9	5.3	0.3
1.4	2.9	1.4	2.6	1.4	3.7	1.5	0.1

Table 4. Particle size distribution of material adjacent to the cores (cont.)

Sample 31A		Sample 32A		Sample 34A		Sample 35A	
Particle Diameter (µm)	% Less Than Diameter	Particle Diameter (µm)	% Less Than Diameter	Particle Diameter (µm)	% Less Than Diameter	Particle Diameter (µm)	% Less Than Diameter
2000	99.8	2000	98.2	2000	87.0	2000	75.7
1000	99.4	1000	86.3	1000	54.4	1000	42.8
500	98.4	500	45.4	500	23.1	500	18.8
250	96.4	250	13.7	250	10.1	250	9.8
106	72.9	106	5.5	106	4.6	106	5.5
75	46.9	75	4.1	75	3.5	75	4.5
53	28.2	53	3.2	53	2.9	53	3.8
51.7	29.2	54.3	7.6	53.6	5.9	53.2	8.5
30.8	15.8	31.5	5.9	31.1	4.5	30.8	6.7
17.0	10.8	17.3	4.8	17.0	4.5	16.9	5.7
9.9	8.3	10.0	3.8	9.8	4.1	9.8	5.0
7.0	7.2	7.1	3.8	7.0	2.7	6.9	4.5
5.7	7.0	5.8	3.8	5.7	2.3	5.7	4.7
5.0	6.2	5.0	3.3	4.9	2.5	4.9	4.5
1.4	5.2	1.4	2.5	1.4	1.8	1.4	2.0

Table 5. Core volume, bulk density, and porosity of the cores

Sample	Core Volume (cm^3)	Bulk Density (g/cm^3)	Porosity (cm^3/cm^3)
B8500-07A	803	1.70	0.377
B8500-10A	803	1.62	0.413
B8500-12A	803	1.74	0.363
B8500-14A	803	1.58	0.416
B8500-15A	803	1.69	0.380
B8500-16A	803	1.58	0.420
B8500-17A	803	1.57	0.423
B8500-19A	803	1.52	0.444
B8500-20A	803	1.58	0.419
B8500-21A	803	1.62	0.403
B8500-22A	1,069	1.78	0.352
B8500-23A	1,069	1.72	0.371
B8500-24A	1,069	1.85	0.321
B8500-25A	1,069	1.80	0.345
B8500-27A	1,069	1.71	0.377
B8500-29A	1,069	1.76	0.359
B8500-31A	1,069	1.60	0.418
B8500-32A	1,069	1.78	0.359
B8500-34A	1,069	1.92	0.316
B8500-35A	1,069	1.98	0.299

Table 6. Water retention data from the pressure plate technique

7A		10A		12A		14A	
Matric Potential -cm	Water Content g/g	Matric Potential -cm	Water Content g/g	Matric Potential -cm	Water Content g/g	Matric Potential -cm	Water Content g/g
561	0.0503	561	0.0400	561	0.0374	561	0.0357
1020	0.0484	1020	0.0344	1020	0.0324	1020	0.0342
2040	0.0415	2040	0.0320	2040	0.0255	2040	0.0372
4080	0.0395	4080	0.0255	4080	0.0255	4080	0.0303

15A		16A		17A		19A	
Matric Potential -cm	Water Content g/g	Matric Potential -cm	Water Content g/g	Matric Potential -cm	Water Content g/g	Matric Potential -cm	Water Content g/g
561	0.0368	561	0.0403	561	0.0595	561	0.0421
1020	0.0316	1020	0.0338	1020	0.0475	1020	0.0336
2040	0.0307	2040	0.0287	2040	0.0400	2040	0.0265
4080	0.0241	4080	0.0232	4080	0.0366	4080	0.0260

Table 6. Water retention data from the pressure plate technique (cont.)

20A		21A		22A		23A	
Matric Potential -cm	Water Content g/g	Matric Potential -cm	Water Content g/g	Matric Potential -cm	Water Content g/g	Matric Potential -cm	Water Content g/g
561	0.0470	561	0.0334	561	0.0296	561	0.0669
1020	0.0378	1020	0.0284	1020	0.0223	1020	0.0525
2040	0.0351	2040	0.0257	2040	0.0209	2040	0.0421
4080	0.0281	4080	0.0234	4080	0.0191	4080	0.0342

24A		25A		27A		29A	
Matric Potential -cm	Water Content g/g	Matric Potential -cm	Water Content g/g	Matric Potential -cm	Water Content g/g	Matric Potential -cm	Water Content g/g
561	0.0425	561	0.0304	561	0.0291	561	0.0346
1020	0.0364	1020	0.0261	1020	0.0254	1020	0.0272
2040	0.0318	2040	0.0247	2040	0.0232	2040	0.0242
4080	0.0290	4080	0.0199	4080	0.0218	4080	0.0222

31A		32A		34A		35A	
Matric Potential -cm	Water Content g/g	Matric Potential -cm	Water Content g/g	Matric Potential -cm	Water Content g/g	Matric Potential -cm	Water Content g/g
561	0.0603	561	0.0357	561	0.0328	561	0.0329
1020	0.0472	1020	0.0333	1020	0.0290	1020	0.0309
2040	0.0402	2040	0.0342	2040	0.0268	2040	0.0281
4080	0.0375	4080	0.0284	4080	0.0204	4080	0.0214

Table 7. Water retention data from the vapor adsorption technique

7A		10A		12A		14A	
Matric Potential -cm	Water Content g/g	Matric Potential -cm	Water Content g/g	Matric Potential -cm	Water Content g/g	Matric Potential -cm	Water Content g/g
24145	0.0152	8781	0.0170	7396	0.0222	28908	0.0116
21945	0.0206	16766	0.0167	45690	0.0112	16298	0.0200
78701	0.0077	113305	0.0048	152030	0.0043	138301	0.0052
129149	0.0045	137994	0.0034	140282	0.0037	188749	0.0036
207546	0.0027	161833	0.0029	121521	0.0042	392007	0.0023
1075921	0.0000	1082660	0.0003	1087258	0.0006	1054326	0.0009

15A		16A		17A		19A	
Matric Potential -cm	Water Content g/g	Matric Potential -cm	Water Content g/g	Matric Potential -cm	Water Content g/g	Matric Potential -cm	Water Content g/g
10683	0.0405	32690	0.0093	7873	0.0230	4628	0.0375
22817	0.0124	39451	0.0107	33754	0.0170	4632	0.0291
364967	0.0023	182999	0.0038	203274	0.0048	238015	0.0038
168294	0.0034	188513	0.0019	221937	0.0038	186010	0.0039
1082928	0.0008	181075	0.0034	252444	0.0035	349726	0.0027
		1063482	0.0009	1070939	0.0009	1042683	0.0011

Table 7. Water retention data from the vapor adsorption technique (cont.)

20A		21A		22A		23A	
Matric Potential -cm	Water Content g/g	Matric Potential -cm	Water Content g/g	Matric Potential -cm	Water Content g/g	Matric Potential -cm	Water Content g/g
6485	0.0258	8349	0.0276	4633	0.0562	10211	0.0289
8341	0.0216	6021	0.0237	11175	0.0460	142403	0.0078
235350	0.0045	234127	0.0039	215747	0.0059	134462	0.0071
232477	0.0043	277628	0.0033	197216	0.0045	225253	0.0054
322711	0.0034	278460	0.0030	1090154	0.0015	223222	0.0048
1105338	0.0014	1092187	0.0008			1075491	0.0024

24A		25A		27A		29A	
Matric Potential -cm	Water Content g/g	Matric Potential -cm	Water Content g/g	Matric Potential -cm	Water Content g/g	Matric Potential -cm	Water Content g/g
4171	0.0392	18992	0.0140	17232	0.0206	5566	0.0268
120958	0.0118	245392	0.0064	55936	0.0148	32360	0.0156
135542	0.0112	316708	0.0061	248841	0.0099	226565	0.0068
257943	0.0088	258559	0.0051	277107	0.0083	250807	0.0068
251919	0.0078	285889	0.0052	252086	0.0085	247094	0.0059
1072363	0.0051	1062967	0.0034	1061386	0.0058	1054101	0.0037

31A		32A		34A		35A	
Matric Potential -cm	Water Content g/g	Matric Potential -cm	Water Content g/g	Matric Potential -cm	Water Content g/g	Matric Potential -cm	Water Content g/g
7894	0.0329	6033	0.0236	7432	0.0197	32783	0.0218
46384	0.0196	73280	0.0161	12568	0.0214	7432	0.0457
226164	0.0076	270140	0.0096	252391	0.0095	43717	0.0135
282406	0.0058	255850	0.0093	283862	0.0083	343812	0.0155
261127	0.0063	268249	0.0090	306591	0.0083	335749	0.0082
1047364	0.0030	1036466	0.0060	1023601	0.0047	1029646	0.0058

Table 8. Saturated hydraulic conductivity of the cores

Sample	Saturated Hydraulic Conductivity (cm/s)			Average Saturated Hydraulic Conductivity (cm/s)	Method
	Rep 1	Rep 2	Rep 3		
B8500-07A	7.81E-04	9.78E-04	1.35E-03	1.04E-03	Falling head
B8500-10A	1.96E-03	2.22E-03	4.68E-03	2.95E-03	Falling head
B8500-12A	2.27E-03	2.35E-03	1.82E-03	2.15E-03	Falling head
B8500-14A	1.47E-03	2.08E-03	2.41E-03	1.99E-03	Falling head
B8500-15A	1.50E-03	1.90E-03	2.87E-03	2.09E-03	Falling head
B8500-16A	8.37E-03	1.05E-02	9.87E-03	9.57E-03	Falling head
B8500-17A	1.88E-03	1.96E-03	2.12E-03	1.99E-03	Falling head
B8500-19A	3.74E-03	4.30E-03	4.88E-03	4.31E-03	Falling head
B8500-20A	2.24E-03	2.54E-03	2.83E-03	2.54E-03	Falling head
B8500-21A	2.84E-03	2.89E-03	3.09E-03	2.94E-03	Falling head
B8500-22A	4.89E-03	5.23E-03	5.05E-03	5.06E-03	Constant head
B8500-23A	2.57E-04	2.76E-04	2.61E-04	2.65E-04	Constant head
B8500-24A	5.88E-04	5.61E-04	5.58E-04	5.69E-04	Constant head
B8500-25A	5.37E-03	5.42E-03	5.43E-03	5.41E-03	Constant head
B8500-27A	8.22E-03	8.10E-03	8.09E-03	8.14E-03	Constant head
B8500-29A	3.77E-03	3.75E-03	3.73E-03	3.75E-03	Constant head
B8500-31A	8.49E-04	8.14E-04	8.01E-04	8.21E-04	Constant head
B8500-32A	6.68E-03	6.71E-03	6.74E-03	6.71E-03	Constant head
B8500-34A	1.32E-02	1.31E-02	1.32E-02	1.32E-02	Constant head
B8500-35A	1.07E-02	1.06E-02	1.06E-02	1.06E-02	Constant head

Table 9. Van Genuchten parameters (based on the multistep method) for 20 ILAW borehole samples from the sandy sequence. Parameters α and n were fitted to matric potential data, drainage data, and a single retention point using a weighting scheme to adjust the importance of each. The typical weightings were 1, 1, and 1, respectively. The superscript a indicates the weightings were 0.5, 1, and 1. The superscript b indicates the weightings were 0, 1, and 1. In these special cases, the matric potential weighting was reduced until the R^2 exceeded 0.6.

Sample	θ_s (cm^3/cm^3)	θ_r (cm^3/cm^3)	Fitted α (1/cm)	Fitted n (-)	R^2
7A1#	0.377	0.0404	0.0290[a]	1.825[a]	0.816
10A2#	0.413	0.0279	0.1161	1.784	0.687
12A1	0.363	0.0309	0.0650	1.755	0.621
14A1	0.416	0.0324	0.0445[b]	1.728[b]	0.966
15A1	0.380	0.0254	0.0487	1.844	0.744
16A1	0.420	0.0228	0.0682	1.710	0.862
17A2	0.423	0.0382	0.0689	1.899	0.741
19A1	0.444	0.0279	0.2010[a]	1.542[a]	0.715
20A1	0.419	0.0321	0.0305	2.081	0.942
21A1	0.403	0.0276	0.0545	1.926	0.813
22A1	0.352	0.0252	0.1078	1.585	0.879
23A1	0.371	0.0411	0.0079	1.553	0.900
24A1	0.321	0.0413	0.0130	1.684	0.983
25A2	0.345	0.0267	0.0842	2.158	0.930
27A2	0.377	0.0354	0.0830	1.532	0.884
29A1	0.359	0.0317	0.0784	1.732	0.777
31A2	0.418	0.0444	0.0058[a]	2.012[a]	0.915
32A2	0.359	0.0401	0.0931	1.703	0.826
34A2	0.316	0.0324	0.0819	2.398	0.854
35A1	0.299	0.0428	0.0897	2.160	0.945

1 and 2 following A indicate tensiometer locations near the top and bottom, respectively (Fig. 2)

Table 10. Water retention and unsaturated conductivity data for each sample during the steady state tests (nd = no data)

Sample	Matric Potential -cm	Water Content cm^3/cm^3	Unsaturated Hydraulic Conductivity cm/s
7A	-10.3	0.403	9.1E-04
7A	-13.5	0.405	9.5E-04
7A	-16.5	0.407	9.02E-4
7A	-19.9	0.406	9.0E-04
7A	-41.6	0.227	5.4E-05
10A	-6.1	0.391	1.1E-03
10A	-36.8	0.206	3.4E-05
12A	-8.5	0.336	9.7E-04
12A	-28.2	0.238	1.1E-04
12A	-29.8	0.234	1.1E-04
14A	-23.1	0.245	4.5E-05
15A	-8.8	0.392	2.2E-03
16A	-16.8	nd	2.0E-03
16A	-30.4	nd	2.9E-05
17A	-5.9	0.372	2.1E-04
17A	-23.3	0.249	6.5E-05
17A	-25.3	0.236	4.3E-06
19A	-6.4	0.422	2.3E-03
20A	-8.4	0.377	1.9E-03
21A	-20.8	0.289	6.7E-04
22A	-6.0	0.363	2.2E-03
22A	-22.8	nd	3.9E-04
22A	-25.6	nd	2.3E-04
23A	-20.2	0.374	1.6E-04
24A	-9.9	0.328	5.8E-04
24A	-25.3	nd	4.8E-04
25A	-8.8	0.326	5.1E-04
25A	-26.6	0.227	2.7E-04
27A	-12.7	0.298	2.4E-03
27A	-15.1	0.298	4.3E-04
27A	-19.7	0.285	2.9E-04
29A	-12.7	0.343	4.8E-04
29A	-14.0	0.315	1.0E-04
31A	-12.7	0.383	3.0E-04
31A	-20.3	0.369	3.0E-04
31A	-20.5	0.371	3.0E-04
31A	-28.2	0.370	2.9E-04
32A	-10.1	0.333	1.5E-03
32A	-12.3	nd	7.7E-04
34A	-6.9	0.313	6.3E-04
34A	-15.2	0.197	1.3E-04
35A	-20.3	0.278	1.9E-05

Figure 3. Comparison of predictive model, based on MULSTP-derived parameters, and observed data on matric potential (-cm) and cumulative drainage (mL) for 20 samples (No tension data were available for sample 14A1).

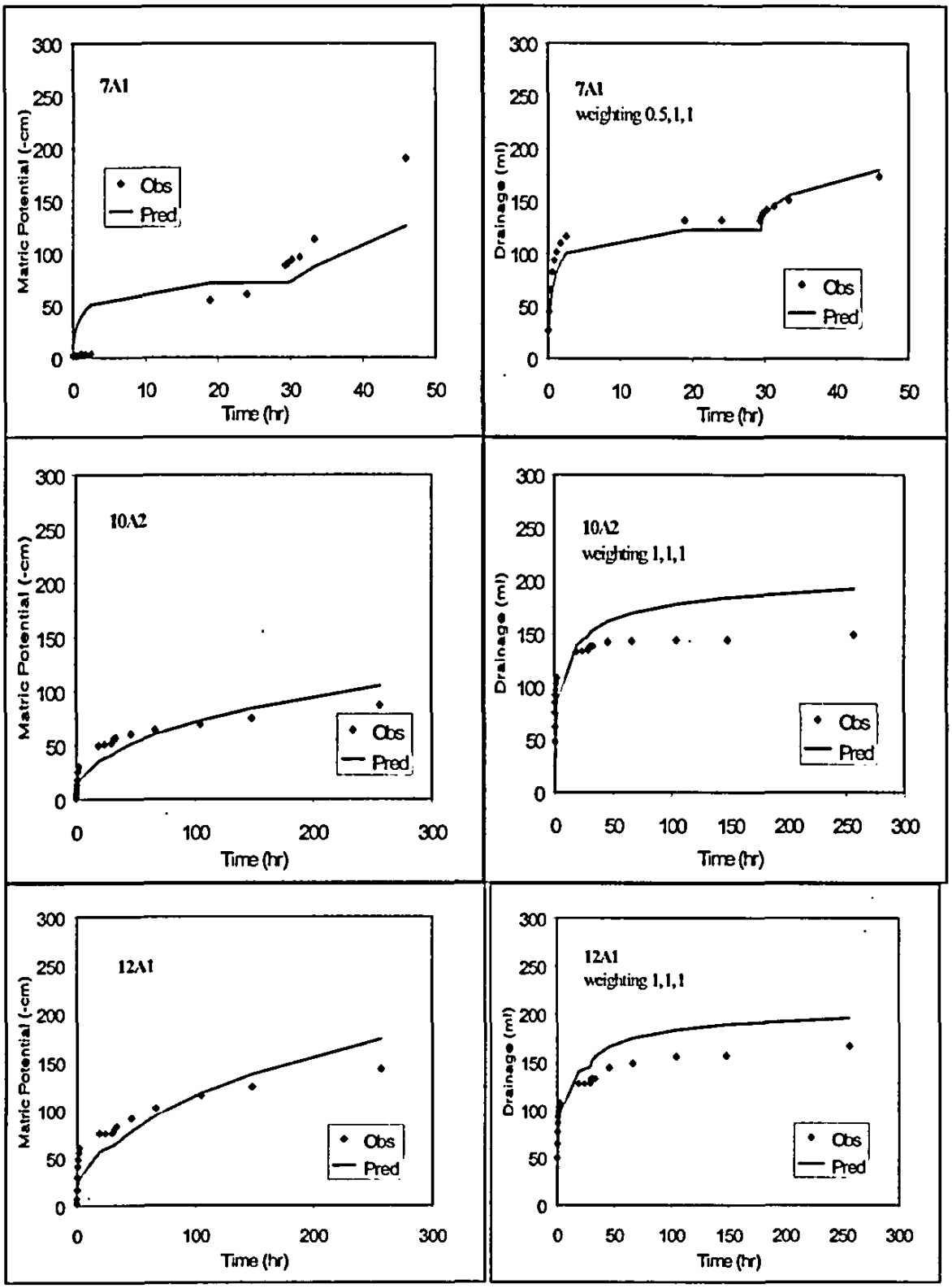

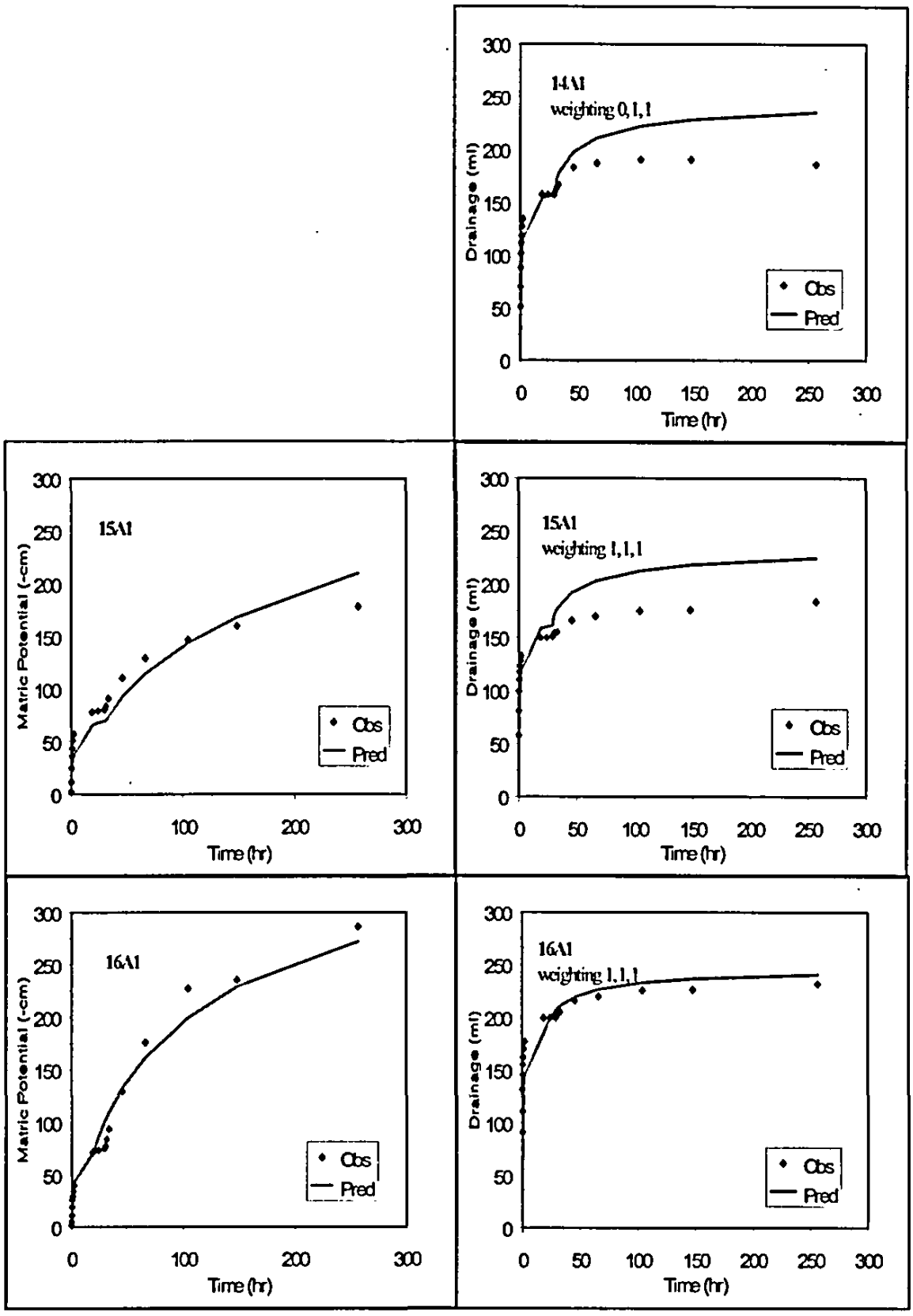
14A1
weighting 0,1,1
Drainage (ml)
Time (hr)
Obs
Pred
15A1
Matric Potential (-cm)
Time (hr)
Obs
Pred
15A1
weighting 1,1,1
Drainage (ml)
Time (hr)
Obs
Pred
16A1
Matric Potential (-cm)
Time (hr)
Obs
Pred
16A1
weighting 1,1,1
Drainage (ml)
Time (hr)
Obs
Pred

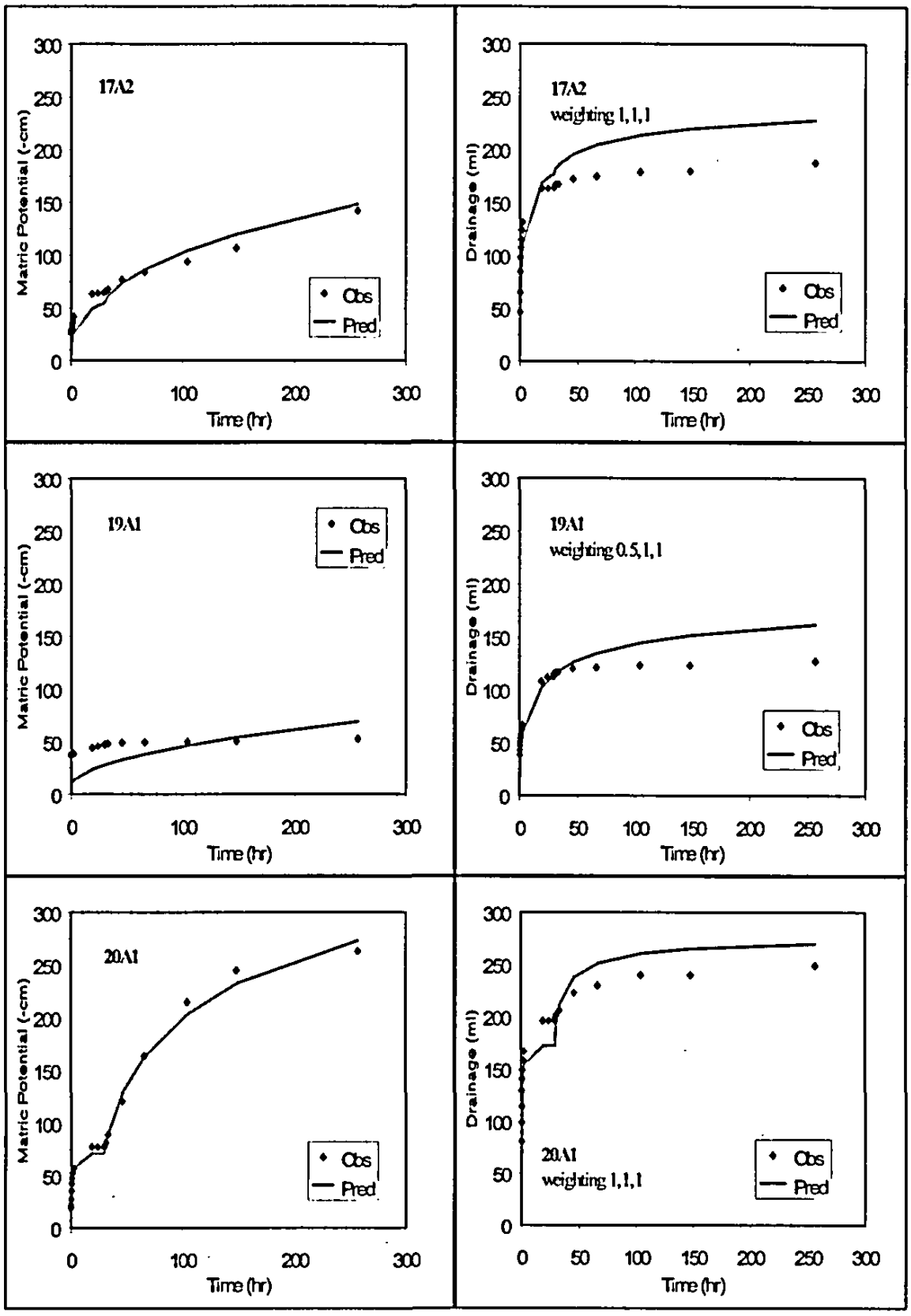
17A2
Matric Potential (-cm)
Time (hr)
Obs
Pred
17A2
weighting 1,1,1
Drainage (ml)
Time (hr)
Obs
Pred
19A1
Matric Potential (-cm)
Time (hr)
Obs
Pred
19A1
weighting 0.5,1,1
Drainage (ml)
Time (hr)
Obs
Pred
20A1
Matric Potential (-cm)
Time (hr)
Obs
Pred
20A1
weighting 1,1,1
Drainage (ml)
Time (hr)
Obs
Pred

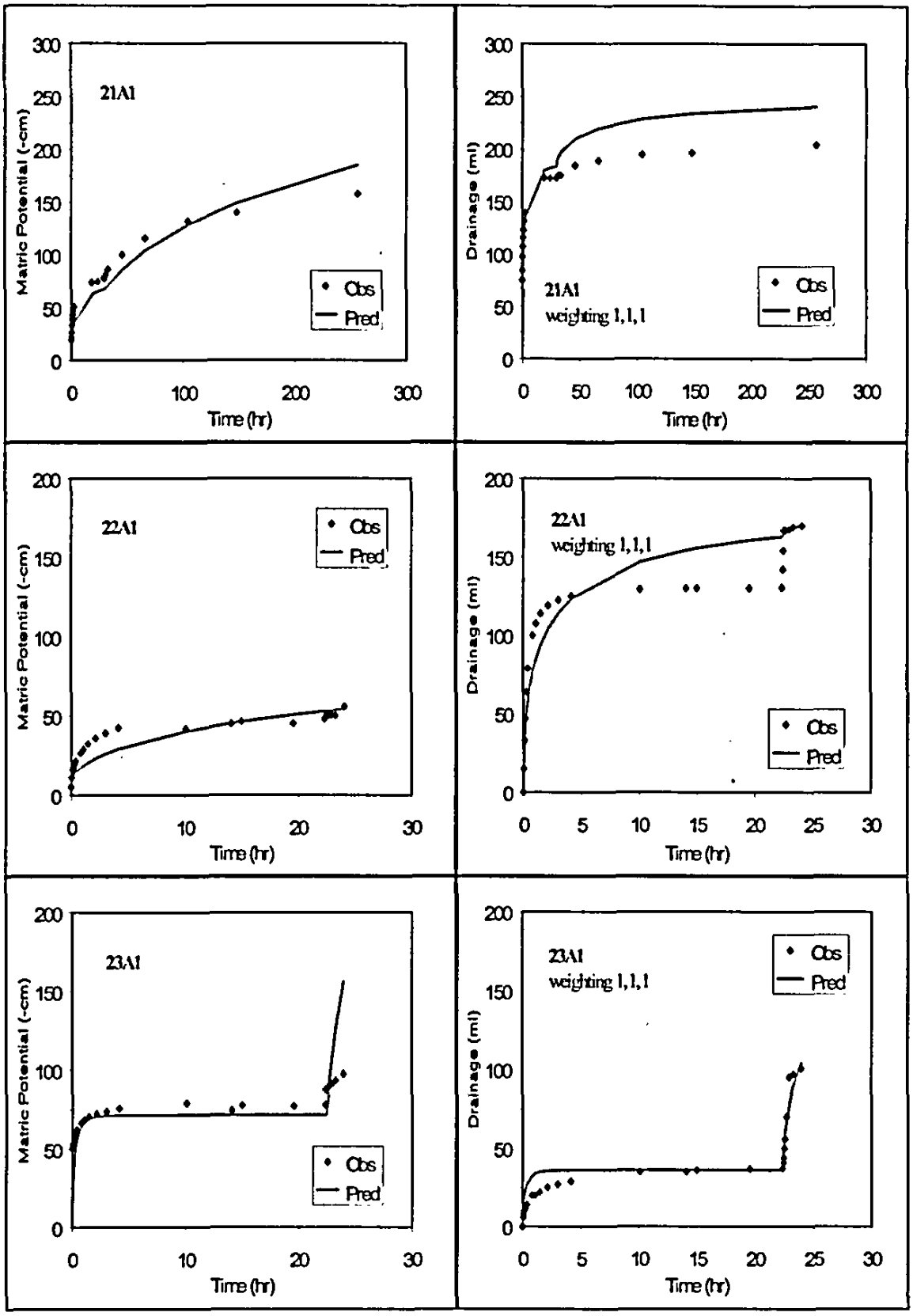
21A1
Matric Potential (-cm)
Time (hr)
Obs
Pred
21A1
weighting 1,1,1
Drainage (ml)
22A1
22A1
weighting 1,1,1
23A1
23A1
weighting 1,1,1

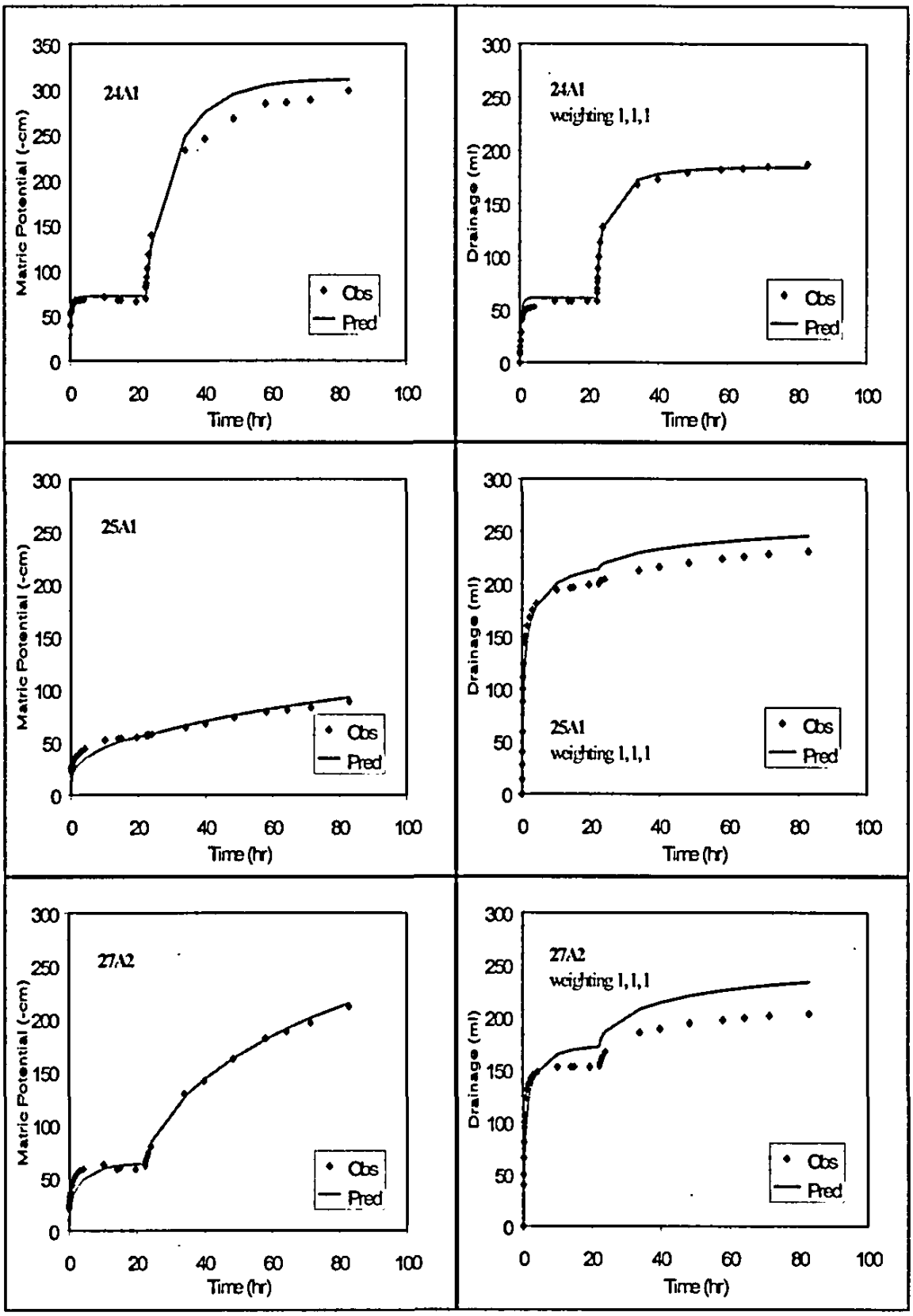
24A1
Matric Potential (-cm)
Time (hr)
Obs
Pred
24A1
weighting 1,1,1
Drainage (ml)
Time (hr)
Obs
Pred
25A1
Matric Potential (-cm)
Time (hr)
Obs
Pred
25A1
weighting 1,1,1
Drainage (ml)
Time (hr)
Obs
Pred
27A2
Matric Potential (-cm)
Time (hr)
Obs
Pred
27A2
weighting 1,1,1
Drainage (ml)
Time (hr)
Obs
Pred

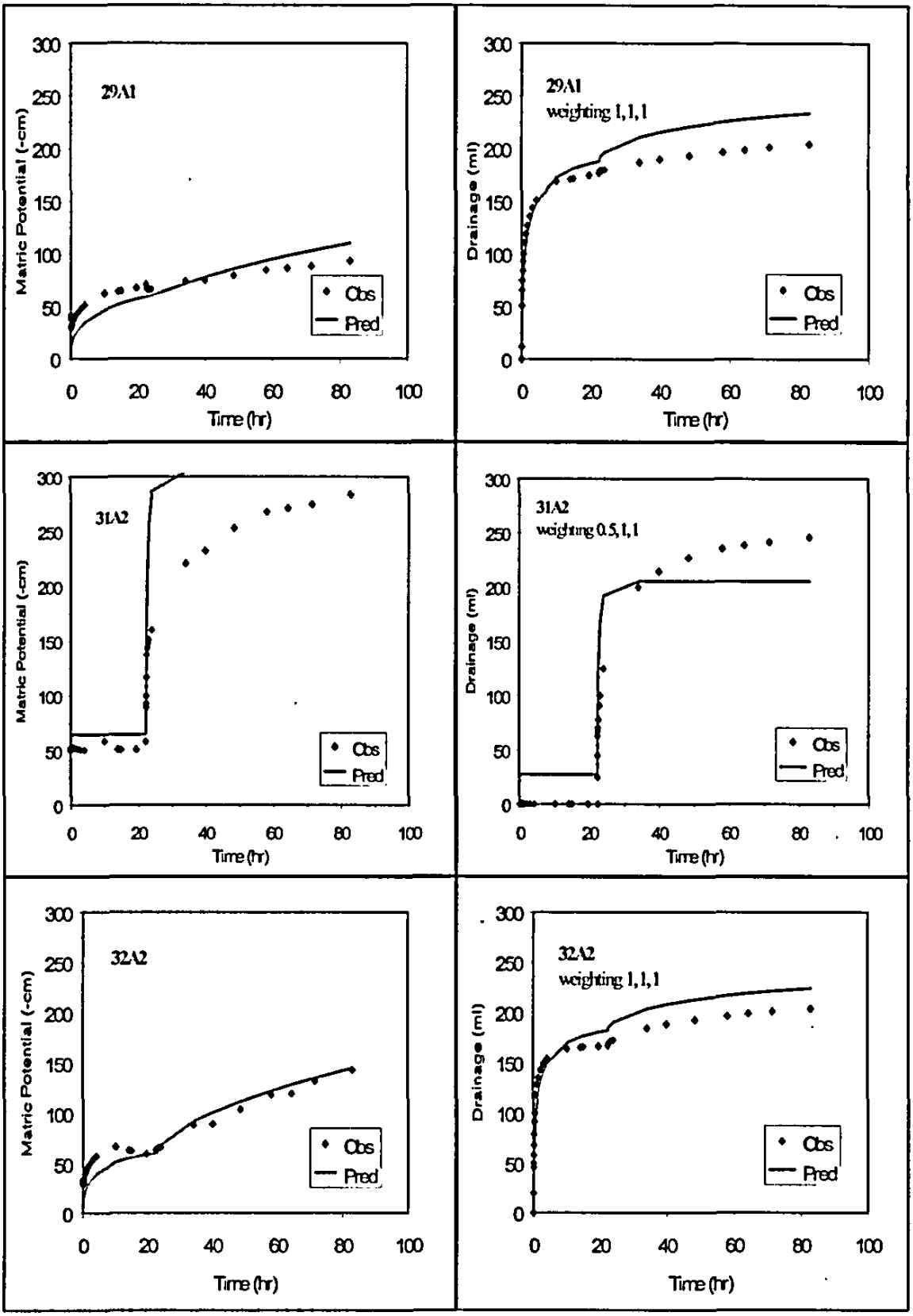
29A1
Matric Potential (-cm)
Time (hr)
Obs
Pred
29A1
weighting 1,1,1
Drainage (ml)
Time (hr)
Obs
Pred
31A2
Matric Potential (-cm)
Time (hr)
Obs
Pred
31A2
weighting 0.5,1,1
Drainage (ml)
Time (hr)
Obs
Pred
32A2
Matric Potential (-cm)
Time (hr)
Obs
Pred
32A2
weighting 1,1,1
Drainage (ml)
Time (hr)
Obs
Pred

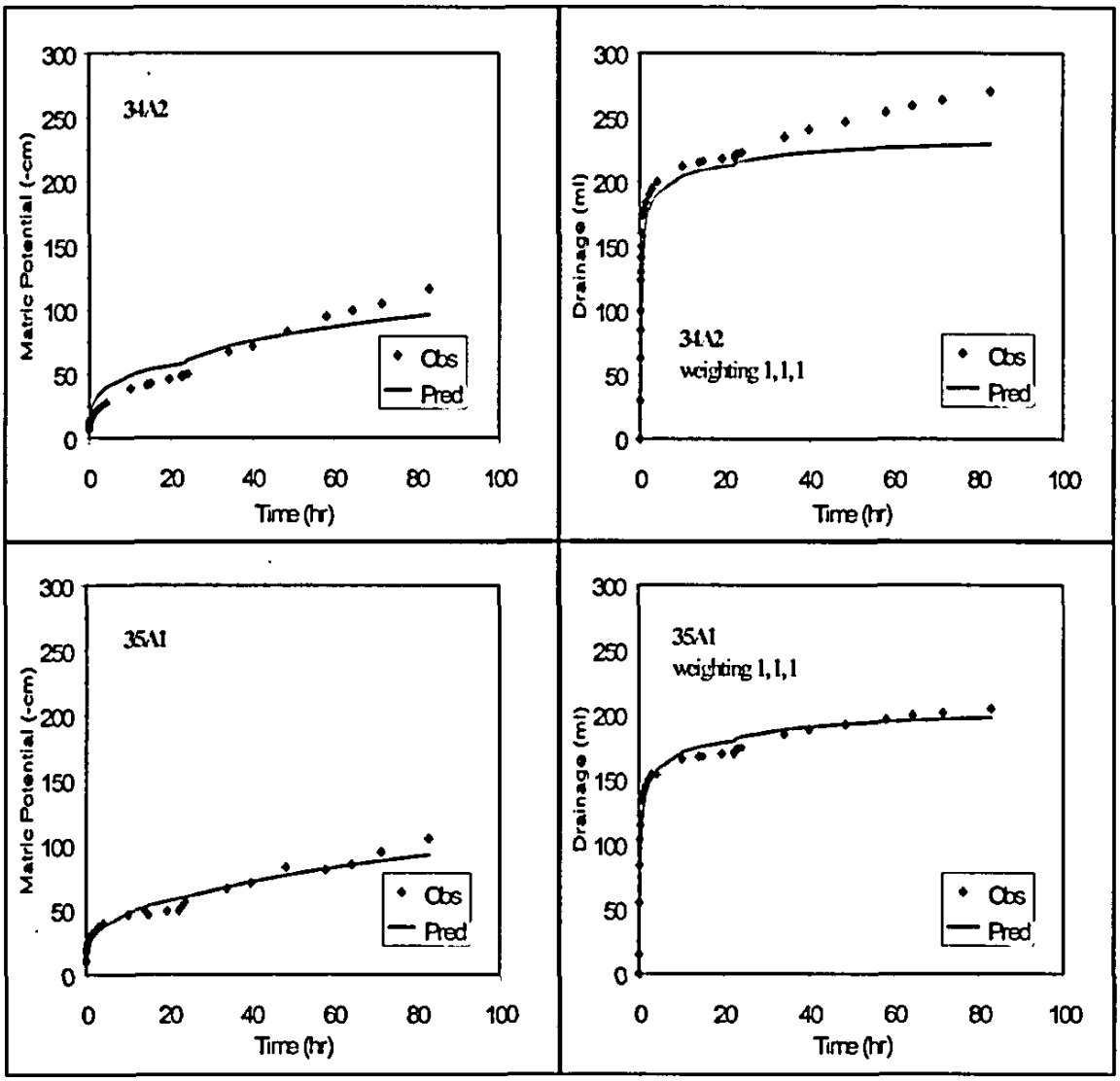
34A2
Matric Potential (-cm)
Time (hr)
Obs
Pred
34A2
weighting 1,1,1
Drainage (ml)
35A1
35A1
weighting 1,1,1

References

American Society for Testing and Materials. 1985. "Standard Test Method for Particle-size Analysis of Soils. D 422-63 (1972)." 1985 Annual Book of ASTM Standards 04.08:117- 127. American Society for Testing and Materials, PA.

Blake GR, and KH Hartge. 1986a. "Particle Density." In Methods of Soil Analysis, Part 1, ed. A. Klute, pp. 377-382. American Society of Agronomy, Madison, WI.

Blake GR, and KH Hartge. 1986b. "Bulk Density." In Methods of Soil Analysis, Part 1, ed. A. Klute, pp. 363-375. American Society of Agronomy, Madison, WI.

Eching SO, and JW Hopmans, 1993. "Optimization of hydraulic functions from transient outflow and soil water pressure data," Soil Sci. Soc. Am. J. 57:1167-1175.

Freeze RA and JA Cherry, 1979. *Groundwater*. Prentice-Hall, Inc., Englewood Cliffs, NJ.

Gardner W.H. 1986. Water Content. In Methods of Soils Analysis, Part 1,, A. Klute, ed., pp. 493-544, Am. Soc. Agron., Madison, WI.

Gee GW and JW Bauder, 1986. "Particle-Size Analysis." In Methods of Soil Analysis, Part 1, ed. A. Klute, pp. 383-409. American Society of Agronomy, Madison, WI.

Khaleel R, and EJ Freeman, 1995. "Variability and scaling of hydraulic properties for 200 Area soils, Hanford Site, WHC-EP-0883, Westinghouse Hanford Company, Richland, Washington.

Khaleel R, and JF Relyea, 1997. "Correcting laboratory-measured moisture retention data for gravels," Water Resour. Res. 33:1875-1878.

Klute A, 1986. " Water Retention: Laboratory Methods," In Methods of Soil Analysis, Part 1, ed A. Klute, pp. 635-662. American Society of Agronomy, Madison, Wisconsin.

Klute A and C Dirksen, 1986. "Hydraulic conductivity and diffusivity: Laboratory methods," In Methods of Soil Analysis, Part 1, ed A. Klute, pp. 687-734. American Society of Agronomy, Madison, Wisconsin.

Kool JB, JC Parker, and MT van Genuchten, 1985a. "Determining soil hydraulic properties from one-step outflow experiments by parameter estimation, I, Theory and numerical studies," Soil Sci. Soc. Am. J. 49:1348-1354.

Kool JB, JC Parker, and MT van Genuchten, 1985b. "Determining soil hydraulic properties from one-step outflow experiments by parameter estimation, I, Experimental studies," Soil Sci. Soc. Am. J. 49:1354-1359.

LMHC, 1997. "Statements of work for FY 1998 to 2003 for the Hanford low-level tank waste performance assessment activity," HNF-SD-WM-PAP-062, Rev. 2, Lockheed Martin Hanford Company, Richland, Washington.

Mann FM, RJ Puigh, II, PD Rittmann, NW Kline, JA Voogd, Y Chen, CR Eiholzer, CT Kincaid, BP McGrail, AH Lu, GF Williamson, NR Brown, PE LaMont, 1998. "Hanford Immobilized Low-Activity Tank Waste Performance Assessment," DOE/RL-97-69, U. S. Department of Energy, Richland, Washington.

Reidel SP, and KD Reynolds, 1998. "Characterization plan for the immobilized low-activity waste borehole," Pacific Northwest National Laboratory, Richland, Washington.

Reidel SP, KD Reynolds, and DG Horton, 1998. "Immobilized low-activity waste disposal complex borehole 299-E17-21," PNNL-11957, Pacific Northwest National Laboratory, Richland, Washington.

This page intentionally left blank.

APPENDIX B

PHYSICAL AND HYDRAULIC MEASUREMENTS OF ILAW BOREHOLE NO. 2 WELL 299-E24-21 [C3177] CORES

This page intentionally left blank.

Physical and Hydraulic Measurements of ILAW Borehole No. 2 Well 299-E24-21 [C3177] Cores

M. Oostrom, K. Waters-Husted, J.S. Ritter, M. Fayer
March 17, 2001

Introduction

Pacific Northwest National Laboratory (PNNL) supports the Immobilized Waste Program (IWP) of the Hanford Site's River Protection Project. The IWP is designing and assessing the performance of on-site disposal facilities to receive radioactive wastes that are currently stored in single and double shell tanks at the Hanford Site (Mann and Puigh 2000). To predict contaminant migration from these facilities requires estimates of the physical and hydraulic properties of sediments within the vadose zone beneath and around the disposal facility.

The site characterization activities of the IWP included a borehole drilling and sampling program in early 2001 to obtain undisturbed cores of the vadose zone sediments (Reidel 2000). A work plan was prepared that provides details on the measurement and analysis of borehole samples (Khaleel 2001). Based on the work plan, PNNL initiated a task entitled "Borehole No. 2: Hydraulic Analyses." The objective of this task is to measure and analyze the properties of the borehole samples originating from Well 299-E24-21. An overview of the location of this well at the ILAW site is shown in Fig. 1 The resulting data will be used to predict the movement of contaminants from the disposal facility to the groundwater. This letter report documents the results of the borehole measurements and analyses of 12 cores.

The cores were selected for physical and hydraulic analysis. The location of the cores within the borehole are shown in Fig. 2. The core selection with respect to target zones is shown in Table 1. The depths associated with the cores are used in this report as the sample or core names. The inside diameter of the cores was 9.9 cm.

Table 1. Core selection relation to target zones.

Target zone	Hanford Formation Description	Split Tube No.; Depth (ft)
Above the upper interface (above 55 ft)	Sand sequence, Layer 3	1 ; 47 ft 2 ; 52 ft
In the middle unit (80 and 140 ft)	Sand sequence, Layer 2	8 ; 80 ft 9 ; 85 ft 14 ; 110 ft 18 ; 130 ft 22 ; 150 ft
In the lower sand unit (180 and 230 ft)	Sand sequence, Layer 1	32 ; 200 ft 35 ; 215 ft 38 ; 230 ft
In compacted sand (241-260 ft)	Sand sequence, Layer 1	41 ; 251 ft
In deepest sands (261 to 270 ft)	Sand sequence, Layer 1	43 ; 261 ft

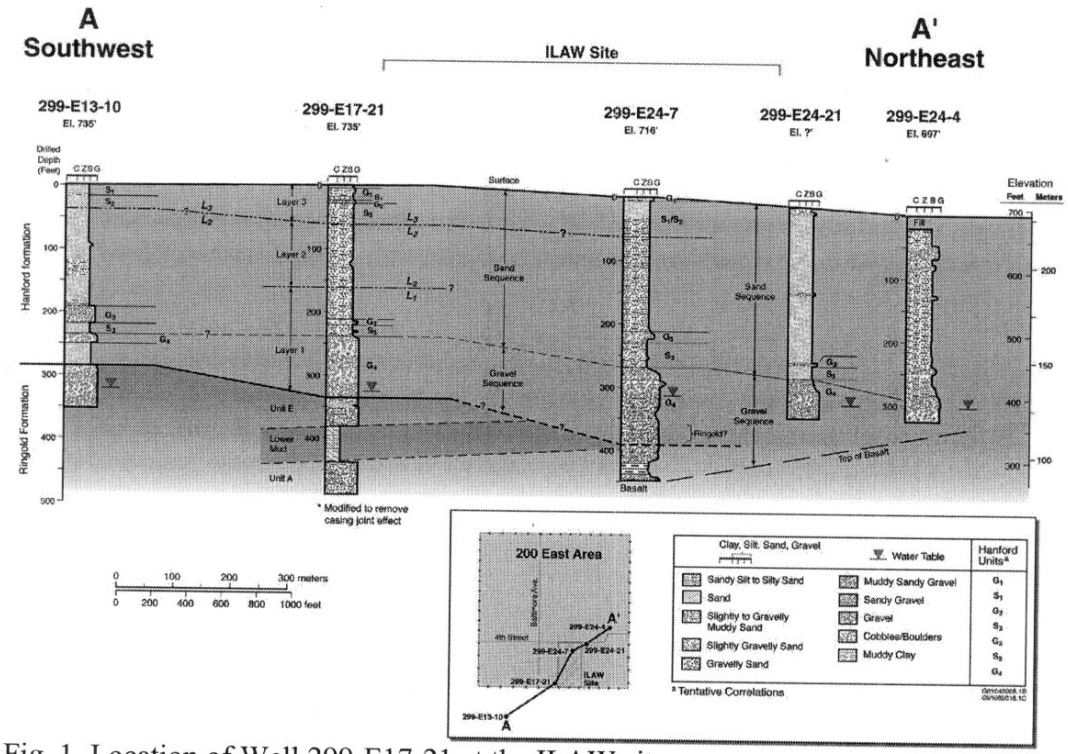

Fig. 1. Location of Well 299-E17-21 at the ILAW site.

Fig. 2. Location of cores within borehole 299-E17-21

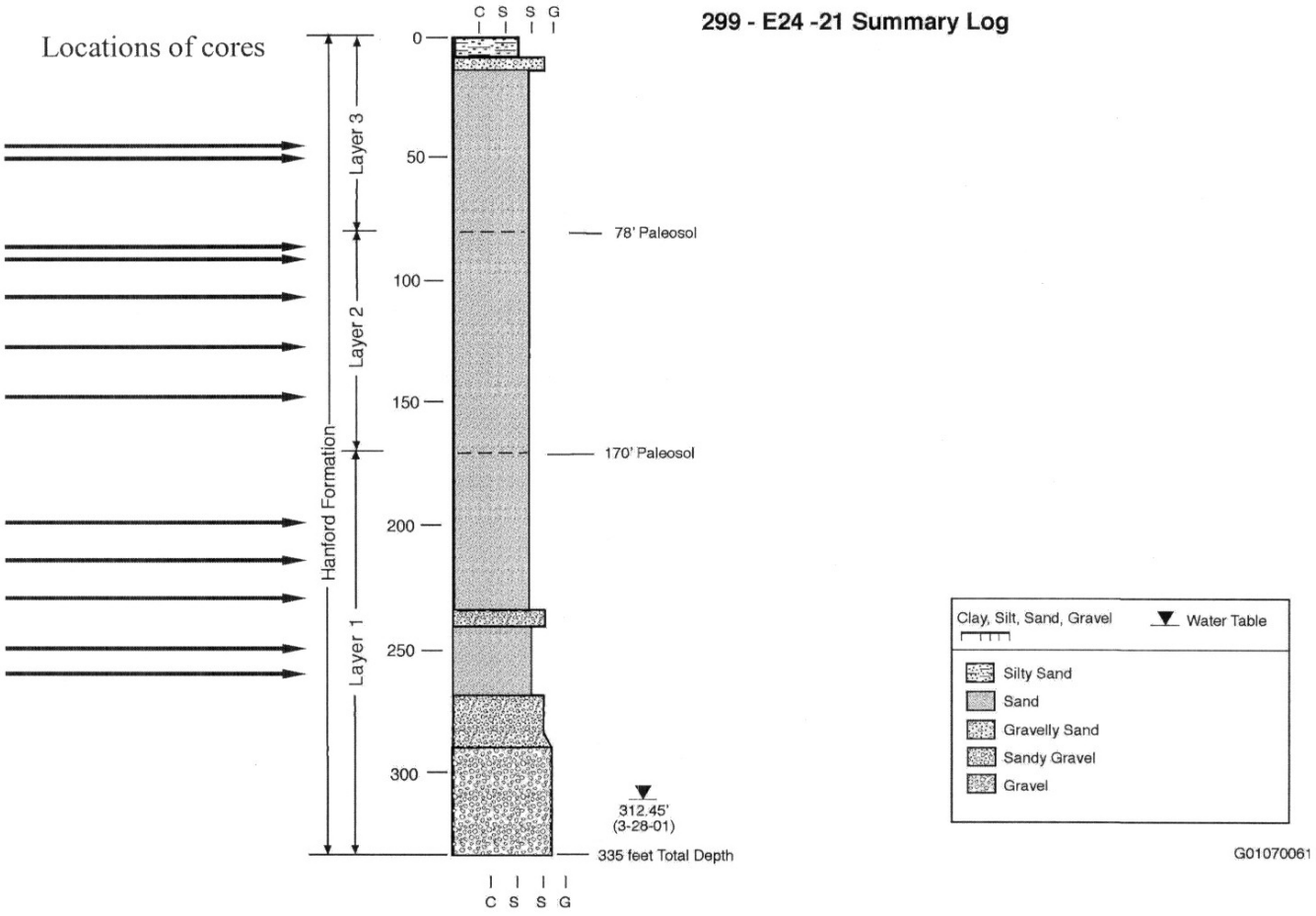

Properties

Physical and hydraulic properties are required for the ILAW samples. Multiple measurements of these properties are required to give some estimate of the degree of variability within each geologic material. The properties are:

Particle Size Distribution. Particle size distribution (PSD) refers to the fractions of the various particle-size classes (e.g., the fraction of particles with diameters between 1 and 2 mm).

Particle Density (ρ_p). Particle density is the mass of the sediment or construction material particles per unit volume of the same sediment or material. This property is used to relate the bulk density to the porosity.

Bulk Density (ρ_b). Bulk density is the mass of oven-dry material per unit bulk volume. The unit bulk volume is the combined volume of material, water, and air prior to oven drying.

Porosity (ϕ). Porosity is the volume of voids per unit bulk volume.

Water Retention. Water retention refers to the retention of water by the sediment at various matric potentials. Mathematical functions are fit to the retention data and the resulting parameters are used directly in computer models for predicting water and contaminant movement. Numerous functions are available, but the van Genuchten function is most commonly used:

$$\theta = \theta_r + (\theta_s - \theta_r)\left[(1 + (\alpha h)^n\right]^m$$

where θ_s = saturated water content (cm^3/cm^3)
θ_r = residual water content (cm^3/cm^3)
h = matric potential (-cm)
α, n, m = empirical fitting parameters (α units are 1/cm; n and m are dimensionless)

Typically, m is approximated as $m = 1 - 1/n$

Saturated Hydraulic Conductivity (K_s). Saturated hydraulic conductivity is the proportionality constant in the Darcy equation that relates the flux density to a unit potential gradient.

Unsaturated Hydraulic Conductivity [$K = f(\theta, h)$]. Unsaturated hydraulic conductivity is the proportionality factor in the Richards equation that relates the flux density to a unit potential gradient at a specific water content. Because the water content varies in the unsaturated zone, the unsaturated conductivity varies also.

Mathematical functions are used to represent the unsaturated conductivity data; these functions are typically estimated using the water retention functions and saturated conductivity. When measured unsaturated conductivity values are available, the conductivity and retention data can be fit to optimize both the retention and conductivity functions. Several functions are available, but the Mualem conductivity function is most commonly used (in conjunction with the van Genuchten retention function, assuming $m = 1 - 1/n$):

$$K = K_s \frac{\left\{ -(\alpha h)^{n-1} \left[1 + (\alpha h)^n \right]^m \right\}^2}{\left[1 + (\alpha h)^n \right]^m}$$

Methods

The core samples were tested with the multistep and steady-state methods, then sectioned for the tests of particle size distribution, particle density, and water retention using pressure plates and vapor adsorption. The cores were prepared for the multistep and steady-state tests according to the procedures described by Fayer et al. (1998)[1].

Procedures

Table 2 lists the procedures used to analyze the samples. Additional details for each procedure are discussed below. These additional details are almost exactly the same as those used by Fayer et al. In general, the cores were cut to 20-cm length and caps were applied. Two tensiometesrs were installed per core, about 3 cm from each end cap. The cores were subsequently tests for leaks using 700 mb air pressure. After the cores were saturated, the hydraulic conductivity test was completed first. After that, the multistep outflow test was performed followed by the steady-state controlled flux test. Before the controlled flux test, the cores were resaturated. After the unsaturated flow test, the core liners was sliced lengthwise on two sides and opened for visual inspection. The entire core was subsequently over dried and separated into gravel and <2 mm particles. The remaining tests were conducted on homogenized <2 mm samples.

Particle Density. Three replicates of the particle density test were performed using the pycnometer method (Blake and Hartge 1986a).

Particle Size Distribution. The PSD test was performed using the methods ASTM 1985 and Gee and Bauder (1986).

Bulk Density. A single measurement of bulk density was made for each core. Following the conductivity test, the sediment in the core was oven dried and weighed. Dividing this

[1] Fayer MJ, AL Ward, JS Ritter, and RE Clayton, 1998. "Physical and hydraulic measurements of FY 1998 borehole cores," Letter Report to Mr. Fred Mann, Fluor Daniel Northwest, September 10, 1998.

weight by the volume of the core yielded the bulk density, as per the method of Blake and Hartge (1986b).

Porosity. A single estimate of porosity was made using the bulk density of the intact cores and the average particle density. The formula used was $\phi = 1 - \rho_b / \rho_s$ (Freeze and Cherry 1979).

Water Retention. Water retention data for the samples were measured using the pressure-plate extraction and vapor equilibrium methods described by Klute (1986). The tests were conducted on the subsample created after the bulk density core was homogenized. Additional retention measurements were obtained during the unsaturated conductivity tests.

Table 2. Procedures for measuring physical and hydraulic properties.

Number	Title	Comment
PNL-MA-567, SA-2	Sieve Procedure	For materials > 50 μm effective diameter
PNL-MA-567, SA-3	Particle-Size Analysis	Hydrometer method for materials < 50 μm effective diameter
PNL-MA-567, SA-4	Constant Head Hydraulic Conductivity (HC)	Laboratory measurement for materials with HC> 10^{-6} cm/s
PNL-MA-567, SA-5	Falling Head--Saturated Hydraulic Conductivity (HC)	Laboratory measurement for materials with HC <10^{-6} cm/s
PNL-MA-567, SA-6	Water Retention Procedure	Laboratory method for core or bulk sample (saturation to air dry)
PNL-MA-567, SA-7	Water Content	Necessary for constant head hydraulic conductivity
PNL-MA-567, SA-8	Clod Density/Bulk Density	Necessary for constant head hydraulic Conductivity
PNL-MA-567, SA-9	Determining Particle Density	Necessary for constant head hydraulic conductivity
Klute (1986)	Water Retention: Laboratory Methods	Pressure plate and vapor adsorption methods
Klute and Dirksen (1986)	Hydraulic Conductivity and Diffusivity: Laboratory Methods	Steady-state flux control method for unsaturated conductivity
Eching and Hopmans (1993)	Unsaturated Hydraulic Properties	Multistep outflow method for unsaturated conductivity and water retention estimation

Saturated Hydraulic Conductivity. Saturated hydraulic conductivity for the cores was measured on the intact cores prior to the unsaturated conductivity tests using the method of Klute and Dirkson (1986). The measurement of saturated conductivity was conducted several times to verify that a steady value of conductivity was achieved.

Unsaturated Hydraulic Conductivity. The multistep and steady state methods were used to measure unsaturated conductivity of the cores. An picture of the multistep outflow method is shown in Fig.3. Pictures of the constant flux steady state tests are shown in Fig.

4a and b. Both methods were performed on the same core using the same sensor locations. The multistep method, which is an improvement of the one-step method of Kool et al. (1985 a,b), provides θ-h pairs and cumulative outflow. These data were used in conjunction with the SFOPT program (a modified version of the MULSTP program of Eching and Hopmans 1993) to determine the optimal set of hydraulic parameters. The constant flux steady state tests were performed in the Multiphase Research Laboratory in room RTL-136. The technique was developed during FY2001. Currently, 4 samples can be analyzed simultaneously.

Because several tests must be performed on the same core, the following test sequence was established: saturated conductivity, multistep unsaturated conductivity, and steady state unsaturated conductivity. Following the saturated conductivity test, the cores were re-wetted to saturation and analyzed using the multistep method. Following the multistep test, the cores were rewetted and tested using the steady-state method.

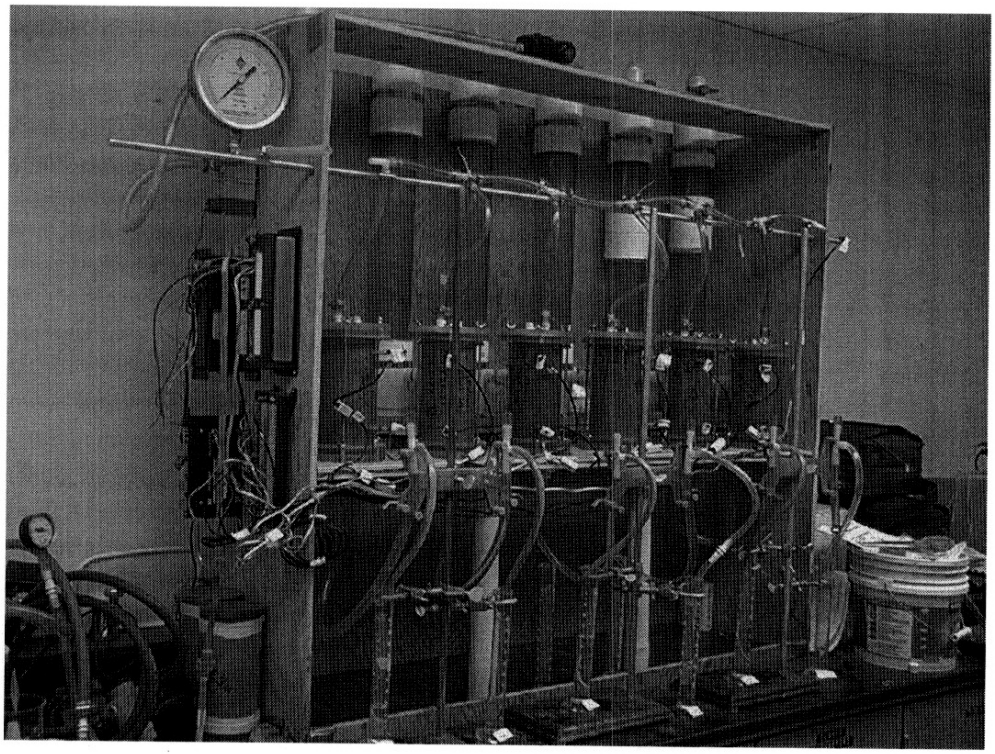

Fig. 3. Picture of the multistep outflow experimental setup.

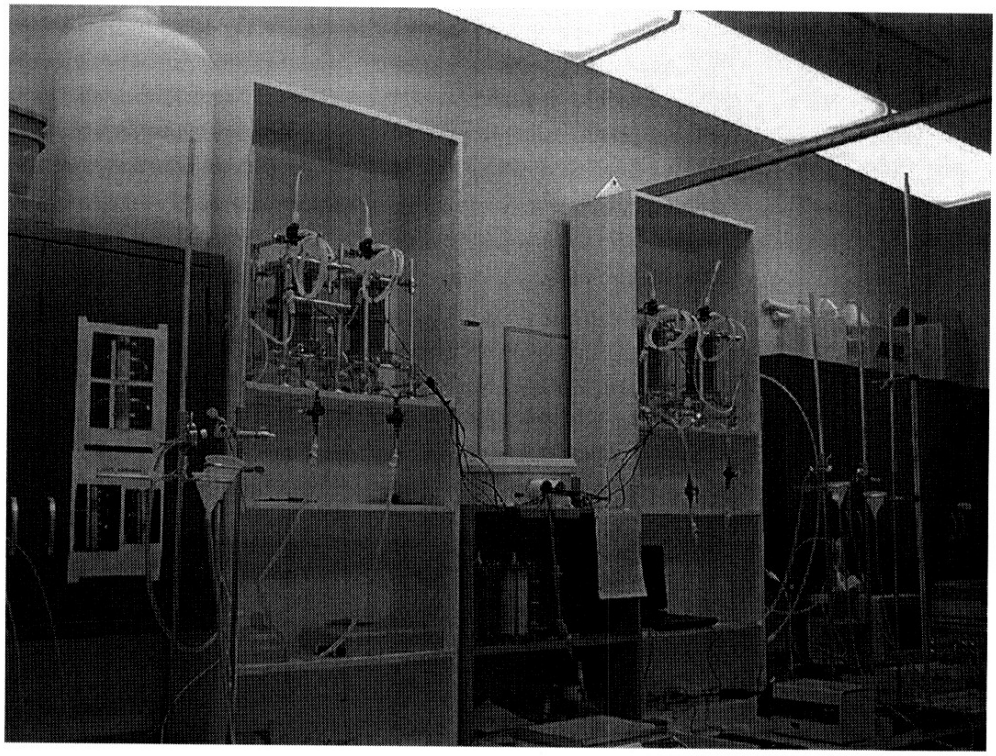

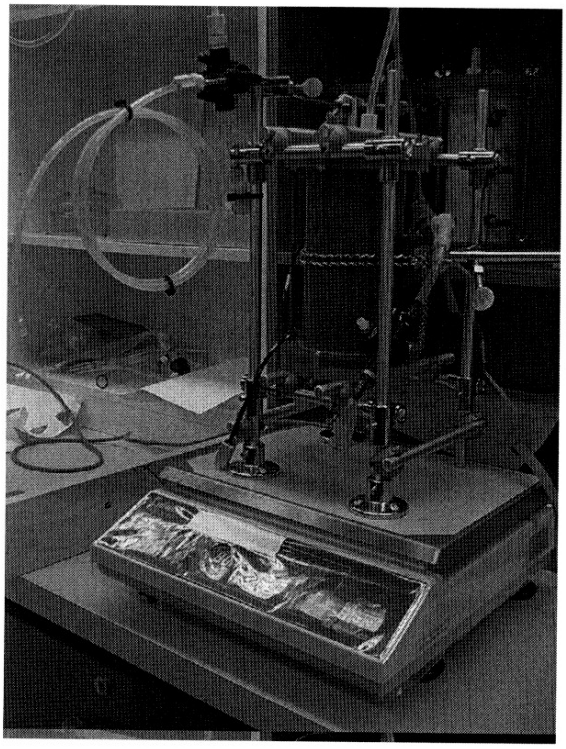

Fig. 4. Pictures of of (a) the steady-state constant flux experimental setup, and (b) method to weigh individual cores after steady-state conditions have been achieved.

Results

After completion of hydraulic conductivity and unsaturated hydraulic parameter tests, the cores were opened and inspected. All cores, expect Core 251, had a fairly homogeneous appearance. In Core 251, a.1.5 to 2 cm thick fine-grained lens was located in the upper half. In all subsequent tests, the bulk material (251a) and the fine-grained material (251b) were analyzed separately. Pictures of the 12 cores are shown in Fig 5a-l.

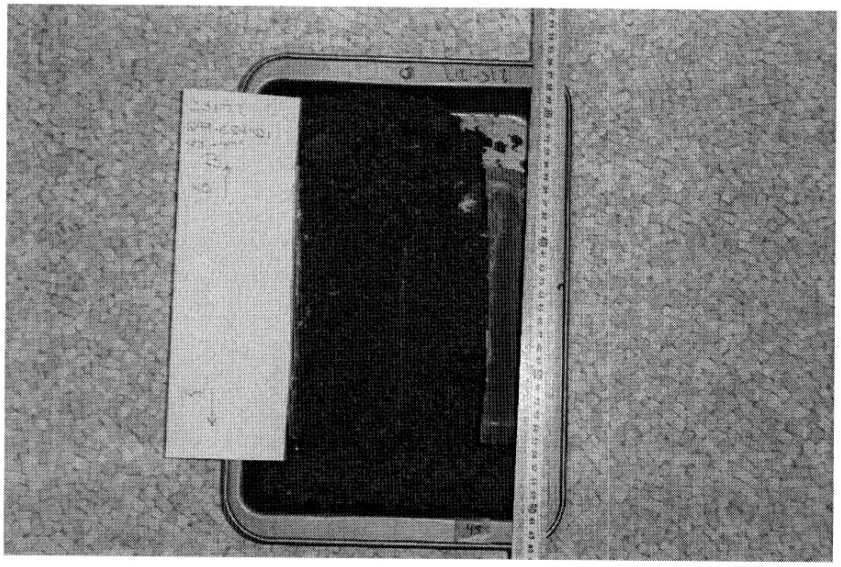

Fig. 5a. Core 45.

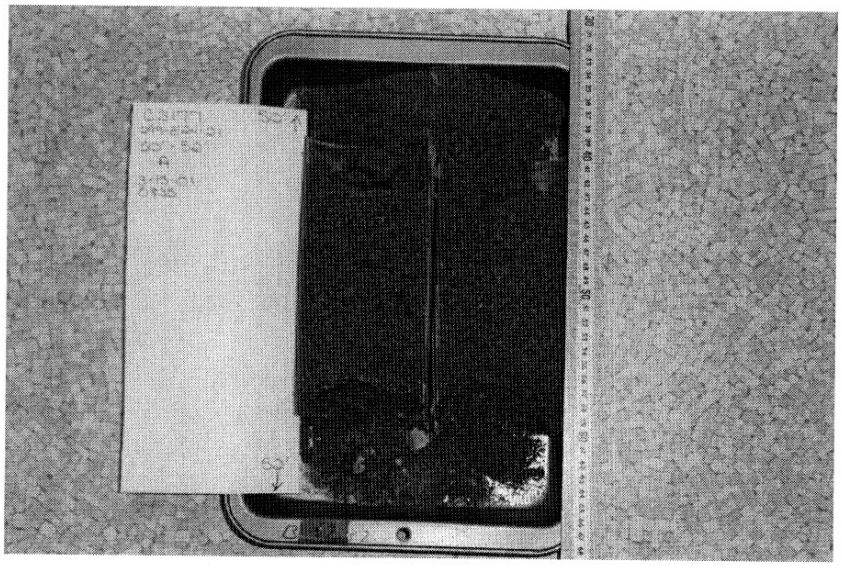

Fig. 5b. Core 52.

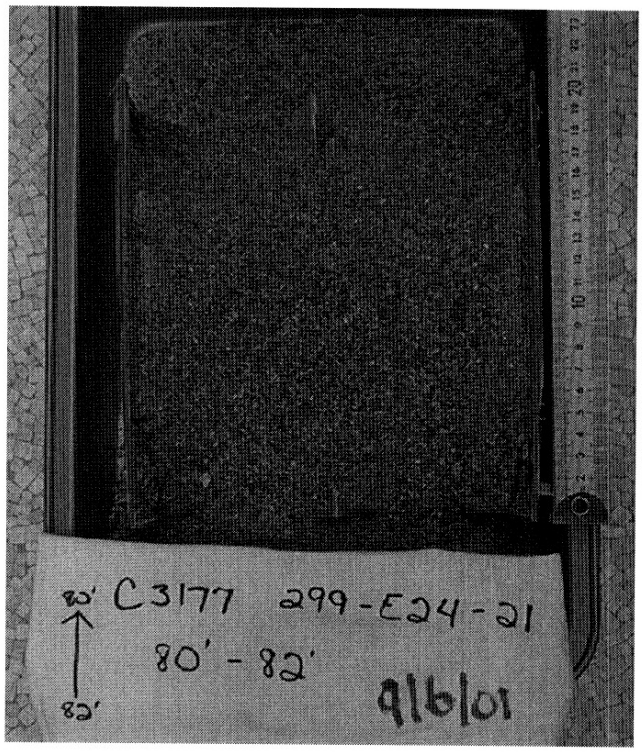

Fig. 5c. Core 80.

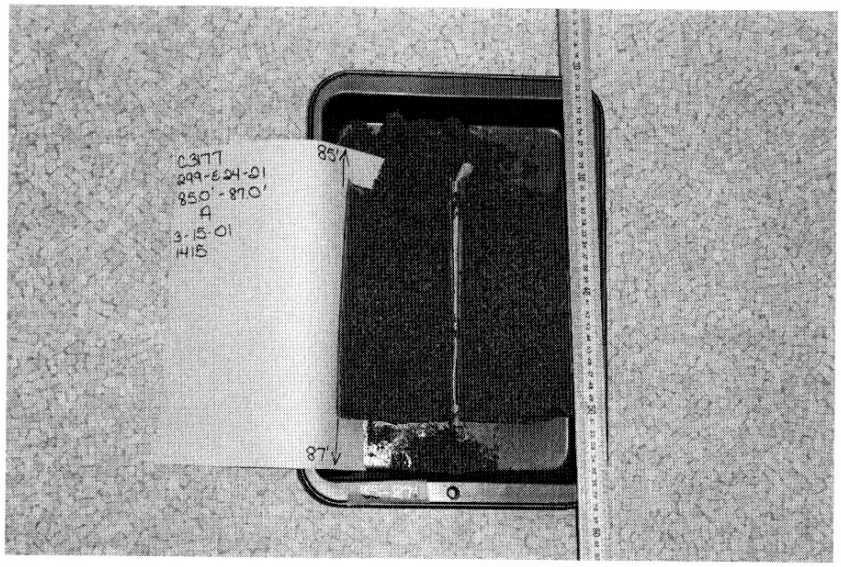

Fig. 5d. Core 85.

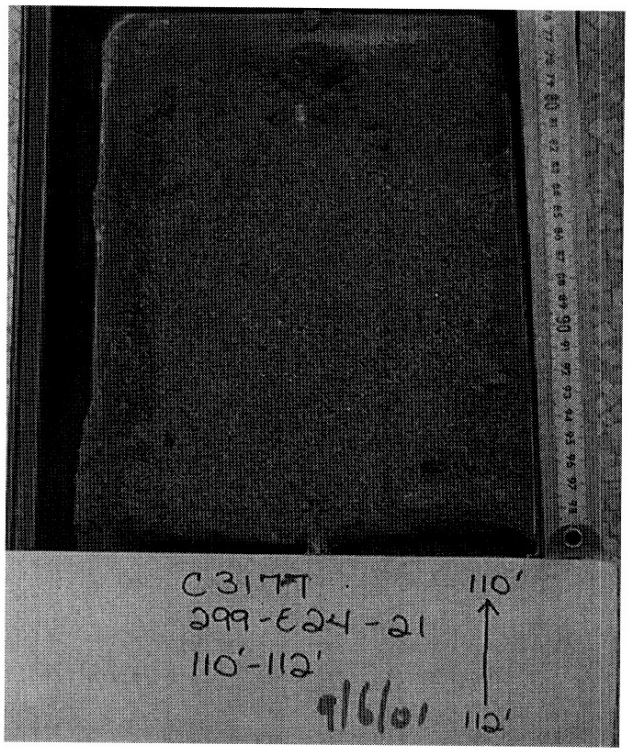

Fig. 5e. Core 110.

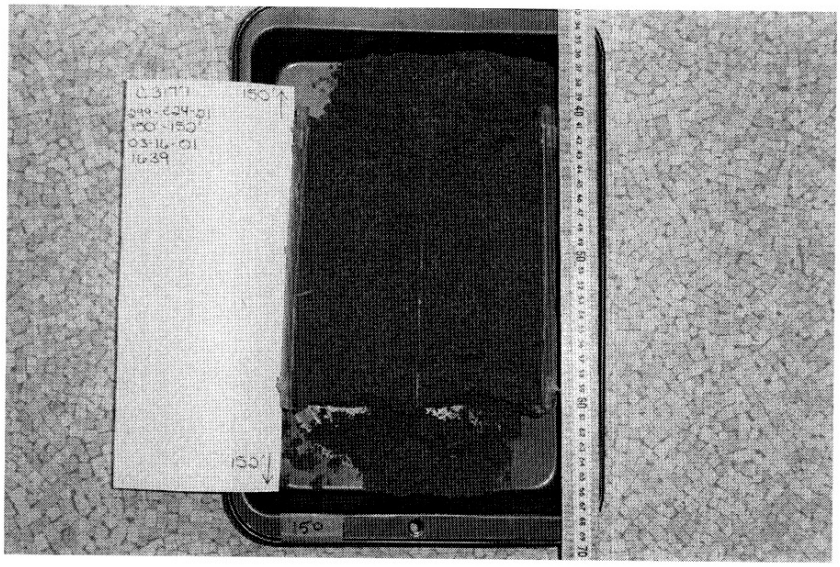

Fig. 5f. Core 130.

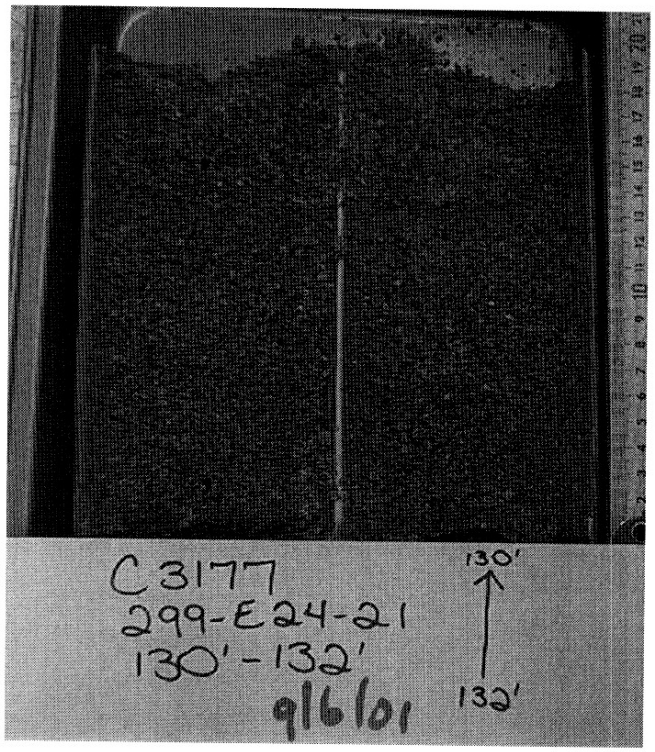

Fig. 5g. Core 150.

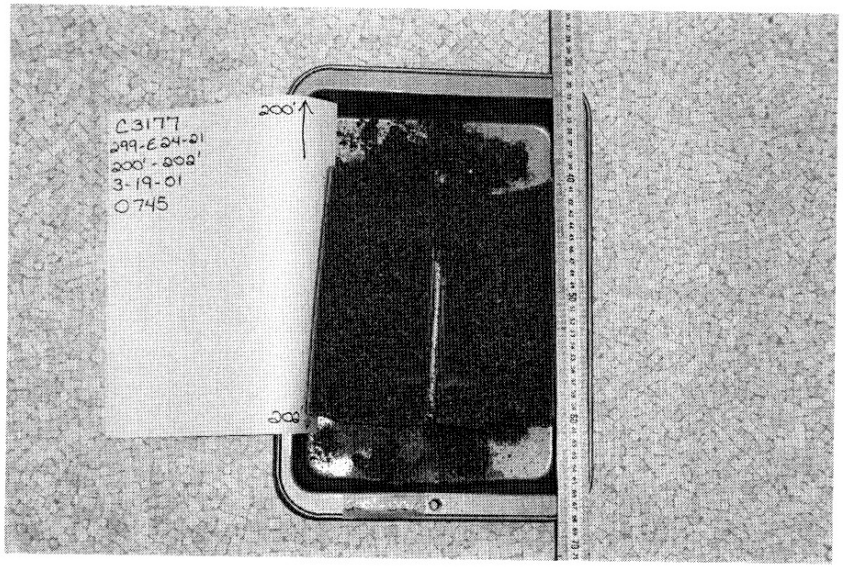

Fig. 5h. Core 200.

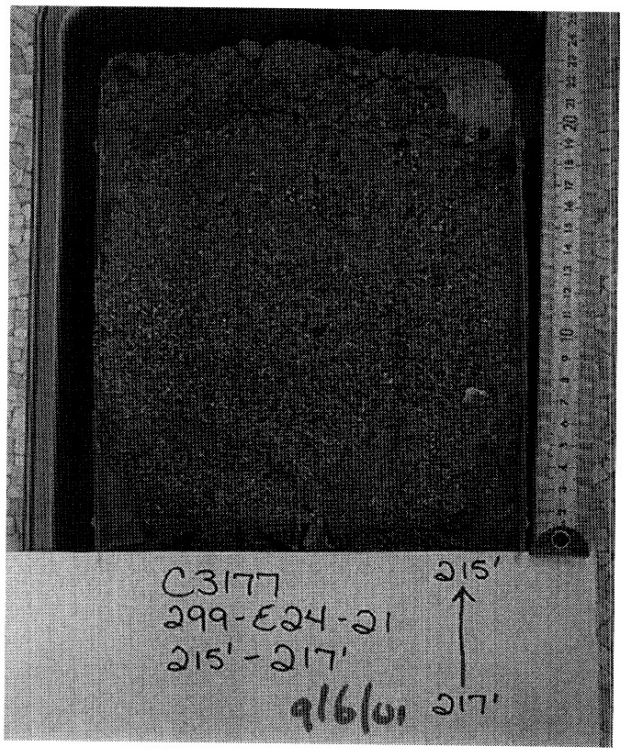

Fig. 5i. Core 215.

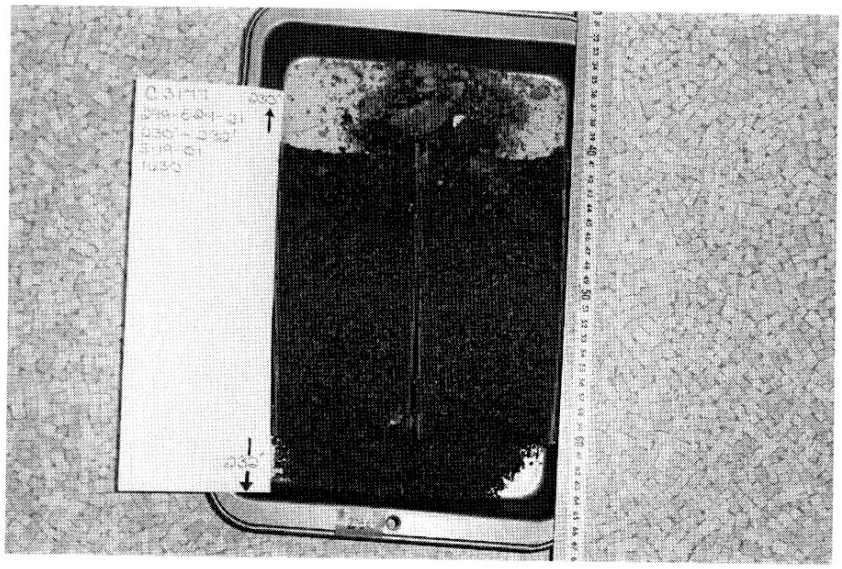

Fig. 5j. Core 230.

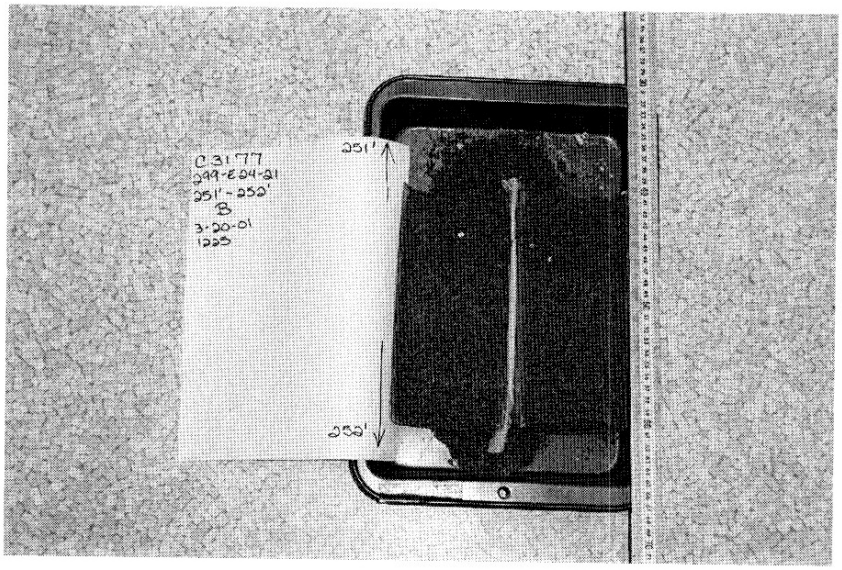

Fig. 5k. Core 251.

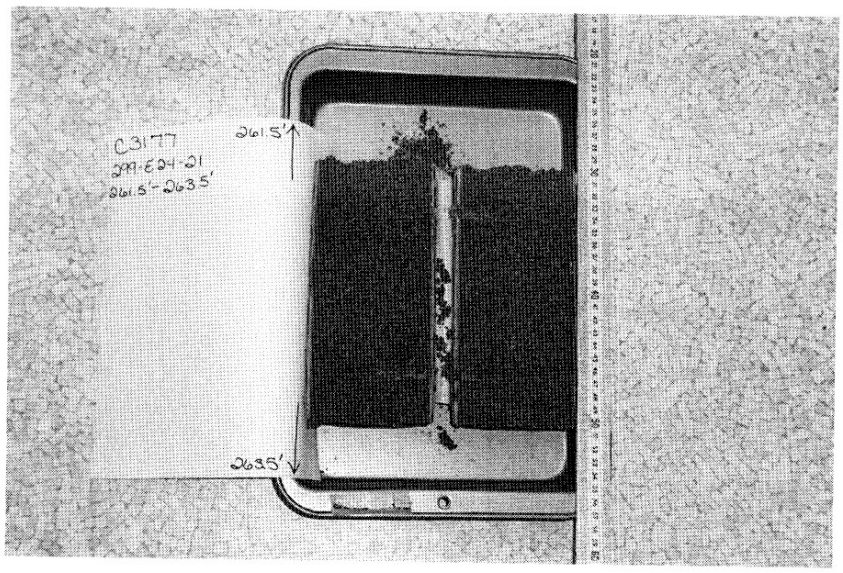

Fig. 5l. Core 261.

Table 3 shows the saturated hydraulic conductivity values for the 12 ILAW cores range from 5.16×10^{-4} to 4.93×10^{-2} cm/s. In Fig. 6, the saturated hydraulic conductivity is plotted as function of depth.

Table 3. Saturated hydraulic conductivity of the core samples. The constant head method was used for all samples

Sample	Saturated Hydraulic Conductivity (cm/s)
45	3.24e-2
50	1.75e-3
80	1.05e-3
85	3.84e-2
110	5.16e-4
130	1.97e-2
150	7.48e-3
200	4.93e-2
215	2.24e-3
230	3.56e-3
251	1.43e-2
261	5.53e-4

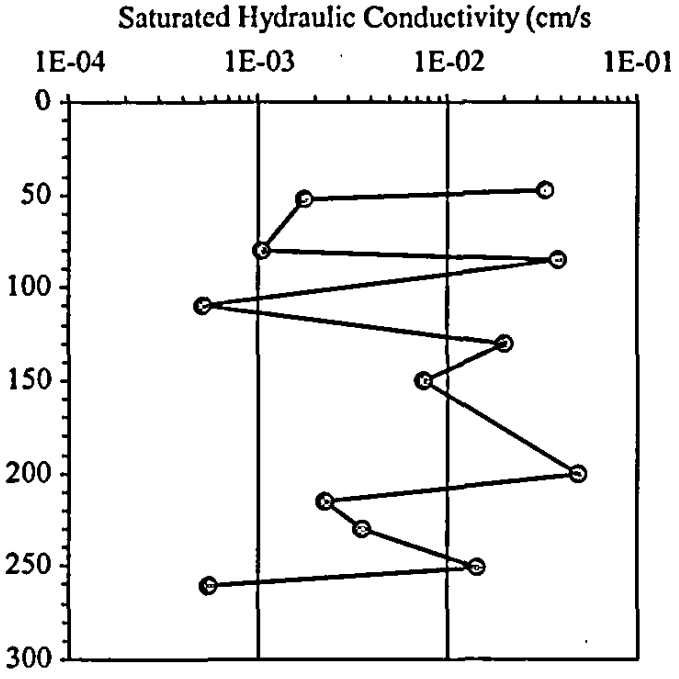

Fig. 6. Saturated hydraulic conductivity (cm/s) of cores as a function of depth.

Table 4 shows that particle density varies between 2.67 and 2.76 g/cm^3 for the four analyzed samples. The particle density of the fine-grained layer in Core 251 was 0.08 g/cm^3 larger than the bulk material.

Table 4. Particle density of core material.

Sample	Particle Density rep 1 (g/cm^3)	Particle Density rep 2 (g/cm^3)	Particle Density rep 3 (g/cm^3)	Average Particle Density, g/cm^3
45	2.70	2.74	2.74	2.73
50	2.69	2.71	2.71	2.71
80	2.72	2.70	2.68	2.70
85	2.73	2.72	2.72	2.72
110	2.71	2.65	2.69	2.69
130	2.67	2.73	2.79	2.73
150	2.69	2.69	2.67	2.68
200	2.76	2.75	2.75	2.76
215	2.67	2.70	2.74	2.70
230	2.72	2.71	2.72	2.72
251a	2.67	2.65	2.68	2.67
251b	2.74	2.75	2.73	2.74
261	2.70	2.70	2.69	2.70

Table 5 shows that the bulk density ranged from 1.54 to 1.83 g/cm^3. Table 5 also shows the porosity data, which ranged from 0.358 to 0.412.

Table 5. Core volume, bulk density, and porosity data for the core samples. The volume of each core was 1620 cm^3.

Sample	Bulk Density (g/cm^3)	Porosity (cm^3/cm^3)
45	1.63	0.385
52	1.54	0.420
80	1.70	0.359
85	1.57	0.406
110	1.56	0.412
130	1.70	0.358
150	1.51	0.431
200	1.56	0.410
215	1.67	0.370
230	1.83	0.309
251 (a and b combined)	1.57	0.406
261	1.62	0.390

Table 6 shows the pressure plate data for four pressures. The results are similar for all samples.

Table 6. Water retention data from the pressure plate technique for the core samples.

45		50		80		85	
Matric Potential -cm	Vol Water Content	Matric Potential -cm	Vol Water Content	Matric Potential -cm	Vol Water Content	Matric Potential -cm	Vol Water Content
530	0.0322	530	0.0439	530	0.0631	530	0.0503
1010	0.0284	1010	0.0410	1010	0.0469	1010	0.0443
2040	0.0245	2040	0.0314	2040	0.0328	2040	0.0253
4080	0.0245	4080	0.0292	4080	0.0148	4080	0.0244

110		130		150		200	
Matric Potential -cm	Vol Water Content	Matric Potential -cm	Vol Water Content	Matric Potential -cm	Vol Water Content	Matric Potential -cm	Vol Water Content
530	0.0656	530	0.0707	530	0.0422	530	0.0480
1010	0.0503	1010	0.0569	1010	0.0394	1010	0.0462
2040	0.0256	2040	0.0253	2040	0.0275	2040	0.0347
4080	0.0168	4080	0.0244	4080	0.0252	4080	0.0257

215		230		251a		251b	
Matric Potential -cm	Vol Water Content	Matric Potential -cm	Vol Water Content	Matric Potential -cm	Vol Water Content	Matric Potential -cm	Vol Water Content
530	0.0682	530	0.0481	530	0.0347	530	0.0516
1010	0.0511	1010	0.0478	1010	0.0330	1010	0.0490
2040	0.0284	2040	0.0331	2040	0.0298	2040	0.0307
4080	0.0282	4080	0.0292	4080	0.0225	4080	0.0281

261	
Matric Potential -cm	Vol Water Content
530	0.0614
1010	0.0597
2040	0.0347
4080	0.0322

The particle size distribution is listed in Table 7, while an overview of the percentages >= than 2 mm is given in Table 8. Gravel percentages vary from 0.4 to 31.9 % (core 230). Eight of the 12 cores have gravel percentages < 5%.

Table 7. Particle size distribution for < mm fraction.

Sample 45		Sample 50		Sample 80		Sample 110	
Particle Diameter (µm)	% Less Than Diameter	Particle Diameter (µm)	% Less Than Diameter	Particle Diameter (µm)	% Less Than Diameter	Particle Diameter (µm)	% Less Than Diameter
2000	100	2000	99.9	2000	99.6	2000	100
1000	86.9	1000	92.1	1000	78.7	1000	90.5
500	33.9	500	49.9	500	44.2	500	49.1
250	16.1	250	24.6	250	19.2	250	19.1
106	9.6	106	12.6	106	10.7	106	10.5
75	6.7	75	8.6	75	8.3	75	8.2
53	4.2	53	6.5	53	7.2	53	7.3
72.0	4.9	72.2	7.9	71.3	6.0	71.5	9.2
51.1	3.9	51.2	6.0	50.7	6.0	50.7	5.5
29.6	2.9	29.6	5.0	29.3	6.0	29.4	3.7
16.2	1.9	16.3	4.0	16.1	2.0	16.4	3.7
9.4	1.9	9.4	3.0	9.3	2.0	9.3	3.7
6.6	1.9	6.7	3.0	6.6	2.0	6.6	3.7
5.4	1.9	5.4	2.0	5.4	2.0	5.4	3.7
4.7	1.9	4.7	2.0	4.7	2.0	4.7	3.7
1.3	1.9	0.0	2.0	1.3	1.0	1.4	0.9

Sample 110		Sample 130		Sample 150		Sample 200	
Particle Diameter (µm)	% Less Than Diameter	Particle Diameter (µm)	% Less Than Diameter	Particle Diameter (µm)	% Less Than Diameter	Particle Diameter (µm)	% Less Than Diameter
2000	100	2000	99.9	2000	99.9	2000	99.9
1000	96.3	1000	82.5	1000	97.0	1000	91.9
500	71.1	500	54.6	500	84.8	500	41.5
250	27.5	250	20.5	250	36.2	250	18.7
106	9.9	106	11.1	106	14.5	106	10.6
75	7.6	75	4.7	75	9.9	75	8.4
53	6.4	53	3.7	53	8.2	53	7.2
71.9	5.9	72.3	5.8	72.5	8.5	71.1	8.5
50.8	4.9	51.3	3.8	51.5	6.4	50.3	6.3
29.3	4.0	29.7	3.8	29.9	4.2	29.2	4.2
16.3	3.0	16.3	2.9	16.4	3.2	16.0	3.2
9.4	3.0	9.4	2.9	9.5	3.2	9.3	3.2
6.6	2.0	6.7	1.9	6.7	2.1	6.5	3.2
5.4	2.0	5.4	1.9	5.8	2.1	5.4	3.2
4.7	2.0	4.7	1.9	4.8	2.1	4.7	3.2
1.7	1.0	0.0	1.0	1.3	2.1	1.4	0

Table 7. Continued

Sample 215		Sample 230		Sample 251a		Sample 251b	
Particle Diameter (µm)	% Less Than Diameter	Particle Diameter (µm)	% Less Than Diameter	Particle Diameter (µm)	% Less Than Diameter	Particle Diameter (µm)	% Less Than Diameter
2000	99.9	2000	99.4	2000	99.9	2000	99.8
1000	86.7	1000	72.8	1000	85.3	1000	79.3
500	52.9	500	38.5	500	44.6	500	44.3
250	22.6	250	21.0	250	12.3	250	24.0
106	12.4	106	12.5	106	5.6	106	14.7
75	9.9	75	7.7	75	4.3	75	12.1
53	8.0	53	6.4	53	3.8	53	10
71.9	7.7	71.6	7.5	73.2	4.9	70.8	9.9
50.8	6.8	50.8	6.5	51.9	3.9	50.3	7.9
29.3	4.8	29.4	5.6	29.3	2.9	29.2	5.9
16.3	3.9	16.2	3.7	30.1	1.9	16.1	4.0
9.4	3.9	9.3	3.7	16.5	1.9	9.3	4.0
6.6	3.9	6.6	2.8	6.7	1.9	6.6	4.0
5.4	3.9	5.4	1.9	5.5	1.9	5.4	3.0
4.7	2.9	4.7	1.9	4.8	1.0	4.7	2.0
1.7	1.9	0.0	1.9	1.3	0.0	1.4	1.0

Sample 261	
Particle Diameter (µm)	% Less Than Diameter
2000	100
1000	96.4
500	76.4
250	33.7
106	16.7
75	12.7
53	10.9
70.8	13.5
50.6	9.6
29.4	7.7
16.2	5.8
9.3	5.8
6.6	3.8
5.4	2.9
4.7	1.9
1.4	1.0

Table 8. Gravel content of cores (>= 2 mm fraction).

Core	% >= 2mm
45	4.1
52	1.9
80	13.0
85	3.6
110	0.4
130	9.8
150	1.7
200	2.9
215	13.4
230	31.9
251 (a and b combined)	3.0
261	0.7

Table 9 shows the parameter estimates and fitting statistics determined using the SFOPT program with data from the multistep test. The parameter α varied from 0.019 to 0.1074, a factor of about 5, and the parameter n ranged from 1.51 to 3.182. For Cores 200, 251 and 261 no data were available from the upper tensiometer.

Table 10 shows the data generated using the steady state method. The maximum matric suction was limited by the minimum injection rates attainable with the laboratory Travcyl pumps. A total of 4 to 7 data points were obtained per sample. Data have been obtained for 10 cores. For Core 251, no convergence could be obtained for the matric potentials. A potential reason for the lack of convergence might be the fine-grained layer in the core (Fig. 5k). No sufficient water drainage could be obtained from Core 261, even after repeatedly servicing the core including replacement of the membrane and applying suctions of up to 200 cm. Based on the multistep test α value, the air entry value of the core should have been in the order of about 50 cm and sufficient water drainage should have occurred at the applied suctions. At this point in time, no reasonable explanation can be offered why the core could not be drainage appropriately during the constant flux test.

Table 9. Parameters and statistics for the van Genuchten function fitted to data from the multistep method using SFOPT (θ_s and K_s were held constant at their measured values; 1-bar pressure plate data and outflow data were used for fitting purposes ; m=1-1/n; ℓ=0.5; all data were weighted by a factor of 1.0) Fitted parameters were α, n, and θ_r.

Core depth	Tensiometer location	α (1/cm)	n	K_{sat} (cm/s)	θ_r	θ_s	R^2	m.b.e. %
45	lower	0.1039	1.737	3.24e-2	0.008	0.385	0.941	0.026
45	upper	0.088	1.664	3.24e-2	0.005	0.385	0.935	0.401
50	lower	0.073	1.710	1.75e-3	0.025	0.420	0.884	0.571
50	upper	0.045	1.667	1.75e-3	0.013	0.420	0.955	0.185
80	lower	0.0403	2.368	1.05e-3	0.031	0.359	0.721	0.044
80	upper	0.0313	2.572	1.05e-3	0.033	0.359	0.743	0.039
85	lower	0.1074	1.697	3.84e-2	0.023	0.406	0.903	0.427
85	upper	0.0847	1.595	3.84e-2	0.027	0.406	0.898	0.238
110	lower	0.0362	2.328	5.16e-4	0.039	0.412	0.916	0.061
110	upper	0.0268	3.182	5.16e-4	0.046	0.412	0.967	0.070
130	lower	0.0940	2.003	1.97e-2	0.032	0.358	0.909	0.031
130	upper	0.0674	1.934	1.97e-2	0.036	0.358	0.948	0.030
150	lower	0.0992	1.547	7.48e-3	0.015	0.431	0.956	0.429
150	upper	0.0703	1.514	7.48e-3	0.024	0.431	0.955	0.186
200	lower	0.0995	2.162	4.93e-2	0.002	0.410	0.931	1.367
215	lower	0.0448	1.918	2.24e-3	0.028	0.370	0.912	0.006
215	upper	0.0333	1.815	2.24e-3	0.023	0.370	0.925	0.013
230	lower	0.0472	1.658	3.56e-3	0.040	0.309	0.895	0.034
230	upper	0.0400	1.658	3.56e-3	0.038	0.309	0.867	0.007
251	lower	0.084	1.845	1.43e-2	0.032	0.427	0.921	0.027
261	lower	0.0191	2.485	5.54e-4	0.045	0.390	0.813	0.059

m.b.e.: mass balance error final run

Table 10. Constant flux test data.

Core 45

injection rate (ml/min)	rel perm (-)	suction upper transducer (cm)	suction lower transducer (cm)	volumetric water content
31.04	0.207	5.3	5.8	0.358
15.52	0.103	8.1	7.4	0.316
7.8	0.052	12.8	13.2	0.277
3.9	0.026	15.4	16.1	0.254
1.02	0.006	25.1	24.2	0.204
0.51	0.003	32.1	31.7	0.181

Core 50

injection rate (ml/min)	rel perm (-)	suction upper transducer (cm)	suction lower transducer (cm)	volumetric water content
1.7	0.211	10.2	10.1	0.365
0.85	0.105	13.9	14.4	0.340
0.46	0.057	15.6	16.4	0.307
0.17	0.011	26.3	27.1	0.273
0.085	0.005	37.1	38.0	0.218

Core 80

injection rate (ml/min)	rel perm (-)	suction upper transducer (cm)	suction lower transducer (cm)	volumetric water content
1.028	0.215	24.2	24.9	0.276
0.514	0.106	33.2	33.5	0.224
0.256	0.053	47.2	47.6	0.186
0.104	0.021	53.2	54.0	0.159
0.051	0.010	72.1	72.3	0.142

Core 85

injection rate (ml/min)	rel perm (-)	suction upper transducer (cm)	suction lower transducer (cm)	volumetric water content
18.66	0.106	8.1	9.0	0.333
9.33	0.053	13.8	13.2	0.292
1.866	0.010	23.7	23.6	0.222
0.933	0.005	26.4	27.3	0.191
0.093	0.0005	54.5	54.3	0.138

Core 110

injection rate (ml/min)	rel perm (-)	suction upper transducer (cm)	suction lower transducer (cm)	volumetric water content
0.524	0.223	31.1	32.0	0.319
0.262	0.112	42.1	43.1	0.286
0.132	0.056	49.8	48.9	0.235
0.052	0.022	74.3	75.0	0.176

Core 130

injection rate (ml/min)	rel perm (-)	suction upper transducer (cm)	suction lower transducer (cm)	volumetric water content
19.5	0.214	18.2	18.8	0.329
9.75	0.107	28.6	29.4	0.287
4.82	0.053	47.3	46.8	0.202
1.02	0.011	68.2	68.5	0.140
0.51	0.005	83.2	84.1	0.118
0.095	0.001	107.3	108.2	0.081

Core 150

injection rate (ml/min)	rel perm (-)	suction upper transducer (cm)	suction lower transducer (cm)	volumetric water content
7.28	0.211	8.3	7.6	0.388
3.64	0.105	12.1	12.0	0.328
1.82	0.053	14.9	15.7	0.306
0.36	0.010	22.1	23.0	0.237
0.071	0.002	38.1	39.1	0.172

Core 200

injection rate (ml/min)	rel perm (-)	suction upper transducer (cm)	suction lower transducer (cm)	volumetric water content
23.94	0.105	13.4	13.0	0.295
12.0	0.053	16.1	15.4	0.258
2.40	0.010	22.1	21.7	0.221
1.2	0.005	26.5	25.7	0.164
0.72	0.003	31.1	30.7	0.135
0.1	0.0004	49.1	49.8	0.099

Core 215

injection rate (ml/min)	rel perm (-)	suction upper transducer (cm)	suction lower transducer (cm)	volumetric water content
2.208	0.214	15.2	15.0	0.308
1.104	0.106	21.2	20.8	0.282
0.552	0.054	32.6	32.8	0.248
0.110	0.010	51.7	50.9	0.194
0.055	0.005	77.8	77.1	0.144

Core 230

injection rate (ml/min)	rel perm (-)	suction upper transducer (cm)	suction lower transducer (cm)	volumetric water content
3.46	0.211	13.1	13.8	0.269
1.73	0.105	16.1	16.7	0.241
0.865	0.053	24.1	23.8	0.213
0.102	0.006	44.2	45.0	0.155
0.05	0.003	60.1	59.4	0.133

Comparisons between water retention results obtained with both methods are shown in Fig. 7a-j for the 10 cores that successfully underwent the constant flux test. The figures show the van Genuchten representation of the parameters obtained in multistep analysis for both tensiometers as solid lines and the constant flux matric suction – water content data as symbols. Fig 8a-j show comparisons of the relative permeability relations obtained with the two methods. The solid lines are computed with the Mualem conductivity function using the n values obtained from the multistep drainage experiments. The symbols are discrete values obtained from the constant flux tests.

Discussion

One of the major goals of the core hydraulic testing was to compare results obtained with the multistep drainage and the controlled flux tests. For Cores 45, 50, 80 and 85 both the matric potential (Fig. 7a-d) and relative permeability figures (Fig. 8a-d) demonstrate good agreement between results obtained with the multistep drainage and the constant flux tests. The figures for Core 110 (Fig 7e and 8e) show good agreement for the relative permeability data but a tendency for the controlled flux test to yield larger water content values for a given matric potential, indicating a more rapid desaturation with increasing matric potential for the multistep drainage test. The controlled-flux data for this core are closer to the predictions for the upper tensiometer than for the lower tensiometer. Larger discrepancies between results of the two methods are observed for Core 130 (Fig. 7f and 8f). In this case, for a given water content, the controlled-flux water retention data are considerably larger than the multistep drainage predictions. However, the controlled-flux relative permeability seems to cross over the multistep drainage relative permeability relations at larger volumetric water contents. It is not clear why the

two methods yielded these markedly different results. The core itself did not show obvious heterogeneities like the layering that was observed in Core 251. For Core 150, the slope of the matric potential data (Fig. 7g) is steeper for the controlled flux data than predicted based the multistep drainage data. The controlled-flux relative permeability data (Fig. 8g) are all larger than the multistep drainage values. For Core 200, only the multistep drainage data associated with the lower tensiometer could be used to obtain retention parameter value. Good agreement between the methods is observed for the relative permeability (Fig. 8h), while the matric potential values measured with the controlled flux test are larger than predicted with the parameters obtained with the multistep drainage data. The figures for Core 215 (Fig. 7i and 8i) show good agreement for both variables and measurement. For Core 230, the controlled flux data, for a given water content, are generally less than the multistep drainage predictions. However, the controlled flux relative permeability values are larger than the associated predictions using the the multistep drainage test.

In general it can be concluded that although some differences were observed, the results produced by both methods are reasonably close for both matric potential and relative permeability values. Based on the comparisons between results of 10 ILAW cores, it appears that the faster multistep drainage method produces generally similar retention and relative permeability data as the slower controlled-flux test.

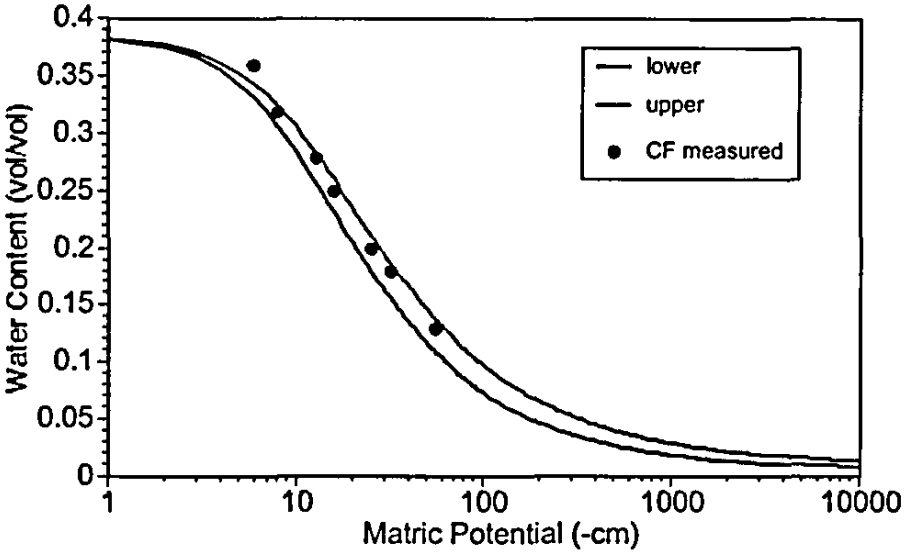

Fig. 7a. Comparison of predicted water contents using the retention parameters obtained with the multistep test and measured water contents obtained with the constant flux test for Core 45.

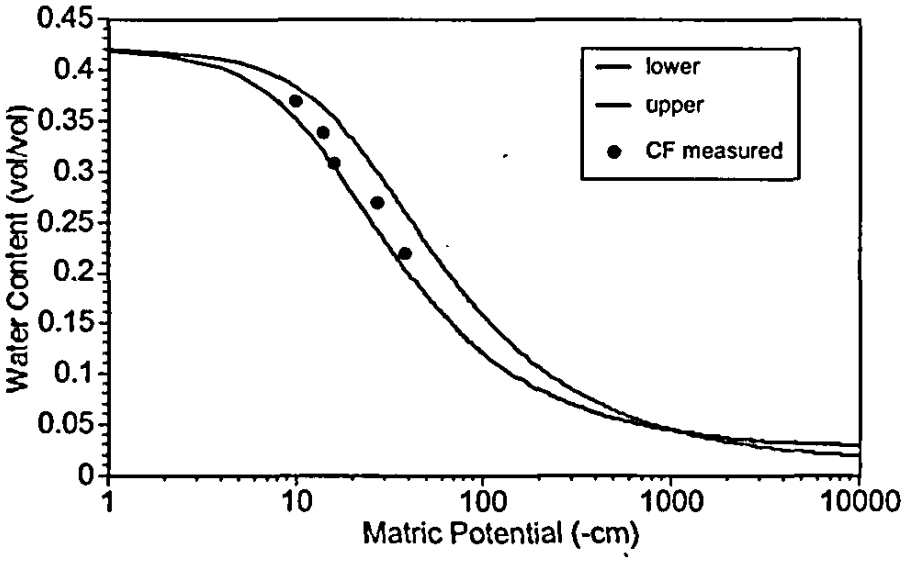

Fig. 7b. Comparison of predicted water contents using the retention parameters obtained with the multistep test and measured water contents obtained with the constant flux test for Core 50.

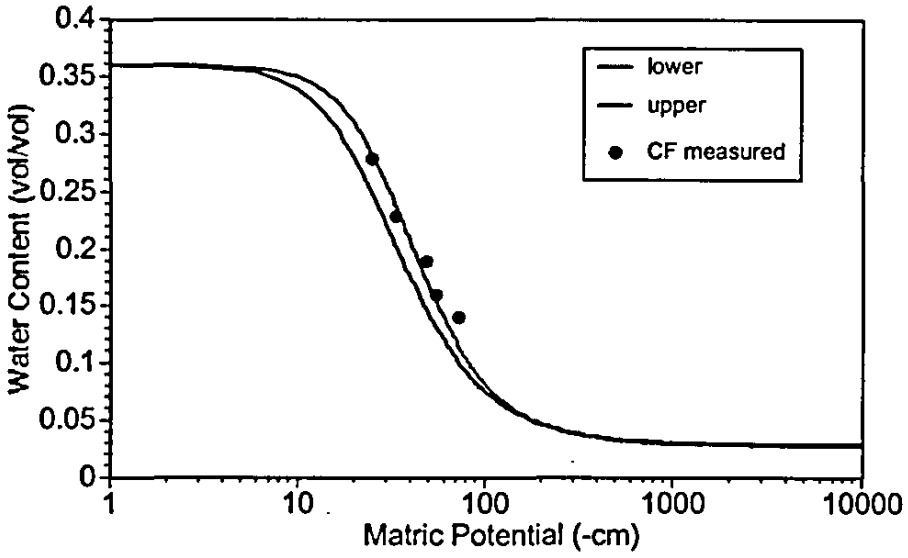

Fig. 7c. Comparison of predicted water contents using the retention parameters obtained with the multistep test and measured water contents obtained with the constant flux test for Core 80.

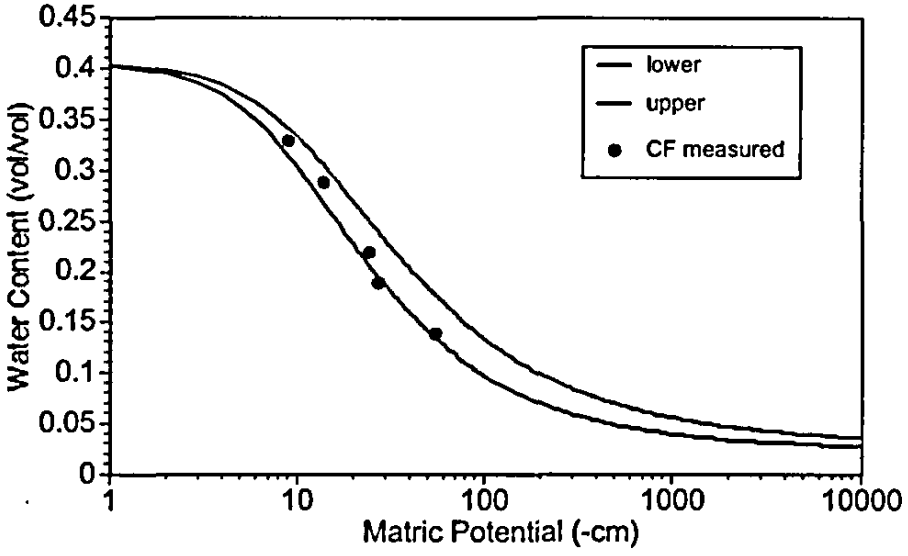

Fig. 7d. Comparison of predicted water contents using the retention parameters obtained with the multistep test and measured water contents obtained with the constant flux test for Core 85.

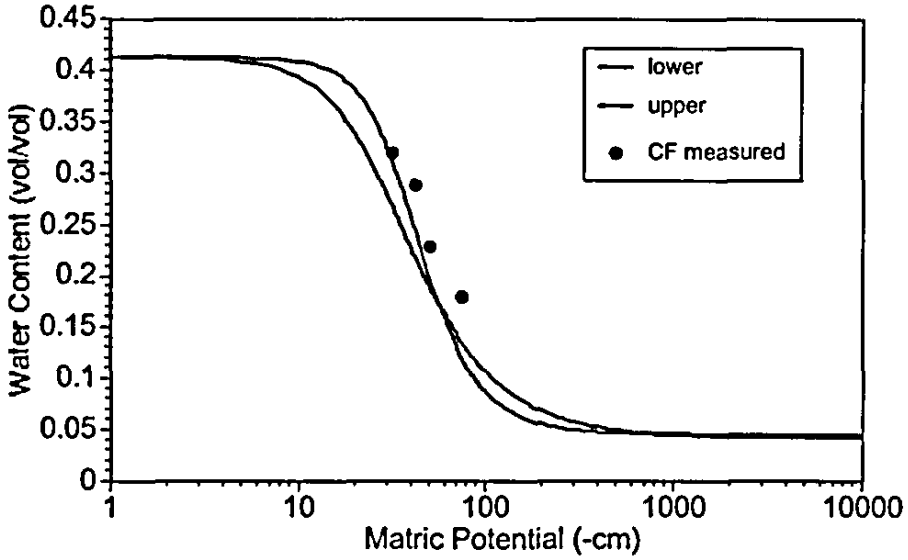

Fig. 7e. Comparison of predicted water contents using the retention parameters obtained with the multistep test and measured water contents obtained with the constant flux test for Core 110.

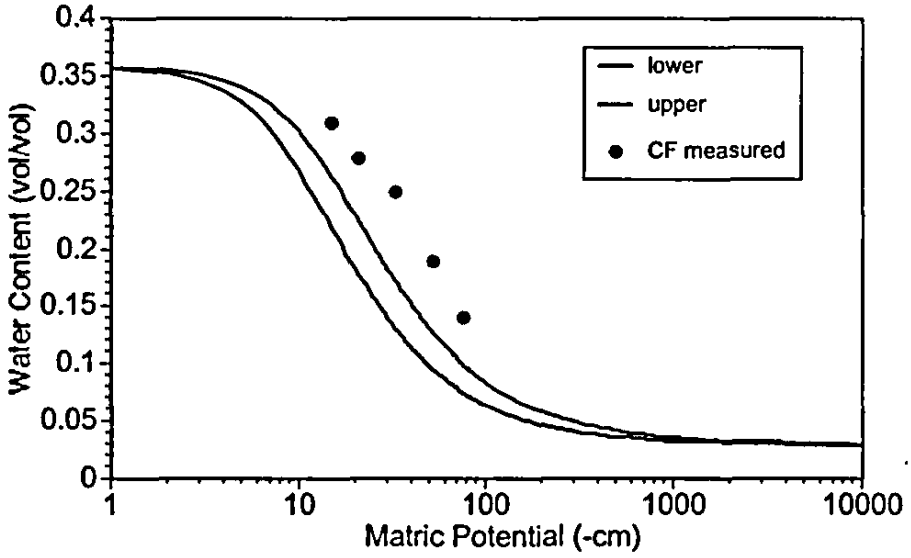

Fig. 7f. Comparison of predicted water contents using the retention parameters obtained with the multistep test and measured water contents obtained with the constant flux test for Core 130.

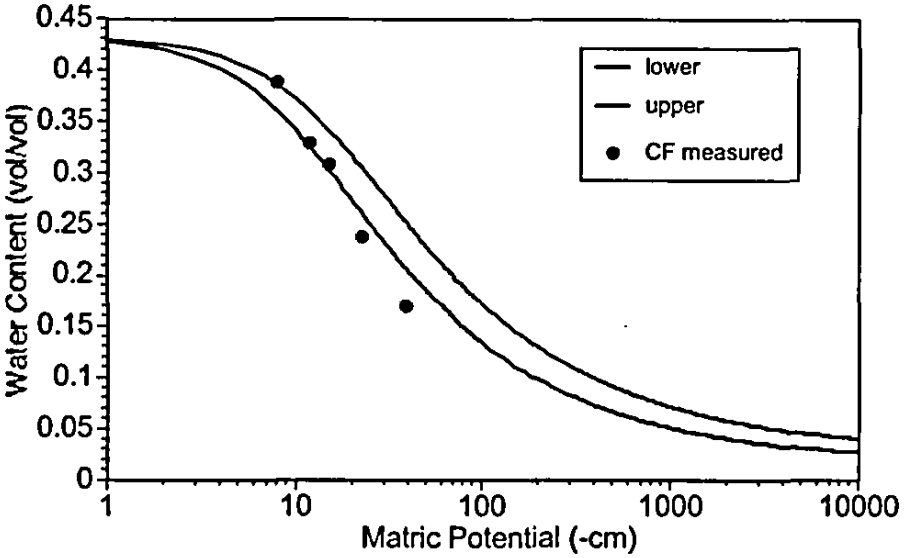

Fig. 7g. Comparison of predicted water contents using the retention parameters obtained with the multistep test and measured water contents obtained with the constant flux test for Core 150.

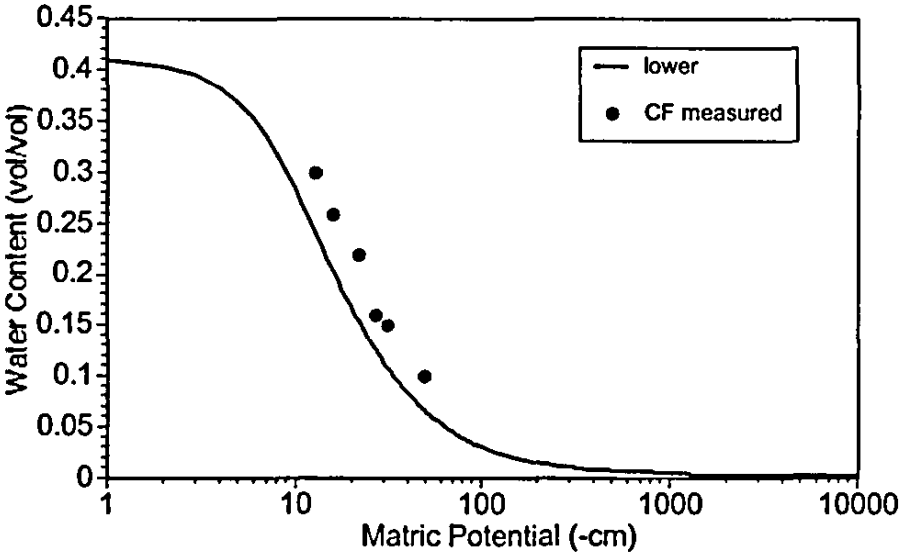

Fig. 7h. Comparison of predicted water contents using the retention parameters obtained with the multistep test and measured water contents obtained with the constant flux test for Core 200.

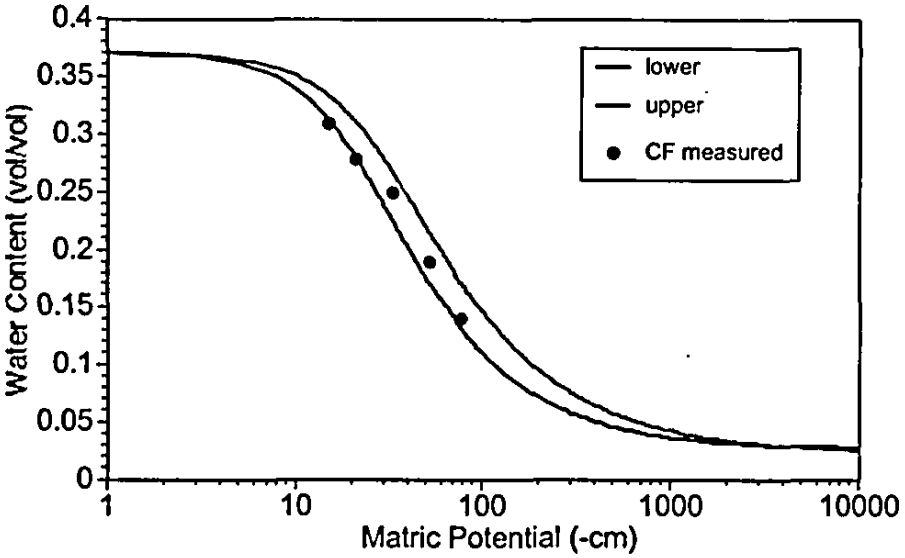

Fig. 7i. Comparison of predicted water contents using the retention parameters obtained with the multistep test and measured water contents obtained with the constant flux test for Core 215.

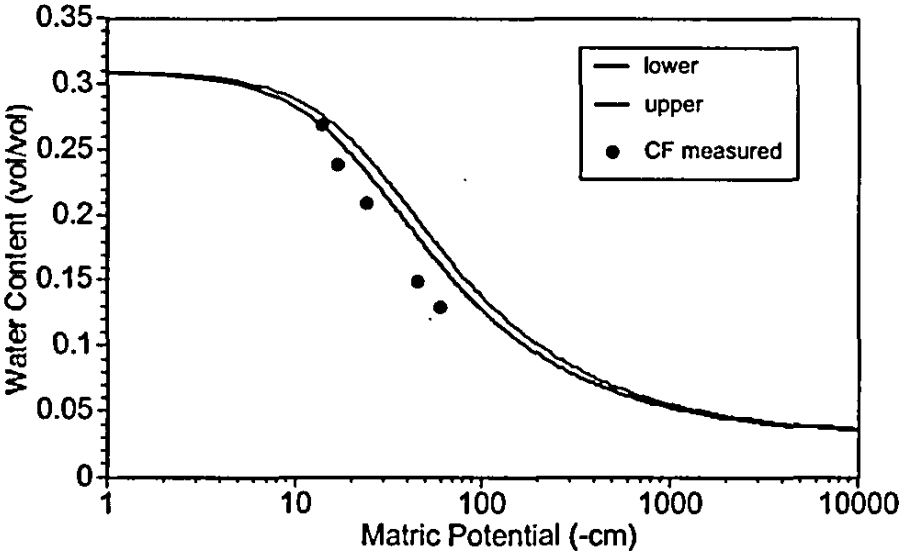

Fig. 7j. Comparison of predicted water contents using the retention parameters obtained with the multistep test and measured water contents obtained with the constant flux test for Core 230.

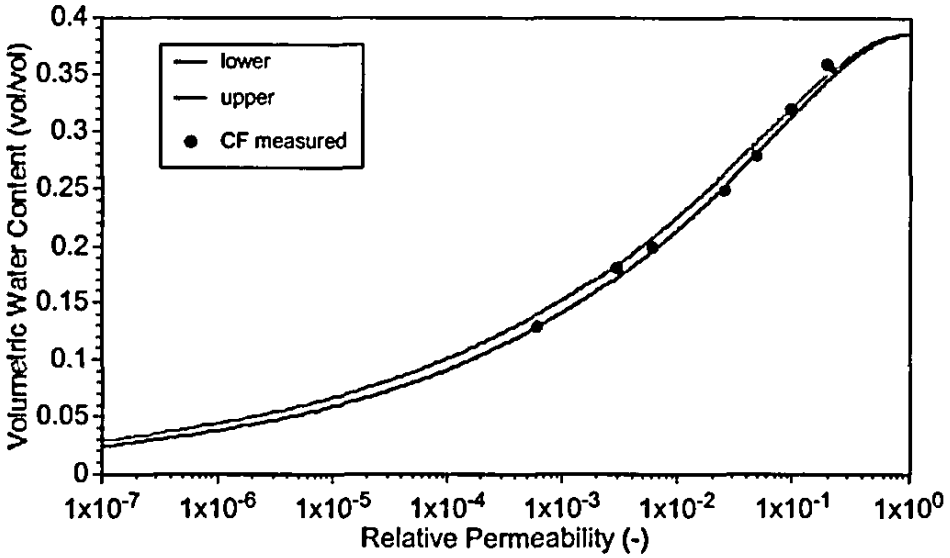

Fig. 8a. Comparison of predicted relative permeabilies using the retention parameters obtained with the multistep test and measured relative permeabilities obtained with the constant flux test for Core 45.

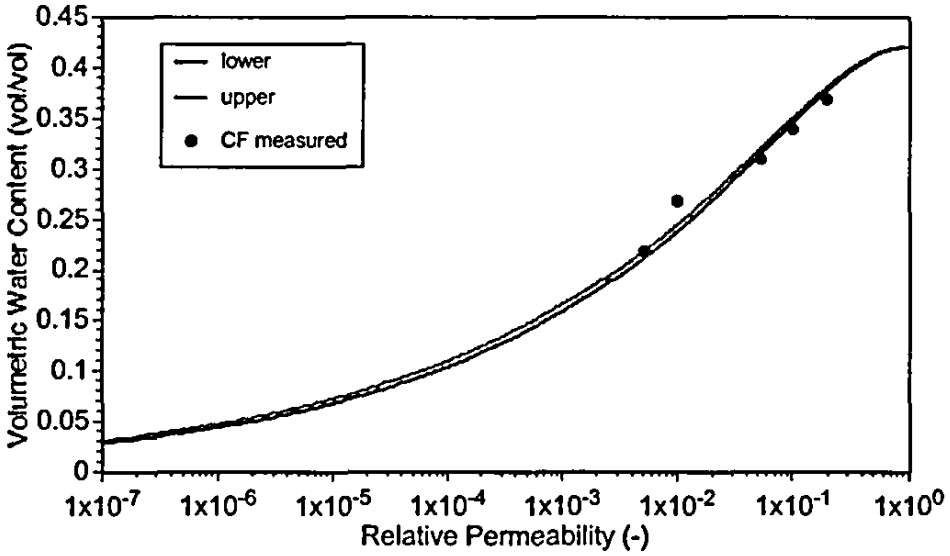

Fig. 8b. Comparison of predicted relative permeabilies using the retention parameters obtained with the multistep test and measured relative permeabilities obtained with the constant flux test for Core 50.

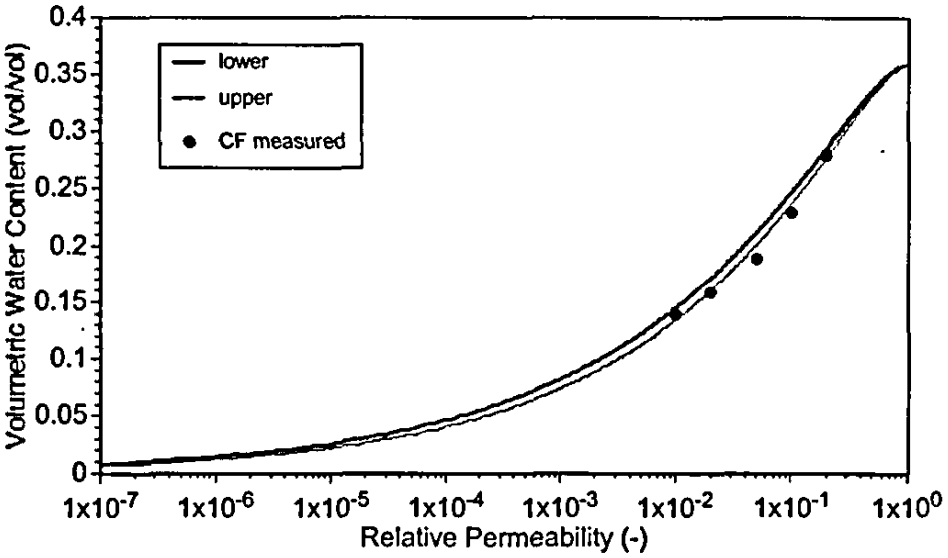

Fig. 8c. Comparison of predicted relative permeabilies using the retention parameters obtained with the multistep test and measured relative permeabilities obtained with the constant flux test for Core 80.

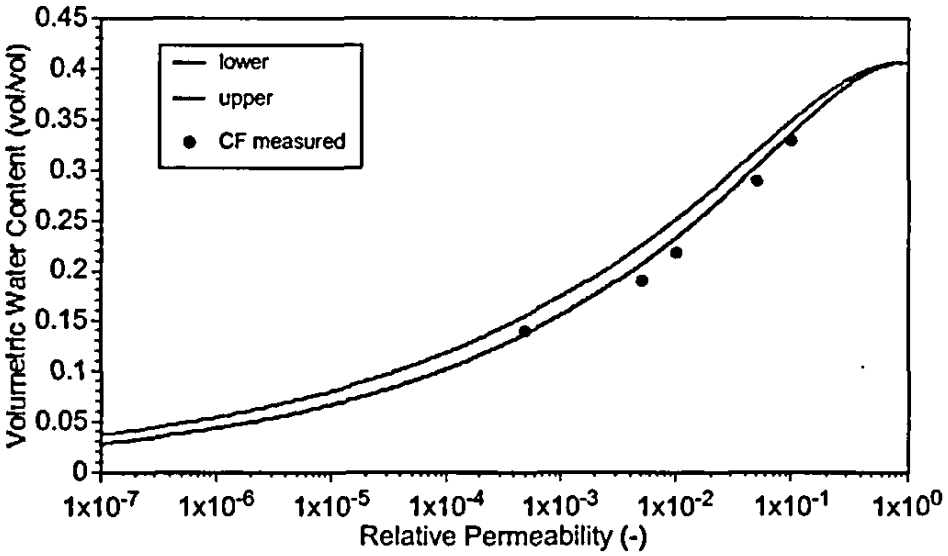

Fig. 8d. Comparison of predicted relative permeabilies using the retention parameters obtained with the multistep test and measured relative permeabilities obtained with the constant flux test for Core 85.

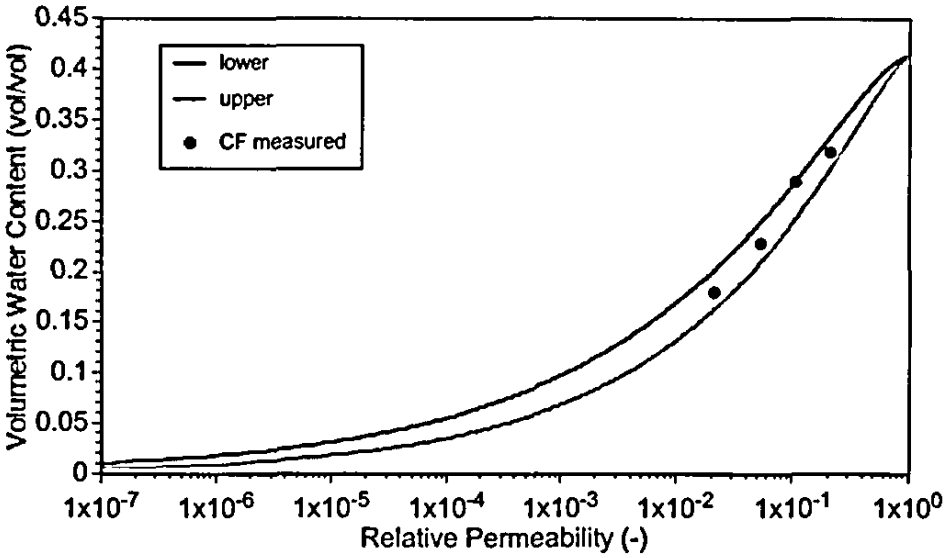

Fig. 8e. Comparison of predicted relative permeabilies using the retention parameters obtained with the multistep test and measured relative permeabilities obtained with the constant flux test for Core 110.

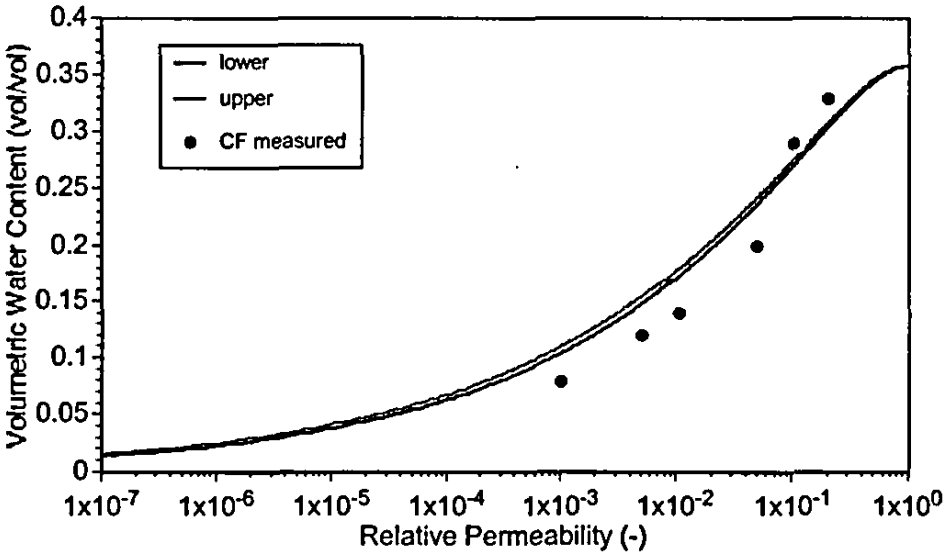

Fig. 8f. Comparison of predicted relative permeabilies using the retention parameters obtained with the multistep test and measured relative permeabilities obtained with the constant flux test for Core 130.

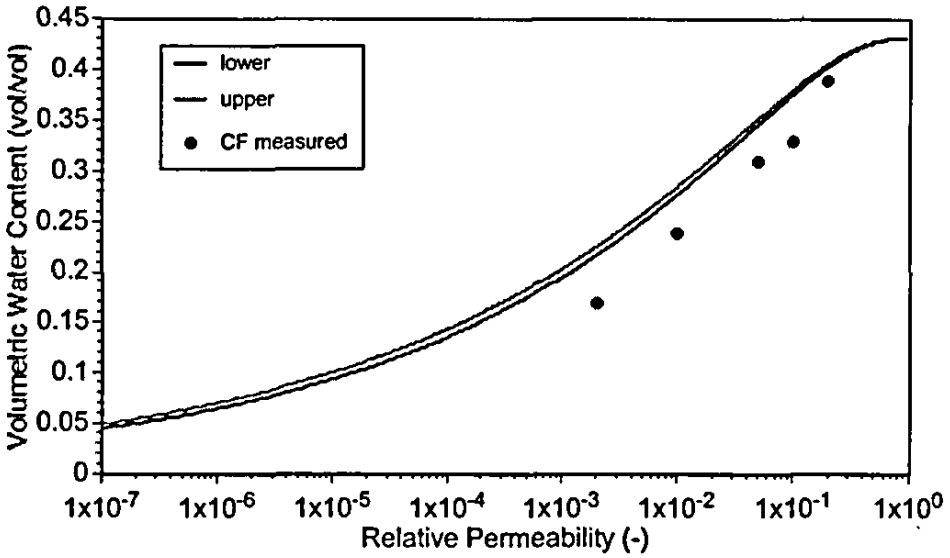

Fig. 8g. Comparison of predicted relative permeabilies using the retention parameters obtained with the multistep test and measured relative permeabilities obtained with the constant flux test for Core 150.

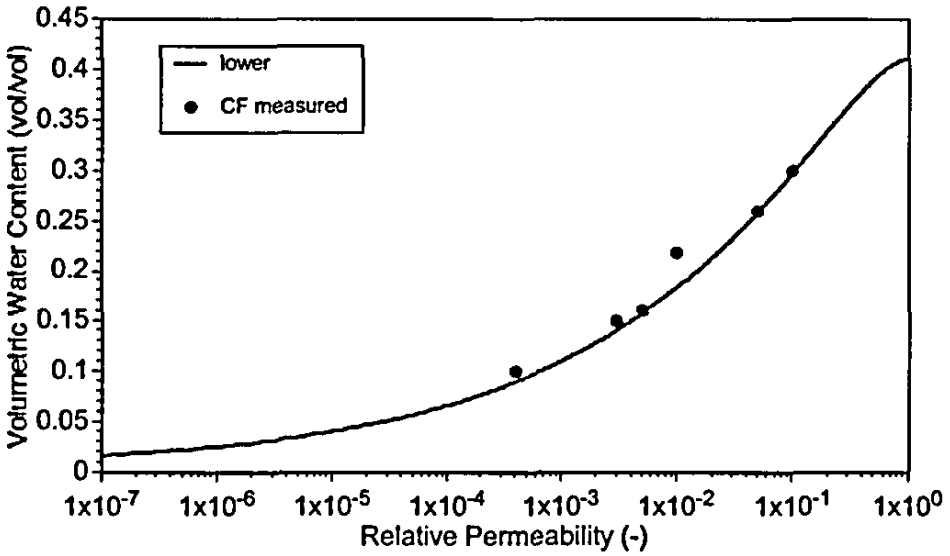

Fig. 8h. Comparison of predicted relative permeabilies using the retention parameters obtained with the multistep test and measured relative permeabilities obtained with the constant flux test for Core 200.

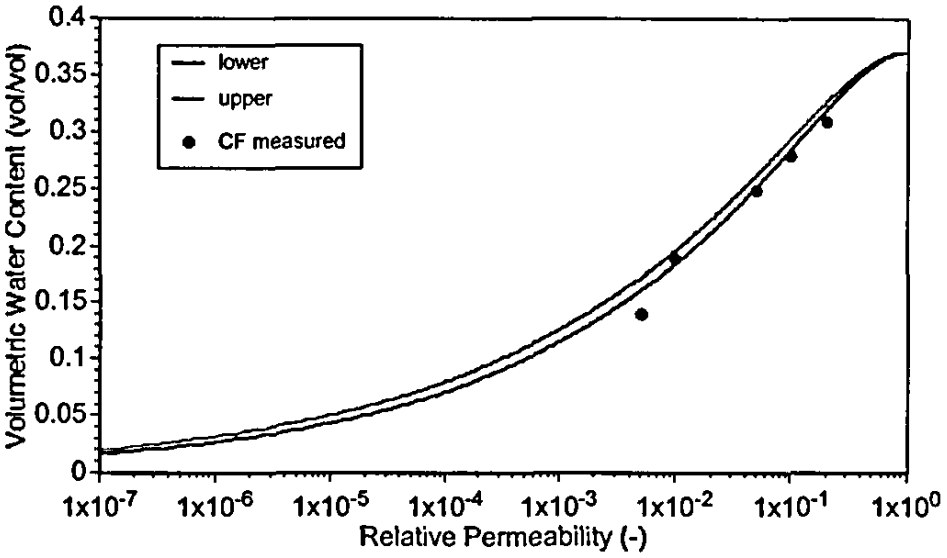

Fig. 8i. Comparison of predicted relative permeabilies using the retention parameters obtained with the multistep test and measured relative permeabilities obtained with the constant flux test for Core 215.

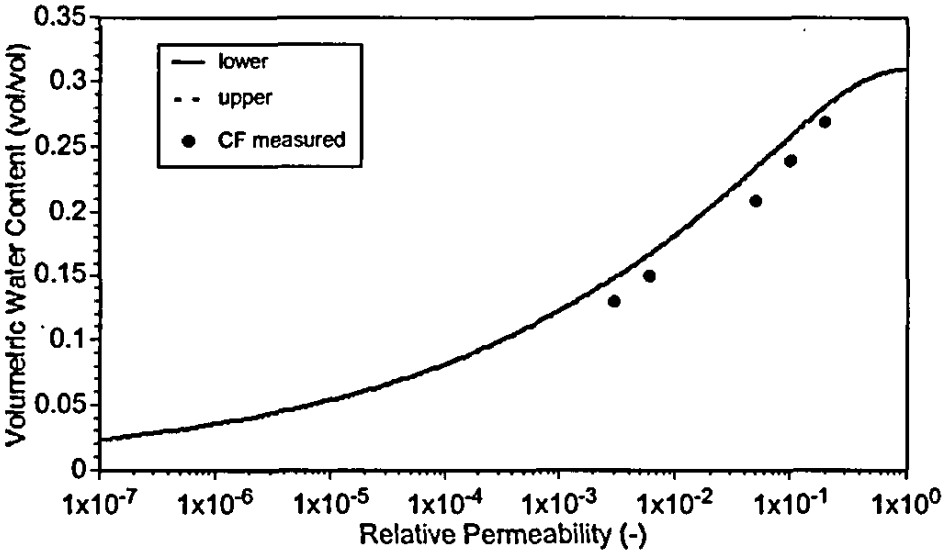

Fig. 8j. Comparison of predicted relative permeabilies using the retention parameters obtained with the multistep test and measured relative permeabilities obtained with the constant flux test for Core 230.

Summary

A total of 12 ILAW 299-E17-21 cores have been analyzed for unsaturated hydraulic properties. Tests to determine unsaturated hydraulic parameters included saturated hydraulic conductivity, multistep drainage, and constant flux experiments. The hydraulic conductivity and multistep drainage tests were completed on all 12 cores. The constant flux experiment was successfully applied to 10 cores. For cores 251 and 261 no useful constant flux data could be obtained because of drainage problems. A thin, fine-grained layer in Core 251 probably prevented appropriate water drainage in Core 251. It is not clear why Core 261 did not allow sufficient water drainage during the constant flux test.

In general it can be concluded that although some differences were observed, the results produced by both methods are reasonably close for both matric potential and relative permeability values. Based on the comparisons between results of 10 ILAW cores, it appears that the multistep drainage method produces generally similar retention and relative permeability data as the controlled-flux test. The correspondence between the data obtained with the multistep and contstant flux techniques is encouraging. Given the considerably longer duration and added complexity of the constant flux test, it appears that a determination of retention parameters through the multistep drainage test might be sufficient.

References

American Society for Testing and Materials. 1985. "Standard Test Method for Particle-size Analysis of Soils. D 422-63 (1972)." 1985 Annual Book of ASTM Standards 04.08:117- 127. American Society for Testing and Materials, PA.

Blake GR, and KH Hartge. 1986a. "Particle Density." In Methods of Soil Analysis, Part 1, ed. A. Klute, pp. 377-382. American Society of Agronomy, Madison, WI.

Blake GR, and KH Hartge. 1986b. "Bulk Density." In Methods of Soil Analysis, Part 1, ed. A. Klute, pp. 363-375. American Society of Agronomy, Madison, WI.

Eching SO, and JW Hopmans, 1993. "Optimization of hydraulic functions from transient outflow and soil water pressure data," Soil Sci. Soc. Am. J. 57:1167-1175.

Freeze RA and JA Cherry, 1979. *Groundwater*. Prentice-Hall, Inc., Englewood Cliffs, NJ.

Gee GW and JW Bauder, 1986. "Particle-Size Analysis." In Methods of Soil Analysis, Part 1, ed. A. Klute, pp. 383-409. American Society of Agronomy, Madison, WI.

Khaleel, R., and J.F. Relyea. 1997. Correcting laboratory-measured moisture retention data for gravels. Water Res. Research 33: 1875-1878.

Khaleel R, and EJ Freeman, 1995. "Variability and scaling of hydraulic properties for 200 Area soils, Hanford Site, WHC-EP-0883, Westinghouse Hanford Company, Richland, Washington.

Klute A, 1986. " Water Retention: Laboratory Methods," In Methods of Soil Analysis, Part 1, ed A. Klute, pp. 635-662. American Society of Agronomy, Madison, Wisconsin.

Klute A and C Dirksen, 1986. "Hydraulic conductivity and diffusivity: Laboratory methods," In Methods of Soil Analysis, Part 1, ed A. Klute, pp. 687-734. American Society of Agronomy, Madison, Wisconsin.

Kool JB, JC Parker, and MT van Genuchten, 1985a. "Determining soil hydraulic properties from one-step outflow experiments by parameter estimation, I, Theory and numerical studies," Soil Sci. Soc. Am. J. 49:1348-1354.

Kool JB, JC Parker, and MT van Genuchten, 1985b. "Determining soil hydraulic properties from one-step outflow experiments by parameter estimation, I, Experimental studies," Soil Sci. Soc. Am. J. 49:1354-1359.

Mann FM, and RJ Puigh. 2000. "Statements of Work for FY 2001 to 2006 for the Hanford Low-Activity Tank Waste Performance Assessment Program," RPP-6702, Rev. 0, Fluor Federal Services, Richland, Washington.

Reidel SP, 2000. "Second ILAW Site Borehole Characterization Plan," PNNL-13283, Pacific Northwest National Laboratory, Richland, Washington

This page intentionally left blank.

APPENDIX C

ILAW BOREHOLE NO. 3 HYDRAULIC PROPERTIES MULTISTEP TEST RESULTS

This page intentionally left blank

ILAW Borehole No. 3 Hydraulic Properties Multistep Test Results

MJ Fayer, M Oostrom, K Waters-Husted,
15 March 2003

In support of FY 2003 Milestone No. HY.2 of the Immobilized Waste Project
"Letter report on measurement of hydraulic properties for FY02 ILAW borehole samples"

Introduction

Pacific Northwest National Laboratory (PNNL) supports the Immobilized Waste Program (IWP) of the Hanford Site's River Protection Project. The IWP is designing and assessing the performance of on-site disposal facilities to receive radioactive wastes that are currently stored in single and double shell tanks at the Hanford Site (Puigh and Mann 2001). To predict contaminant migration from these facilities requires estimates of the physical and hydraulic properties of sediments within the vadose zone beneath and around the disposal facility.

The objective of the PNNL task titled "Borehole Hydraulic Measurements" is to measure the physical and hydraulic properties of sediment cores taken from the ILAW Disposal Site. In FY 2002, the site characterization activities of the IWP included a borehole drilling and sampling program to obtain undisturbed cores of vadose zone sediments (Reidel and Ho 2002). Of particular interest was obtaining cores of paleosols potentially located at 3 separate depths. Fayer et al.[1] described the sample selection, preparation, and saturated conductivity test results from FY 2002. This report summarizes the hydraulic parameters that were derived in FY 2003 from analyses of data from the multistep test.

Method

The multistep test was used to estimate the hydraulic parameters of the 10 ILAW borehole cores from FY 2002. The test, which has been used on previous ILAW cores, is based on the methodology described by Eching and Hopmans (1993). Basically, each cores is saturated, then subjected to progressively greater atmospheric pressures. The resulting outflow from the core is recorded and then used in an inverse model to estimate the hydraulic parameters.

Table 1 describes the 10 cores from the FY 2002 boreholes. The cores were fitted with 600-mbar mesh screening and saturated by passing three pore volumes of de-aired water through the cores. Once saturated, the cores were equilibrated with zero suction at the base (where the plate was located). The cores were then subjected to pressure increments of 20, 40, 60, 100, 300, and 500 mbar. During each pressure increment, the outflow was monitored. Once the outflow rate decreased substantially,

[1] Fayer MJ, M Oostrom, and K Waters-Husted. "ILAW Borehole No. 3 Hydraulic Properties: Status Report for FY 2002," Letter Report to Fred Mann dated 2 October 2002.

Table 1. Cores Selected from ILAW Boreholes Drilled in FY 2002 (adapted from FY2002 Status Report)

Borehole	Core Liner Depths (ft)	Approximate Depth of Test Sample (ft)	Sample ID	Comments (visual estimate of texture)
C3826	63.5-64.5	63'8"-64'4"	C3826-63.5	Medium sand
C3826	65.5-66.5	65'8"-66'4"	C3826-65.5	Fine sand
C3826	171-172	171'2"-171'10"	C3826-171	Medium sand
C3827	63.5-64.5	63'8"-64'4"	C3827-63.5	Medium sand; no evidence of anything that might indicate a paleosol
C3827	64.5-65.5	64'8"-65'4"	C3827-64.5	Coarse to very coarse sand
C3827	163.5-164.5	163'8"-164'4"	C3827-163.5	Fine sand
C3827	221-222	221'2"-221'10"	C3827-221	Sandy; some fines and gravel (<5%)
C3828	60-62	60'2"-60'10"	C3828-60	Coarse sand packed tightly; regular vertical features spaced evenly 1"., appear to be result of the drill string
C3828	155.5-157.5	155'8"-156'4"	C3828-155.5	Marked as suspected paleosol, but it's a clastic dike (associated with paleosol?)
C3828	155.5-157.5	156'6"-157'2"	C3828-156.5	Coarse sand; possible clastic dike barely visible on upper end, nothing on lower end

the applied pressure was increased to the next increment. In several instances, a seal or tensiometer failed during a pressure increment, in which case the test of that particular core was stopped.

Outflow data from the multistep test were analyzed using the SFOPT program. SFOPT is based on the van Genuchten water retention function and the Mualem conductivity function. The retention function is:

$$\theta = \theta_r + (\theta_s - \theta_r)\left[(1 + (\alpha h)^n\right]^m$$

where θ_s = saturated water content (cm^3/cm^3)
θ_r = residual water content (cm^3/cm^3)
h = matric potential (-cm)
α, n, m = empirical fitting parameters (α units are 1/cm; n and m are dimensionless; for all analyses, the parameter m was approximated as $m = 1 - 1/n$)

In combination with the van Genuchten retention function, the Mualem conductivity function is expressed as:

$$K = K_s \frac{\left\{1-(\alpha h)^{n-1}\left[1+(\alpha h)^n\right]^m\right\}^2}{\left[1+(\alpha h)^n\right]^{m\ell}}$$

where ℓ is an additional fitting parameter that is almost always set equal 0.5 based on observed values.

Results

Table 2 shows the parameter estimates and fitting statistics determined using the SFOPT program and data from the multistep tests. In all cases, an attempt was made to fit the parameters α, n, θ_r, and θ_s. Typically, measured porosity values and water retention data would be used, but these data were not available because the cores are currently being tested with the controlled flux method. In lieu of porosity data, the fitting program was constrained so that the estimated porosity never exceeded a value of 0.444, which is the maximum porosity observed in the cores from ILAW boreholes 1 and 2. The K_s parameter was held constant at the measured value.

The data from some of the cores in the first set of tests (Tests 1 to 5) were difficult to fit with SFOPT. After multiple attempts, one or more parameters were fixed at values that the program indicated were reasonable (prior to the program terminating prematurely for non-convergence).

The fitted parameter values in Table 2 are similar to parameter values reported for cores from ILAW boreholes 1 and 2. We did not quantify the comparisons because we expect the final parameters may be somewhat different once the porosity and water retention data are determined. The only measured parameter that can be said to differ significantly from previous results is the saturated conductivity of one sample, C3828-155.5. The Ks value for this sample is nearly 40-fold less than all other ILAW samples tested. The reason is that this particular sample contains portions of a clastic dike. Although the core has not yet been sectioned to reveal it, the clastic dike feature was evident on the end of the core when it was prepared for testing.

One of the objectives of this task was to determine the physical and hydraulic properties of possible paleosols at the ILAW site. Although the parameters have not been finalized, the initial estimates shown in Table 2 suggest that the paleosols have properties that do not differ much from previous cores samples taken from other portions of the vadose zone at the ILAW site. This observation is preliminary and could change when the remainder of the data are collected and assimilated.

Table 2. Parameters and statistics for the van Genuchten/Mualem function fitted to data from the multistep method using SFOPT (θ_s was constrained to ≤ 0.444; K_s was held constant at the measured value; m=1-1/n; ℓ=0.5; all data were weighted by a factor of 1.0; fitted parameters are in bold type).

Sample ID	Test Order	α (1/cm)	n (-)	θ_r (vol/vol)	θ_s (vol/vol)	K_{sat} (cm/s)	R^2	m.b.e. %
C3826-63.5	3	0.0300	3.06	0.148	0.444	1.84E-02	0.942	0.71
C3826-65.5	4	0.0200	2.62	0.127	0.444	2.00E-03	0.971	0.95
C3826-171	2	0.0390	1.84	0.0226	0.382	7.96E-03	0.969	0.82
C3827-63.5	5	0.0914	1.50	0.0	0.444	2.23E-02	0.978	0.71
C3827-64.5	6	0.0537	2.25	0.0721	0.412	3.66E-03	0.998	0.17
C3827-163.5	1	0.169	4.55	0.115	0.398	6.85E-03	0.986	0.15
C3827-221	10	0.0660	1.77	0.0220	0.361	7.30E-03	0.999	0.61
C3828-60	7	0.0115	1.17	0.0	0.444	2.55E-04	0.977	1.72
C3828-155.5	8	0.0572	1.29	0.0	0.444	6.95E-06	0.977	1.72
C3828-156.5	9	0.0223	1.92	0.121	0.301	4.92E-04	0.999	0.45

m.b.e.: mass balance error

Summary of Multistep Test

The 10 cores from the FY 2002 ILAW boreholes were tested using the multistep method. Preliminary hydraulic property parameters were estimated using the SFOPT program. The preliminary parameter estimates do not differ much from parameters determined on other ILAW cores. One core had a clastic dike feature; its measured saturated conductivity was 40-fold lower than all other values ever measured on ILAW cores. Once the remainder of the testing is complete, the parameters for the FY 2002 cores will be updated and finalized.

References

Eching SO, and JW Hopmans, 1993. "Optimization of hydraulic functions from transient outflow and soil water pressure data," Soil Sci. Soc. Am. J. 57:1167-1175.

Puigh RJ, and Mann FM. 2001. *Statements of Work for FY 2002 to 2007 for the Hanford Low-Activity Tank Waste Performance Assessment Program*, RPP-6702, Rev. 1, Fluor Federal Services, Richland, Washington.

Reidel SP, and AM Ho. 2002. *Geologic and Wireline Summaries from Fiscal Year 2002 ILAW Boreholes.* PNNL-14029, Pacific Northwest National Laboratory, Richland, Washington.

This page intentionally left blank.

APPENDIX D

LABORATORY DATA ON PHYSICAL AND HYDRAULIC PROPERTIES FOR 100 AREA SAMPLES (RETC INPUT FILE)

This page intentionally left blank.

```
   15    1    8
2-1307: mass-based correction    : Drying curve
    1   20   24    3    4    0    1    1    8   30    2
    0.0352    0.2309    0.1000    1.6000    0.3750       0.5       1.       1.0
    1    1    1    1    0    0    1
1 0.27E-03
2-1307
100-HR-3   : 43%gr, 46%cs, 11%fs,  0%silt,  0%clay
       0.1    0.2309
       7.5    0.2309
      21.0    0.2309
      33.0    0.2200
      52.5    0.2112
      69.0    0.2006
     100.5    0.1809
     202.5    0.1441
     300.0    0.1239
     500.0    0.1042
     500.0    0.1010
     700.0    0.0931
     700.0    0.0870
    1000.0    0.0831
    2010.0    0.0663
    3000.0    0.0575
    5000.0    0.0475
    7000.0    0.0346
    8700.0    0.0304
   14400.0    0.0352
      0.10   2.70E-4
      30.0   5.86E-6
      97.0   9.70E-7
     388.0   2.60E-7
2-1308: mass-based correction    : Drying curve
    1   19   23    3    4    0    1    1    8   30    2
    0.0186    0.1176    0.1000    1.6000    0.3750       0.5       1.       1.0
    1    1    1    1    0    0    1
1 0.75E-04
2-1308
100-HR-3   : 58%gr, 22%cs,  9%fs, 11%silt,  0%clay
       0.1    0.1176
       7.5    0.1176
      21.0    0.1176
      33.0    0.1176
      52.5    0.1112
      69.0    0.1005
     100.5    0.0858
     202.5    0.0694
     300.0    0.0604
     500.0    0.0520
     500.0    0.0487
     700.0    0.0483
     700.0    0.0428
    1000.0    0.0398
    2000.0    0.0381
    3200.0    0.0329
    5000.0    0.0411
    7000.0    0.0211
   10000.0    0.0186
      0.10   7.50E-5
      34.0   3.94E-6
      90.0   1.05E-6
     374.0   2.88E-7
2-1318: mass-based correction    : Drying curve
```

```
    1   20   24    3    4    0    1    1    8   30    2
    0.0181    0.1207    0.1000    1.6000    0.3750       0.5       1.       1.0
    1    1    1    1    0    0    1
1 0.11E-03
2-1318
100-HR-3    : 60%gr, 40%cs, 20%fs,  0%silt,  0%clay
       0.1    0.1207
       7.5    0.1207
      21.0    0.1207
      33.0    0.1207
      52.5    0.1207
      69.0    0.1171
     100.5    0.1039
     202.5    0.0859
     300.0    0.0746
     500.0    0.0639
     700.0    0.0588
     700.0    0.0553
    1000.0    0.0507
    1000.0    0.0510
    2000.0    0.0359
    3200.0    0.0512
    5000.0    0.0293
    7000.0    0.0229
   10000.0    0.0183
   15000.0    0.0181
      0.10   1.10E-4
      18.0   9.30E-5
      43.0   4.10E-5
     138.0   3.80E-6
2-2663: mass-based correction    : Drying curve
    1   21   24    3    4    0    1    1    8   30    2
    0.0298    0.1301    0.1000    1.6000    0.3750       0.5       1.       1.0
    1    1    1    1    0    0    1
1 0.39E-03
2-2663
100-BC-5    : 61%gr, 35%cs,  4%fs,  0%silt,  0%clay
       0.1    0.1301
       8.0    0.1301
      11.0    0.1301
      23.5    0.1301
      31.5    0.1301
      53.5    0.1301
      72.1    0.1301
     101.0    0.1301
     203.0    0.1043
     300.0    0.0877
     500.0    0.0741
     700.0    0.0674
     700.0    0.0633
    1000.0    0.0602
    1000.0    0.0594
    2060.0    0.0482
    3020.0    0.0426
    5000.0    0.0370
    7000.0    0.0321
   10000.0    0.0297
   15000.0    0.0298
      0.10   3.90E-4
      27.0   1.40E-5
     101.0   1.60E-6
2-2664: mass-based correction    : Drying curve
    1   23   28    3    4    0    1    1    8   30    2
```

```
    0.0222    0.1214    0.1000    1.6000    0.3750       0.5       1.       1.0
    1    1    1    1    0    0    1
1 0.46E-03
2-2664
100-BC-5   : 73%gr, 19%cs,  8%fs,  0%silt,  0%clay
       0.1    0.1214
       2.0    0.1214
       6.5    0.1214
      10.8    0.1214
      11.0    0.1214
      20.0    0.1214
      30.5    0.1214
      55.0    0.1111
      72.0    0.1047
     101.0    0.0911
     201.5    0.0700
     300.0    0.0593
     500.0    0.0504
     700.0    0.0458
     700.0    0.0512
     850.0    0.0442
    1000.0    0.0416
    1000.0    0.0417
    2000.0    0.0301
    3000.0    0.0291
    5000.0    0.0247
    7000.0    0.0233
   10000.0    0.0222
      0.10   4.60E-4
      16.0   8.60E-5
      90.0   7.40E-7
     100.0   5.70E-7
     296.0   5.80E-8
2-2666: mass-based correction    : Drying curve
    1   20   25    3    4    0    1    1    8   30    2
    0.0365    0.2300    0.1000    1.6000    0.3750       0.5       1.       1.0
    1    1    1    1    0    0    1
1 0.14E-03
2-2666
100-BC-5 :71%gr, 19%cs,  7%fs,  3%silt,  0%clay
       8.0    0.1325
      11.0    0.1325
      23.5    0.1325
      31.5    0.1323
      53.5    0.1276
      72.1    0.1266
     101.0    0.1237
     203.0    0.1161
     300.0    0.1020
     500.0    0.0903
     700.0    0.0836
     700.0    0.0737
    1000.0    0.0753
    1000.0    0.0694
    2060.0    0.0610
    3020.0    0.0544
    5000.0    0.0466
    7000.0    0.0403
   10000.0    0.0358
   15000.0    0.0365
      0.10   1.40E-4
      32.0   3.00E-4
      93.0   3.60E-7
```

```
      98.0   4.50E-7
     294.0   2.20E-7
2-2667: mass-based correction    : Drying curve
    1   22   26    3    4    0    1    1    8   30    2
    0.0241    0.0906    0.1000    1.6000    0.3750       0.5       1.       1.0
    1    1    1    1    0    0    1
1 0.33E-03
2-2667
100-BC-5    : 75%gr, 21%cs,  4%fs,  0%silt,  0%clay
       0.1    0.0906
       2.0    0.0906
       6.5    0.0906
      10.8    0.0906
      20.0    0.0906
      30.5    0.0906
      55.0    0.0906
      72.0    0.0906
     101.0    0.0899
     201.5    0.0684
     300.0    0.0597
     500.0    0.0530
     700.0    0.0488
     700.0    0.0563
     850.0    0.0467
    1000.0    0.0452
    1000.0    0.0508
    2000.0    0.0365
    3000.0    0.0353
    5000.0    0.0294
    7000.0    0.0251
   10000.0    0.0241
      0.10   3.30E-4
      19.0   9.66E-5
      96.0   2.39E-7
     305.0   1.97E-7
3-0570: mass-based correction    : Drying curve
    1   19   25    3    4    0    1    1    8   30    2
    0.0298    0.1500    0.1000    1.6000    0.3750       0.5       1.       1.0
    1    1    1    1    0    0    1
1 0.39E+00
3-0570
100-KR-1    : 60%gr, 33%cs,  7%fs,  0%silt,  0%clay
       3.5    0.1195
       7.3    0.1195
      11.0    0.1195
      21.5    0.1195
      35.5    0.1195
      49.0    0.1195
      74.5    0.1092
      99.0    0.1017
     200.3    0.0856
     300.0    0.0786
     500.0    0.0700
     700.0    0.0628
     850.0    0.0598
    1000.0    0.0565
    2000.0    0.0429
    3000.0    0.0406
    5000.0    0.0387
    7000.0    0.0327
   10000.0    0.0298
      0.10   3.90E-1
      29.0   6.30E-5
```

```
      40.0   1.70E-5
      56.0   1.80E-6
      89.0   4.50E-7
     228.0   1.40E-7
3-0577: mass-based correction    : Drying curve
    1   22   27    3    4    0    1    1    8   30    2
    0.0140    0.1007    0.1000    1.6000    0.3750       0.5        1.       1.0
    1    1    1    1    0    0    1
1 0.90E-01
3-0577
100-FR-3   : 66%gr, 35%cs,  4%fs,  0%silt,  0%clay
       0.1    0.1007
       2.5    0.1007
       6.5    0.1007
      10.0    0.1007
      25.0    0.1007
      33.5    0.1007
      51.0    0.1007
      75.0    0.0961
     102.0    0.0880
     201.5    0.0676
     300.0    0.0574
     500.0    0.0496
     700.0    0.0434
     700.0    0.0437
     850.0    0.0409
    1000.0    0.0379
    1000.0    0.0380
    2000.0    0.0292
    3000.0    0.0268
    5000.0    0.0195
    7000.0    0.0165
   10000.0    0.0140
      0.10   9.00E-2
      31.0   8.70E-6
      59.0   3.10E-6
     153.0   8.80E-8
     232.0   2.70E-8
3-0686: mass-based correction    : Drying curve
    1   21   25    3    4    0    1    1    8   30    2
    0.0237    0.1782    0.1000    1.6000    0.3750       0.5        1.       1.0
    1    1    1    1    0    0    1
1 0.13E-02
3-0686
100-FR-1   : 55%gr, 23%cs, 22%fs,  0%silt,  0%clay
       0.1    0.1782
       3.5    0.1782
       6.0    0.1782
       8.0    0.1782
      10.0    0.1782
      25.0    0.1782
      33.5    0.1782
      54.5    0.1775
      71.5    0.1601
     102.0    0.1282
     202.5    0.0872
     300.0    0.0690
     500.0    0.0551
     700.0    0.0473
     850.0    0.0434
    1000.0    0.0387
    2000.0    0.0248
    3000.0    0.0260
```

```
    5000.0    0.0215
    6300.0    0.0387
   10000.0    0.0237
     0.10   1.30E-3
     23.0   1.60E-4
     48.0   3.40E-5
    202.0   2.60E-6
3-1702: mass-based correction    : Drying curve
    1   23   30    3    4    0    1    1    8   30    2
   0.0216    0.0976    0.1000    1.6000    0.3750       0.5       1.       1.0
    1    1    1    1    0    0    1
1 0.13E-01
3-1702
100-DR-2   :68 %gr,32 %cs,0 0%fs, 0 %silt,   %clay
      0.1    0.0976
      3.0    0.0976
      5.0    0.0976
      8.0    0.0976
     11.5    0.0976
     23.5    0.0944
     37.0    0.0860
     56.0    0.0788
     71.5    0.0721
    102.5    0.0655
    201.0    0.0554
    300.0    0.0498
    500.0    0.0447
    509.9    0.0400
    700.0    0.0417
    713.8    0.0373
    850.0    0.0395
   1000.0    0.0380
   1019.7    0.0316
   3059.1    0.0308
   5098.5    0.0262
   7137.9    0.0225
  10197.0    0.0216
     0.10   1.30E-2
     30.0   2.30E-6
     44.0   1.70E-6
     65.0   1.10E-6
    111.0   4.40E-7
    153.0   2.30E-7
    258.0   1.00E-7
4-1086: mass-based correction    : Drying curve
    1   23   29    3    4    0    1    1    8   30    2
   0.0173    0.1510    0.1000    1.6000    0.3750       0.5       1.       1.0
    1    1    1    1    0    0    1
1 0.11E-01
4-1086
100-K:65 %gr,24 %cs,11 %fs,0 0%silt,   %clay
      0.1    0.1510
      4.0    0.1103
     12.0    0.1078
     20.0    0.1041
     31.0    0.1005
     52.0    0.0967
     70.1    0.0948
    100.9    0.0912
    213.0    0.0759
    300.0    0.0680
    500.0    0.0602
    510.0    0.0571
```

```
      690.0    0.0563
      714.0    0.0536
     1000.0    0.0520
     1020.0    0.0520
     2039.0    0.0445
     3059.0    0.0430
     5099.0    0.0398
     7138.0    0.0307
     9993.0    0.0360
    10197.0    0.0334
   136538.0    0.0173
       0.10   1.10E-2
       19.0   1.40E-4
       36.0   1.00E-5
       88.0   1.40E-6
      247.0   4.60E-7
      296.0   1.40E-7
4-1090: mass-based correction    : Drying curve
    1   23   28    3    4    0    1    1    8   30    2
    0.0075    0.1740    0.1000    1.6000    0.3750       0.5        1.       1.0
    1    1    1    1    0    0    1
1 0.21E-03
4-1090
100-K:50 %gr,34 %cs,16 %fs,0 0%silt,   %clay
       0.1    0.1740
       4.0    0.1423
      12.0    0.1390
      20.0    0.1379
      31.0    0.1359
      52.0    0.1326
      70.1    0.1166
     100.9    0.1029
     213.0    0.0783
     300.0    0.0653
     500.0    0.0523
     510.0    0.0467
     690.0    0.0460
     714.0    0.0452
    1000.0    0.0393
    1020.0    0.0429
    2039.0    0.0287
    3059.0    0.0278
    5099.0    0.0230
    7138.0    0.0156
    8565.0    0.0253
   10197.0    0.0446
  228311.0    0.0075
       0.10   2.10E-4
       61.0   1.40E-5
      120.0   3.60E-6
      231.0   7.60E-7
      320.0   2.90E-7
4-1118: mass-based correction    : Drying curve
    1   23   29    3    4    0    1    1    8   30    2
    0.0213    0.1760    0.1000    1.6000    0.3750       0.5        1.       1.0
    1    1    1    1    0    0    1
1 0.86E-03
4-1118
100-K:66 %gr,28 %cs,6 0%fs, 0 %silt,   %clay
       0.1    0.1760
       5.0    0.1290
       8.0    0.1293
      11.5    0.1272
```

```
      27.0    0.1144
      49.0    0.1080
      70.5    0.1017
     104.0    0.0856
     202.0    0.0820
     300.0    0.0763
     500.0    0.0704
     510.0    0.0621
     700.0    0.0663
     714.0    0.0697
    1000.0    0.0626
    1020.0    0.0618
    2039.0    0.0496
    3059.0    0.0497
    5099.0    0.0479
    7138.0    0.0353
    9993.0    0.0365
   16927.0    0.0306
   55982.0    0.0213
      0.10   8.60E-4
      49.0   2.20E-6
      83.0   6.60E-7
     131.0   1.80E-7
     240.0   8.30E-8
     327.0   6.70E-8
4-1120: mass-based correction    : Drying curve
    1   23   28    3    4    0    1    1    8   30    2
    0.0069    0.1340    0.1000    1.6000    0.3750       0.5        1.       1.0
    1    1    1    1    0    0    1
1 0.33E-03
4-1120
100-K:63 %gr,20 %cs,17 %fs,0 0%silt,   %clay
       0.1    0.1340
       5.0    0.1261
       8.0    0.1277
      11.5    0.1271
      27.0    0.1238
      49.0    0.1216
      70.5    0.1184
     104.0    0.0823
     202.0    0.0755
     300.0    0.0648
     500.0    0.0519
     510.0    0.0470
     700.0    0.0460
     714.0    0.0593
    1000.0    0.0383
    1020.0    0.0383
    2039.0    0.0294
    3059.0    0.0291
    5099.0    0.0280
    7138.0    0.0143
    9993.0    0.0184
   28450.0    0.0131
  223824.0    0.0069
      0.10   3.30E-4
      27.0   4.10E-5
      61.0   1.10E-5
      88.0   7.40E-6
     118.0   4.80E-6
```

APPENDIX E

HANFORD LOW-ACTIVITY TANK WASTE PERFORMANCE ASSESSMENT ACTIVITY: DETERMINATION OF IN SITU HYDRAULIC PARAMETERS OF THE UPPER HANFORD FORMATION

This page intentionally left blank.

Hanford Low-Activity Tank Waste Performance Assessment Activity:

Determination of In Situ Hydraulic Parameters of the Upper Hanford Formation

AL Ward, RE Clayton and JS Ritter
31 December 1998

Introduction

Under the Hanford Low-Activity Tank Waste Project, the Lockheed Martin Hanford Company (LMHC) is designing and assessing the performance of a disposal facility for radioactive wastes currently stored in single and double shell tanks at the Hanford Site. Part of the performance assessment of such a facility involves the use of numerical models to predict the potential migration and fate of contaminants in through the vadose zone.

A general feature of soils is their spatial heterogeneity, i.e., variation of their hydraulic properties in space. The relation between the matric potential, ψ, and the volumetric water content, θ [the soil water characteristic, $\psi(\theta)$], the hydraulic conductivity tensor, $\mathbf{K}(\theta)$, and the diffusivity, $D(\theta)$] are all spatially variable and have been shown to exhibit scale dependence. Thus, vadose flow and transport is a complex, three-dimensional phenomenon, even in soils that appear to be uniform. In addition to the inherent variability, typical field soils may exhibit a number of other structural elements, e.g. lenses, and clastic dikes, that often cause the redirection and concentration of water and solute flux at the local scale. Consequently, a major hindrance to the interpretation and prediction of vadose zone transport is the difficulty in measuring the constitutive properties and the uncertainty over the range of spatial scales required by numerical models. The associated uncertainty in hydraulic properties and its effect of performance of disposal facility is requirement is recognized in the DOE revised interim policy for waste disposal facilities.

The DOE revised interim policy requirement of a reasonable expectation that a disposal facility will comply with the LAW performance objectives implies consideration for uncertainty in model predictions of facility performance. Thus, any model of transport in the vadose zone requires, in the least, knowledge of the average properties of the medium, as well as the magnitude and characteristic length scale of the variations of those properties. Since a major source of uncertainty in model predictions of facility performance will be due to the uncertainty

in hydraulic and transport parameters, there is a need for information on the unsaturated hydrologic properties of the porous media.

The Pacific Northwest National Laboratory (PNNL) is providing geotechnical support to LMHC to assist in the design and performance assessment of the disposal facility. Two related components of the geotechnical support to be provided by PNNL are the determination of *in situ* unsaturated hydraulic parameters for Hanford surface sediments (Task 4b) and the upper Hanford sand sequence (Task 4c) at the proposed location of the disposal facility. In FY 1998, laboratory and field activities for the two tasks were completed and a letter report for Task 4b prepared (Ward et al., 1998). Data analysis and report preparation for Task 4c were deferred until FY-1999. This report represents the completion of Task 4c.

Methods

The experimental site is located approximately 325 m southwest of PUREX plant and about 220 m west of the injection site in the 200E Area used by Sisson and Lu (1984). On completion of the measurements in the surface sediments, a 1.5-m deep trench was excavated and the bottom of the trench instrumented in a manner identical to the surface. Detailed descriptions of the site, experimental design, and instrumentation have presented in the test plan of Ward (1997) and reiterated in the Task 4b letter report (Ward et al., 1998). Briefly, probes were installed along the centerline of the test plot in 25 short rows spaced 0.2 m apart (Figure 1). Each row consisted of 5 TDR probes installed vertically to depths of 0.25, 0.50, 0.75, 1.0, and 1.50 m (Figure 2).

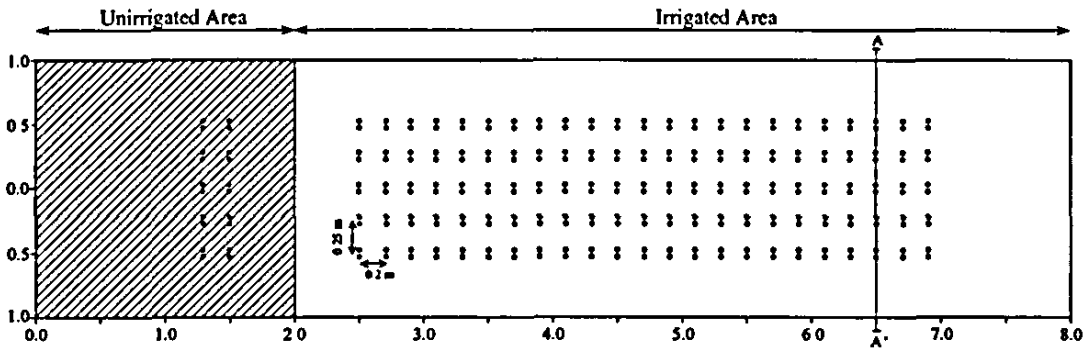

Figure 1. Plan View of Test Plot Showing Instrument Layout. The shaded 2-m section is the unirrigated control.

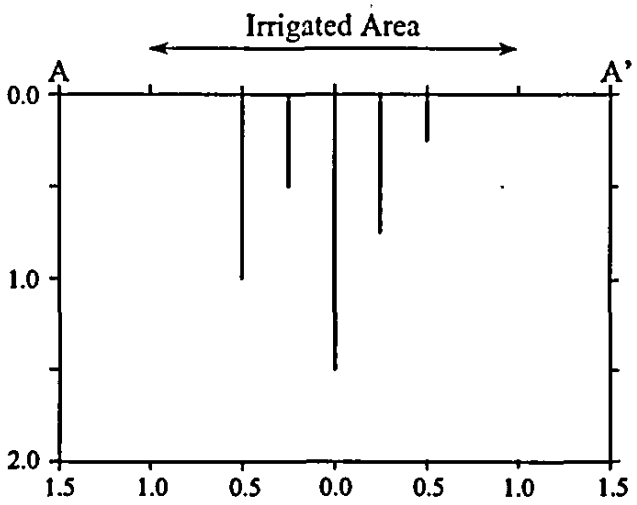

Figure 2. Cross-Sectional View of Test Plot Showing Installation Depths of the Instruments

Six infiltration experiments were conducted over the course of the study. Each experiment was conducted at a different flux density, J_w, to allow determination of $K(\theta_c)$. The values J_w used in the experiment were the same as in the first experiment, i.e., 4.7×10^{-3} cm s^{-1}; 2.5×10^{-3} cm s^{-1}, 1.292×10^{-3} cm s^{-1}, 3.093×10^{-4} cm s^{-1}, 3.54×10^{-5} cm s^{-1}, and 1.35×10^{-5} cm s^{-1}. The maximum application rate during the course of the experiments was determined by the nozzles used on the irrigation system. The lower rates were obtained by increasing the amount of time between each pass by the irrigation system.

Data reduction methods identical to those reported for Task 4b were employed. Briefly, hydraulic parameters for each depth interval were obtained by fitting the van Genuchten (1980) functions to the measured $\psi(\theta)$, and $K(\theta)$ data with the RETC computer program. The RETC program uses non-linear least squares techniques to fit the observed $\theta(\psi)$ and $K(\theta)$ data to closed-form analytical functions (van Genuchten et al., 1991). Unlike in the first experiment, saturated hydraulic conductivity, K_s was measured at fixed intervals along the transect using a tension infiltrometer according to the method of Zhang (1997). The measured K_s provided an additional constraint for the RETC analysis.

Solute breakthrough curves were derived from time domain reflectometry (TDR) measurements of the changes in bulk resistivity, R_L, in response to the application of KCl as a tracer (Ward et al. 1994; Kachanoski and Ward, 1994). The specific mass of tracer applied to the

surface, M_T, was 80 g Cl^- per m^2 of soil surface. At each level of J_w and associated equilibrium water content, θ_e, the specific mass of the tracer present from the surface to depth z=L (L being the length of the TDR probes), as a function of time, $M_L(t)$ [g cm^{-2}], was calculated from R_L at each probe location. The probability density function (pdf) of relative solute mass flux, $f_L(t)$, was calculated from the first derivative of $M_L(t)$ with respect to time. This is equivalent to the measured amount of solute, relative to the amount applied, that fluxes past the end of the TDR probe and represents the solute travel-time pdf.

Three methods were compared for determining transport parameters from measured $f_L(t)$. The first and most common approach fitted the solution to the convection-dispersion equation (CDE) to observed $f_L(t)$ to obtain estimates of the mean transport velocity ($\bar{v}$) and the dispersion coefficient (D). This solution assumes a Dirac delta-function input of solute at the surface and vertical one-dimensional flow. For a semi-infinite soil system, $f_L(t)$ is given by Jury and Roth (1990)

$$f_L(z,t)=\frac{z}{2\sqrt{\pi D t^3}}\exp\left[\frac{-(z-\bar{v}t)^2}{4Dt}\right] \qquad (1)$$

where D [L^2 T^{-1}] is the dispersion coefficient, $\bar{v}$ [L T^{-1}] is the mean pore water velocity, z [L] is distance positive downward, and t [T] is time. The dispersion can also be expressed as $\lambda\bar{v}$, where λ [L] is the dispersivity of the soil, controlled by the geometry of the transport volume. It is assumed that the TDR probes measure the total amount of solute in the range $0 \le z \le L$, regardless of the distribution of the solute along the probes. Then $M_L(t)$ represents the mass of solute, relative to the amount applied, that remains in the region $0 \le z \le L$ and is given by

$$M_L(t)=1-\int_0^t f_L(L,\tau)\,d\tau=1-C_F \qquad (2)$$

where C_F is the flux-averaged, reduced concentration for a step function input of solute, given by (Parker, 1984)

$$C_F=\frac{1}{2}erfc\left[\frac{L-\bar{v}t}{2\sqrt{Dt}}\right]+\frac{1}{2}\exp\left[\frac{\bar{v}L}{D}\right]erfc\left[\frac{L+\bar{v}t}{2\sqrt{Dt}}\right] \qquad (3)$$

A similar development for the convective lognormal transfer function (CLT) model gives the following relationship (Jury, 1983)

$$M_L(t)=\frac{1}{2}erfc\left[\frac{\ln(t)-\mu}{\sqrt{2}}\right] \tag{4}$$

in which μ [ ] is the mean of log transform of the travel time, ln(t), σ is the standard deviation of ln(t). Fitting of Eq. [4] to observed data to obtain μ and σ constitutes the second approach. The third and final approach makes use of time moment analysis to obtain the transport parameters from $M_L(t)$. The mean or expected travel time, E_{LT}, is given by (Kachanoski et al, 1992)

$$E_{LT}=\frac{\int_0^T[-dM_L(t)/dt]t\,dt}{A_{LT}} \tag{5}$$

while the variance of the solute travel time, $Var_{LT}(t)$, is given and by

$$Var_{LT}(t)=\frac{\int_0^T[-dM_L(t)/dt](t-E_{LT})^2\,dt}{A_{LT}} \tag{6}$$

where

$$A_{LT}=\int_0^T[-dM_L(t)/dt]dt \tag{7}$$

and represents the area under the breakthrough curve.

Differences between the three approaches lie in the assumptions made about the transport process. The CDE is essentially the far-field limit for solute transport. It assumes that v is the same at every location and differences in arrival time at an observation plane are due to random diffusion/dispersion processes. Thus, travel time of a solute particle to a depth z = L is assumed to be uncorrelated to its travel time in the next depth increment. In contrast, the CLT does not require any particular assumption about the underlying transport process, except that it is linear and stationary. Information on the transport process is implicit in the measured transfer function. At any particular location, v is constant with depth, but it varies in the horizontal plane. Thus, solute spreading at the field scale is attributed to the horizontal spatial variability in vertical transport velocity. Since the vertical solute velocity at any given location is constant with depth,

the horizontal spatial pattern of travel times to an observation plane at z = L is correlated with the spatial pattern of travel time in the next depth increment. The CLT can be used for all transport regimes and is not restricted to near- or far-field limits. However, because of the assumption of linearity and stationarity, this form of the CLT is not applicable to contaminants that exhibit nonlinear interactions with soil components, or to situations of transient water flow. In addition, it provides an integral description of transport from the surface to depth L and there are no provisions for either predicting transport to depths shallower or deeper than the measurement depth. The method of moment is a direct method and makes no assumption about the transport process. Moments can be used to determine parameters of any stable, linear process that can be represented by a transfer function. The n^{th} moment of $f_L(t)$ is given by

$$M_n = \int_0^\infty f_L(t) t^n \, dt \tag{8}$$

The mean travel time of the system is equal to the first moment, M_1; the second moment M_2 is a measure of the dispersion; while the third moment, M_3, is related to the skewness. The main problem with ordinary moments is that higher moments are unreliable due to magnification of small errors in the tail. Nevertheless, for a particular flow model, specific relations exist between the moments and the model parameters.

In each approach, the dispersivity was calculated from the fitted parameters. The dispersivity for the CDE, λ_{CDE}, was calculated as

$$\lambda_{CDE} = \frac{D}{\bar{v}} \tag{9}$$

An equivalent dispersivity for the CLT, λ_{CLT} was calculated as

$$\lambda_{CLT} = \frac{L}{2}[\exp(\sigma^2) - 1] \tag{10}$$

while from moment analysis method, λ_{MOM} was calculated as

$$\lambda_{MOM} = \frac{L}{2} \frac{Var_{LT}}{E_{LT}^{\ 2}} \tag{11}$$

Results

Saturated Hydraulic Conductivity

Figure 3 shows the mean K_s measured at 40-cm intervals along the surface and 1.5-m deep transects. The three high values at the proximal end of the two transects were likely due to poor surface contact and treatment as outliers can be statistically justified (Acton, 1966). Overall, the results show an unexpected similarity in K_s at the two depths. At the surface, measured K_s (minus the outlier at x = 1.6 m) was 0.0013 ± 0.0006 cm s^{-1}, while at z = 1.5 m, K_s was 0.0008 ± 0.0003 cm s^{-1}. An analysis of variance was performed to test the null hypothesis of no difference between K_s measured in the two transects (Snedecor and Cochran, 1980). The value of F was significant at the 1% level ($F^{**} = 7.82 < F[0.99;1,24]=8.25$). Thus, measured K_s are from two different populations or soil types.

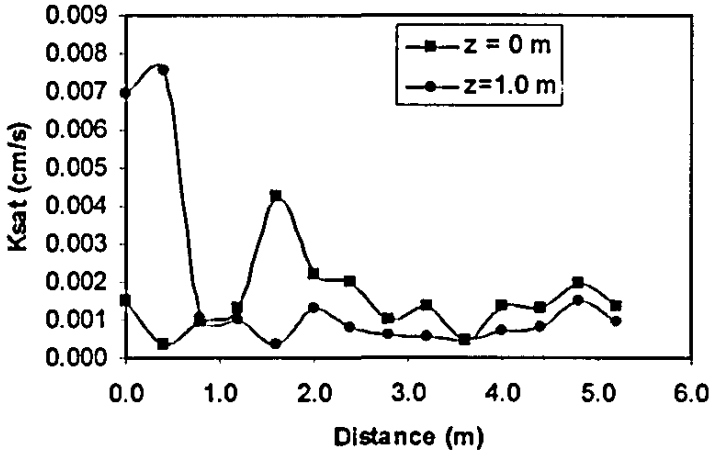

Figure 3. Mean saturated hydraulic conductivity measured along the surface and 1.5-m deep transects. Measurements were made using a tension infiltrometer at a head of -2 cm. Values at x =0 and 0.4 m (z = 0 m) and x=1.6 m(z=1.5 m) were treated as outliers in calculating the mean and variance of K_s.

Spatial Variation in Water Flux Density

An added advantage of using the TDR system for infiltration measurements is its ability to measure soil water storage, *W*, as a function of time, *t*. For a given probe length, *W(t)* is given

simply by $\theta(t) \cdot L$, where $\theta(t)$ is the water content averaged over the length of the probe. During the time before the wetting front first reaches a depth L, the derivative of cumulative W with respect to time should be equal to the water flux at the soil surface, assuming no plant water uptake or evaporation (Parkin et al., 1992). Thus, spatial variation in water flux density, from which the variation in infiltration rates can be inferred, can be determined from early time measurements of $W(t)$.

Figure 4 shows the W(t) (L =0 .25 m; x=0 m) and the linear relationship fitted at early time. The rate of application at the soil surface was 2.5×10^{-6} cm s^{-1}. The calculated flux is 3.95×10^{-5} cm s^{-1}, an indication of the variability in the hydraulic conductivity.

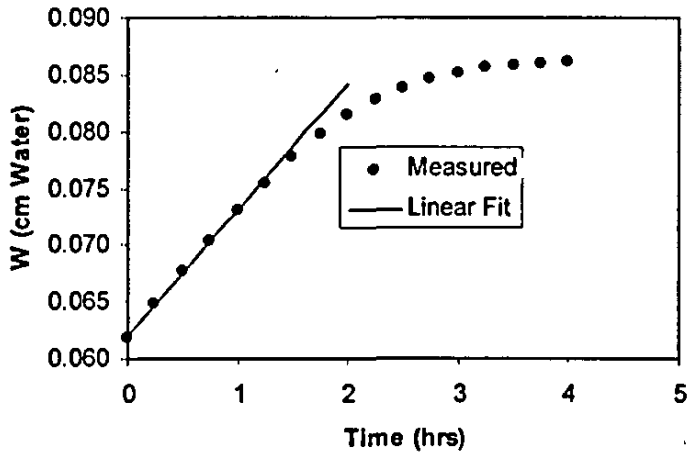

Figure 4. Cumulative storage versus time with a 25-cm probe at x = 0 m. The solid line shows a linear fit used to determine water flux density.

Figure 5 shows the distribution of flux along the transect based on measurements at the 25-cm depth. This result show that even under a constant flux of water at the surface, the actual infiltration rate can be quite variable. The local-scale average (an average of the 24 measurements) is 2.38×10^{-6} cm s^{-1}, while the field-scale average (valued fitted to the average $W(t)$ curve) is 2.61×10^{-6} cm s^{-1}. Similar increases in flow and transport properties from the local scale to the field scale have been made by other researchers (e.g. Kachanoski et al., 1990). The increase from the local scale to field scale is related to the scale dependence of the lateral

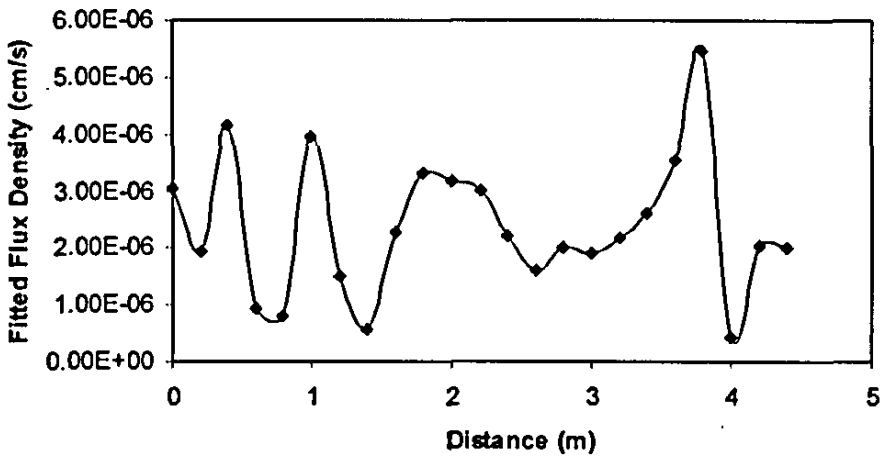

Figure 5. Spatial variation in measured surface flux density. Measurements were made with a 25-cm probe.

variations in water flux density. In this case, most of the variation can probably be explained by the distribution of sagebrush root channels (many of which were present) and micro-topography.

Water Retention Properties

Figure 6 shows the field-averaged moisture characteristic and the fitted van Genuchten relationship for the plot. Figures 7 through 11 show the plots of the individual depths. These data represent mostly imbibition data, collected as the profile was wetted to steady state at each flux of interest. There are some desorption data, mostly obtained between wetting cycles as maintenance was performed on the system. There was generally very little drainage during these periods and the data are not obvious from the plots.

As seen from the data presented, there are not many measurements at matric suctions greater than around 500 cm. The profile remained relatively wet following the first experiment, except very near the surface. In addition, most of the joints between the transducer and tensiometer failed at suctions greater than 400 to 500 cm.

Figure 6 shows that the data can be treated as essentially one population, suggesting some degree of homogeneity. To determine whether there was any advantage to be gained from treating the data otherwise, the measurements were separated out by depth interval and the

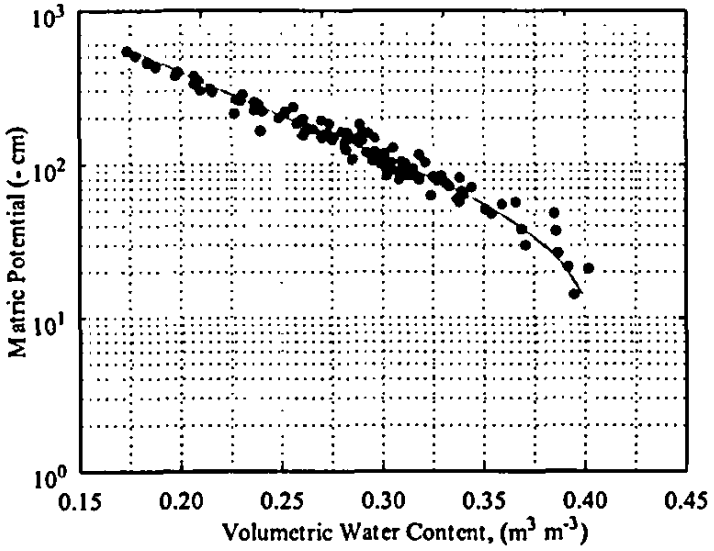

Figure 6. Fitted and observed field-averaged moisture characteristic function. This plot includes measurements from all depth intervals.

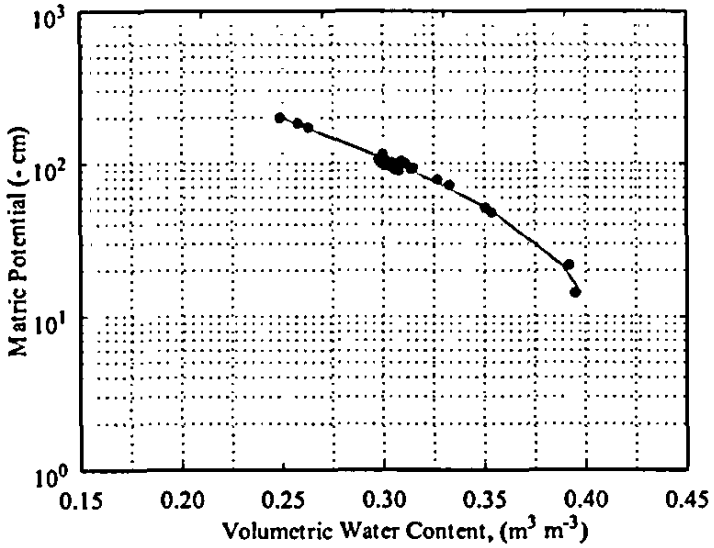

Figure 7. Fitted and observed field-averaged moisture characteristic function for the 0-25 cm depth.

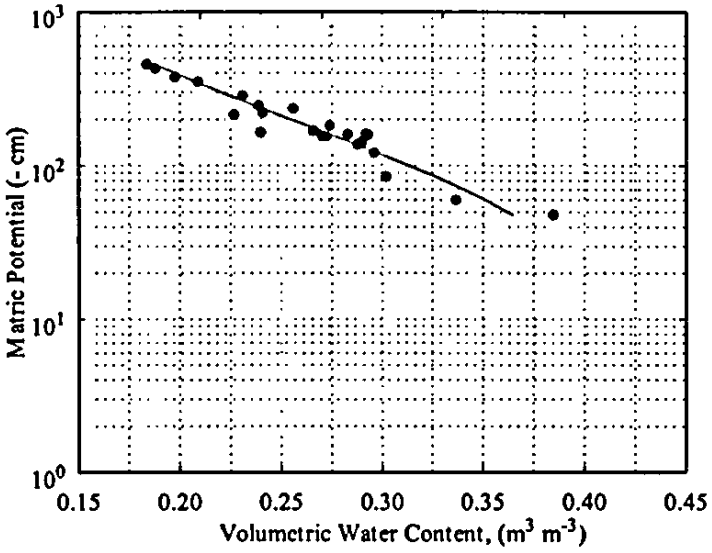

Figure 8. Fitted and observed field-averaged moisture characteristic function for the 25-50 cm depth.

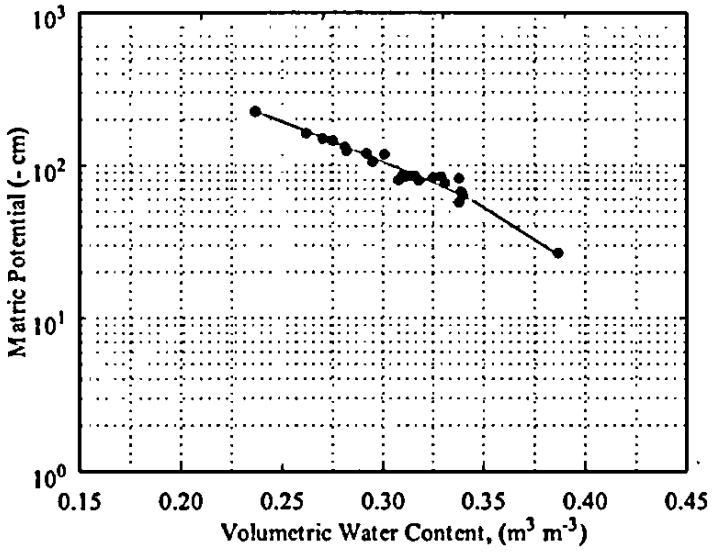

Figure 9. Fitted and observed field-averaged moisture characteristic function for the 50-75 cm depth.

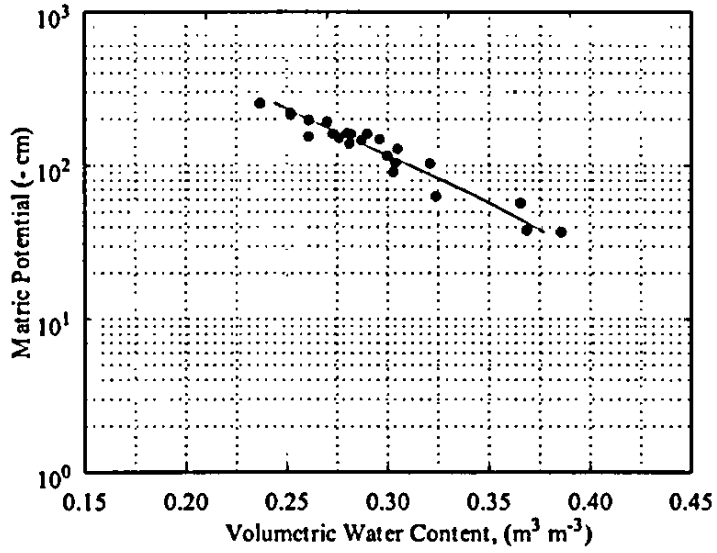

Figure 10. Fitted and observed field-averaged moisture characteristic function for the 75-100 cm depth.

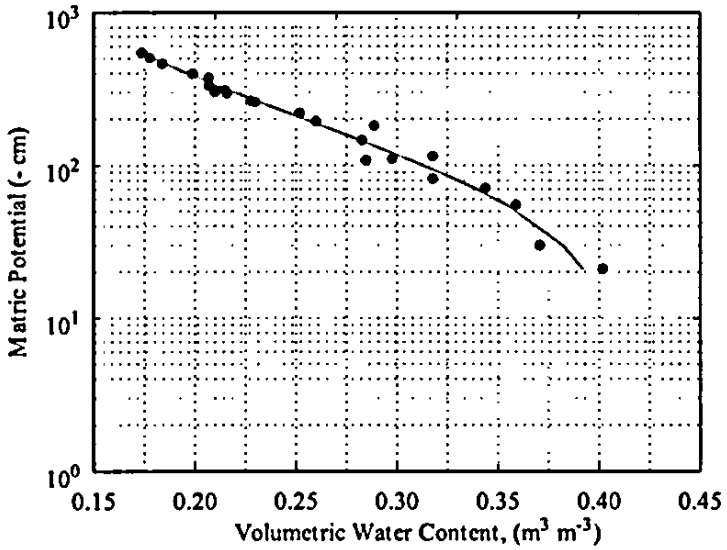

Figure 11. Fitted and observed field-averaged moisture characteristic function for the 100-125 cm depth.

Table 1. A comparison of Fitted Moisture Retention Parameters.

Sample	Depth (m)	Fitted Parameters				Measured K_s (cm s^{-1})
		θ_r	θ_s	α (cm^{-1})	n	
1[a]	1.5	0.0187	0.4131	0.148	1.309	$5.73x10^{-4}$
2	1.5	0.0336	0.3367	0.0211	1.536	$5.73x10^{-4}$
299-E24-95[b]	1.83	0.000	0.3550	0.0061	1.538	$1.40x10^{-4}$
Task 4b[c]	0-0.25	0.007	0.3566	0.1554	1.724	Not measured
	0.25-0.50	0.007	0.3863	0.0741	1.595	Not measured
	0.50-0.75	0.029	0.4215	0.0381	2.468	Not measured
	0.75-1.0	0.035	0.4083	0.0355	2.036	Not measured
	1.0-1.5	0.024	0.3980	0.0290	2.497	Not measured
Task 4c[d]	0-0.25	0.00	0.3172	0.0015	2.024	$8.37x10^{-4}$
	0.25-0.50	0.00	0.4163	0.0162	1.400	Not measured
	0.50-0.75	0.00	0.4164	0.0139	1.419	Not measured
	0.75-1.0	0.00	0.4403	0.0256	1.303	Not measured
	1.0-1.25	0.00	0.4089	0.0127	1.433	Not measured
	Plot Avg.	0.00	0.4117	0.015	1.390	Not measured

(a) Khaleel and Freeman (1995), from the former Grout Site, on the east side of the 200E Area.
(b) Khaleel et al., (1995), one of 15 repacked, 5.1-cm diameter cores.
(c) Surface sediments values are plot averages for each depth interval with 24 samples.
(d) This experiment, values are plot averages for each depth interval with 24 samples.

parameters fitted for each depth. The van Genuchten parameters θ_r, α, n, and θ_s were all fitted and are summarized in Table 1. Table 1 also compares these results with those from the surface sediments and from a set of independent measurements conducted on cores.

The results from this study (Task 4c) compare reasonably well with the previous results, falling within the range of values observed on samples 1 and 2 from the former Grout Site (Khaleel and Freeman, 1995). However, the fitted parameters suggest soil of a somewhat finer texture than expected for this site. As further verification of the field-measured properties, soil samples were taken from the pit on completion of the infiltration experiments and an analysis of particle sizes performed in the laboratory. Results of the analysis show a mean distribution 70.6% sand, 17.7% silt and 11.6% clay. The high silt and clay content may explain the low values of n and α observed in this study.

Solute Transport Parameters

Figure 12 shows the TDR-measured relative mass flux, M(t), at L=0.25 m. The variability in transport, even at such a shallow depth is clear. This behavior is consistent with the variability in water flux density and K_s observed at the surface.

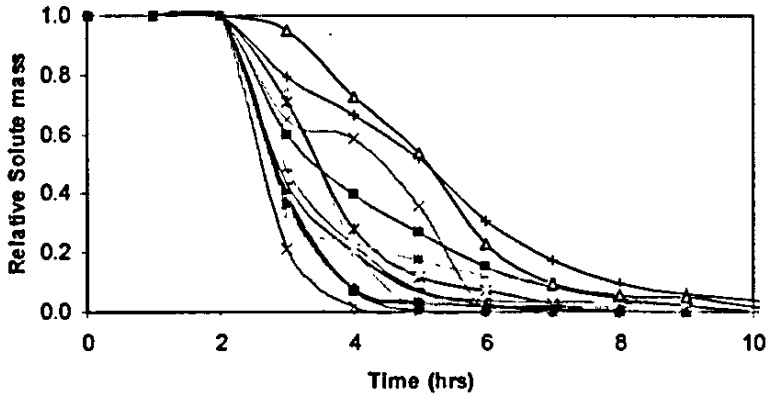

Figure 12. Spatial variability in TDR-measured relative solute mass flux at a depth of 0.25 m. Twenty four measurements were obtained along a 5 m transect at 0.20 m intervals.

Figure 13 shows an example of the observed data, and the fitted results obtained with the CDE and CLT transport models. In both cases, the models diverge from the observed data at late time ($t \geq 5$ hrs), leading to a higher predicted dispersion coefficient and travel-time variance. Although the discrepancy is not large, it suggests that these models may not be the most appropriate for predicting field-scale solute transport.

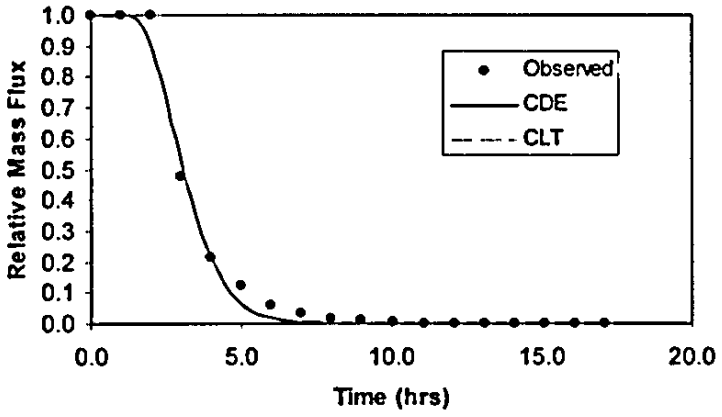

Figure 13. Example of $M_L(t)$ and the least squares fit of the convective dispersion equation (CDE) and convective lognormal transfer function (CLT) models.

Figure 14 shows an example of the solute travel time probability density function obtained by taking the first derivative of an M(t) curve. Theoretically, the area under $f_L(t)$ should equal exactly 1.0, provided all of the solute mass applied can be accounted for. In most cases, the value was less than 1.0, suggesting that either some of the solute may have moved beyond the measurement depth without being detected (preferential flow); moved laterally; or experienced some other delay in vertical transport. The long tails observed in Figure 12 support the hypothesis of delayed vertical movement. The results of the transport analysis are summarized in Table 2.

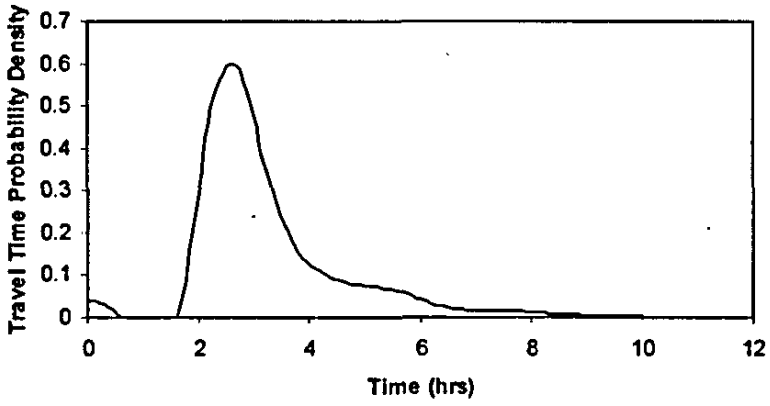

Figure 14. Solute travel time probability density function obtained by taking the first time derivative of the relative mass flux shown on Figure 13.

Table 2. Parameter estimates for the upper Hanford Formation from field transport experiments. D and v are the dispersion coefficient and pore water velocity of the convective dispersion equation (CDE); μ_p and σ_p are the population mean and variance of the convective lognormal transfer function (CLT); M_1 and M_2 are the expected travel time and travel time variance obtained by moment analysis; and λ_{CDE}, λ_{CLT} and λ_{MOM} are the dispersivities obtained by the three techniques.

		CDE				CLT			MOM		
L	θ_v	D	v	λ_{CDE}	t_L	μ_p	σ_p	λ_{CLT}	M_1	M_2	λ_{MOM}
m	m^3/m^3	Cm^2/h	cm	cm	h	h	h^2	cm	h	h^2	cm
0.25	0.331	10.79	8.14	1.32	3.07	3.23	0.106	1.39	3.43	1.98	2.03
0.50	0.312	11.74	8.64	1.36	5.78	5.95	0.056	1.44	6.03	3.88	2.67
0.75	0.294	42.40	9.18	4.62	8.17	8.29	0.12	4.79	8.44	9.59	5.05
1.00	0.283	66.61	9.54	6.98	10.48	10.75	0.137	7.32	10.85	16.88	7.17
1.25	0.283	66.04	9.54	6.92	13.10	13.78	0.112	7.44	13.95	24.32	7.81

Generally the CDE and CLT models predict the same average transport velocity, but differ in their predicted dispersion or degree of solute spread. A useful comparison of the CDE and CLT

has been given in terms of the existence or absence of correlated travel times with depth (Jury, 1982). For uncorrelated flow, the CDE predicts a linear increase in travel time variance with depth. For correlated flow, the CLT predicts an increase in travel time variance as the square of the distance. By comparing the results of the analysis, conclusions can be made on the appropriateness of different transport models.

The CDE, CLT and moment analysis shows reasonably good agreement in the transport parameters. All three methods predict essentially the same mean travel times to the depths of interest. Travel time was linear with depth, except for a small decrease (increase in v) that corresponded to a decrease in θ_c. This is probably due to increasing coarseness of the soil with depth.

The change in travel time variance with depth show that M_2 at the 0.50-m depth was 2 times that at the 25-cm depth, while M_2 at 100 cm was 4 times that at 50 cm. The 2x increase from 25 cm to 50 cm does not meet the criterion for correlated flow required by the CLT model but satisfies the 2x increase required for uncorrelated flow described by the CDE (Jury, 1982). In general, a 4x increase in variance requires constant velocity with depth, which does not exist initially, but becomes more so at greater depth. A CDE approach would be appropriate for modeling transport in this soil.

Table 2 also shows generally good agreement in the dispersivities obtained with the two models. However, λ_{MOM} was almost double the α_{CDE} and α_{CLT}, particularly at the smaller depths. The higher λ_{MOM} values reflect the larger travel time variance used in their derivation. Nevertheless, the range $1.32 \geq \lambda \geq 2.67$ cm observed in the shallow depths is comparable to the $0.01 \geq \lambda \geq 2.0$ cm reported for unconsolidated cores by Freeze and Cherry (1979). Another point worth noting is the increase in λ with depth down to 0.75 m, after which it essentially becomes constant. This result is consistent with the concept of a scale-dependent dispersivity and suggests for vertical transport in this soil, the scale over which λ becomes constant may be smaller than predicted from literature values obtained from horizontal transport in the saturated zone. With respect to upscaling and the extrapolation of data from one site to the next, these observations suggest a need for site-specific transport measurements at a range of scales and concomitant measurements of $\psi(\theta)$ in the same transport volume.

Summary and Conclusions

Field-measured hydraulic properties have been shown to be more representative of natural flow and transport processes but are generally difficult to measure. In this study, it was shown that vertically-installed time domain reflectometry (TDR) probes, when combined with a sprinkler-imposed constant flux system, can be used to measure the spatially variable hydraulic properties. The infiltration rate, when combined with the measured equilibrium water content and matric potential, provide direct measurements of the moisture characteristic function, $\psi(\theta)$, and the unsaturated hydraulic conductivity function, $K(\theta)$ at the field scale.

A series of infiltration tests were conducted at the site of the proposed LLTWDS during the summer of 1998. Measurements of K_s were made using a tension infiltrometer. The spatial distribution of K_s and water flux density determined from water storage measurements appear to be related to micro-topogrpahy and root channels.

Saturated water content and the other van Genuchten parameters, α, n, and θ_r were fitted with the program RETC. The goodness of fit was generally good with coefficients of determination (r^2) all exceeding 0.95.

The fitted mean saturated water content ranged from 0.3172 $m^3\ m^{-3}$ to 0.440 $m^3\ m^{-3}$, increasing slightly with depth. Neither the fitted α nor n showed any dependence on depth. Both parameters were less variable than those observed for the surface sediments.

Solute transport parameters were also obtained field measurements using KCl as a tracer. Analysis of the data using the traditional CDE and the less common CLT models, as well as with moment analysis, showed reasonably good agreement in the transport parameters. The three methods predicted the same mean travel times. Fitted dispersivities also showed good agreement between methods and are within the range observed on unconsolidated cores. Dispersivity also increased with depth down to 0.75 m, after which it essentially became constant. This result suggests a scale-dependent dispersivity, which in this soil appears to be somewhat smaller than predicted from measurements in the saturated zone.

This test has resulted in a data set that can be used the development of a catalogue of hydraulic and transport properties, one that will be amenable to geostatistical analysis and will facilitate the testing of upscaling theories. Comparisons of the data from this study with those from previous studies show remarkable similarity.

References

Acton, F. S. 1966. Analysis of straight-line data. Dover Publications Inc. New York., pp 224-229.

Freeze, R. A., and J. A. Cherry. 1979. Groundwater. Prentice Hall, NJ.

Jury, W.A., 1982. Simulation of solute transport using a transfer function. Water Resour. Res. 38:363-368.

Kachanoski, R.G., C. Hamlin, and I. J. van Wesenbeeck. 1990. Spatial variability of water and solute flux in a layered soil. *In* Roth, K., H. Fluhler, H., W. A. Jury, and J. C. Parker (Eds.) Field-scale water and Solute Flux in Soils, . Birkhauser Verlag, Basel.

Kachanoski, R. G., A. L. Ward, and I. J. van Wesenbeeck, 1994. Measurement of Transport Properties at the Field Scale. Transactions of the 15th World Congress of Soil Science. Vol. 2a:106- 126.

Khaleel, R, and E. J. Freeman, 1995. Variability and scaling of hydraulic properties for 200 Area soils, Hanford Site. WHC-EP-0883, Westinghouse Hanford Company, Richland, Washington.

Khaleel, R., J. F. Relyea, and J. L. Conca. 1995. Evlauation of van Genuchten-Maulem relationships to estimate unsaturated hydraulic conductivity at low water contents. Water Res. Resour. 31:2659-2668.

Parkin, G.W., D. E. Elrick, and R. G. Kachanoski. 1992. Cumulative storage of water under constant flux infiltration: Analytical solution. Water Resour. Res. 28:2811-2818.

Snedecor, G.W., and W.G. Cochran. 1980. Statistical methods. Iowa State University Press, Iowa, 507 pp.

van Genuchten, M. Th., 1980. A closed form equation for predicting the hydraulic conductivity of unsaturated soils. Soil Sci. Soc. Am. J. 44: 892-989.

van Genuchten, M. Th., F. J. Liej, and S.R. Yates.1991. The RETC code for quantifying the hydraulic functions of unsaturated soils. EPA/6000/2-91/065. 93 pp. R.S. Kerr Environ. Res. Lab., U.S. Environmental Protection Agency, Ada, OK.

Ward, A.L., R.E. Clayton and J.C. Ritter. 1997. Fabrication and Testing of an Integrated Soil Water Content-Matric Potential Probe. A letter report for activity S1W03490 submitted to the Lockheed Martin Hanford Company, September 1997.

Ward, A.L., R.E. Clayton and J.C. Ritter. 1998. Hanford Low-Activity Tank Waste Performance Assessment Activity: Determination of In Situ Hydraulic Parameters of Hanford Sediments A letter report for activity Task 4b submitted to the Lockheed Martin Hanford Company, September 1998.

Zhang, R., 1997. Infiltration models for the disc infiltrometer. *Soil Sci. Soc. Am. J.* 61:1597-1603

APPENDIX F

PHYSICAL AND HYDRAULIC MEASUREMENTS OF FY1998 CLASTIC DIKE SAMPLES

This page intentionally left blank.

Physical and Hydraulic Measurements of FY 1998 Clastic Dike Samples

MJ Fayer and JS Ritter
19 March 1999

Introduction

Pacific Northwest National Laboratory (PNNL) assists the Lockheed Martin Hanford Company (LMHC) in designing and assessing the performance of disposal facilities for radioactive wastes stored in single and double shell tanks at the Hanford Site. To predict contaminant migration from these facilities requires estimates of the physical and hydraulic properties of sediments within the vadose zone beneath and around the disposal facility. An unusual feature of the Hanford Site is the presence of vertical sediment structures known as clastic dikes in all of the major lithologies of the unsaturated zone. Fecht et al. (1998)[1] discussed dike structure and etiology and summarized some of the measurements that have been made.

Because clastic dikes could impact the performance of the ILAW disposal site, a work plan was prepared that provides details on the measurement and analysis of clastic dikes (Khaleel 1998)[2]. As part of the work plan, a PNNL task was initiated, entitled "Hydraulic Property Lab Tests for ILAW Samples." One objective of this task is to provide the measured data for clastic dike samples. Samples were obtained in fiscal year 1998 for characterization. The objective of this letter report is to document the physical and hydraulic properties of the clastic dike samples.

Properties

Physical and hydraulic properties are required for the clastic dike samples and the samples of the surrounding matrix. Multiple measurements of these properties are required to give some estimate of the degree of variability within each geologic material. The properties are:

Particle Size Distribution. Particle size distribution (PSD) refers to the fractions of the various particle-size classes (e.g., the fraction of particles with diameters between 1 and 2 mm).

Particle Density (ρ_p). Particle density is the mass of the sediment or construction material particles per unit volume of the same sediment or material. This property is used to relate the bulk density to the porosity.

Bulk Density (ρ_b). Bulk density is the mass of oven-dry material per unit bulk volume. The unit bulk volume is the combined volume of material, water, and air prior to oven drying.

Porosity (ϕ). Porosity is the volume of voids per unit bulk volume.

---

[1] Fecht, KR, KA Lindsey, BN Bjornstad, DG Horton, GV Last, and SP Reidel. "An atlas of clastic injection dikes of the Pasco Basin and Vicinity," BHI-1103 Draft A, Bechtel Hanford Inc., May 1998.

[2] Khaleel R, January 1998. "Work plan for measurement and analysis of hydraulic properties for clastic dikes and the ILAW Borehole No. 1 sediment samples," Fluor Daniel Northwest, Inc., P.O. Box 1050, Richland, Washington.

Water Retention. Water retention refers to the retention of water by the sediment at various matric potentials. Mathematical functions are fit to the retention data and the resulting parameters are used directly in computer models for predicting water and contaminant movement. Numerous functions are available, but the van Genuchten function is most commonly used:

$$\theta = \theta_r + (\theta_s - \theta_r)\left[(1 + (\alpha h)^n\right]^{-m}$$

where θ_s = saturated water content (cm^3/cm^3)
θ_r = residual water content (cm^3/cm^3)
h = matric potential (-cm)
α, n, m = empirical fitting parameters (α units are 1/cm; n and m are dimensionless)

Typically, m is approximated as $m = 1 - 1/n$

Saturated Hydraulic Conductivity (K_s). Saturated hydraulic conductivity is the proportionality constant in the Darcy equation that relates the flux density to a unit potential gradient.

Unsaturated Hydraulic Conductivity [$K = f(\theta, \psi)$]. Unsaturated hydraulic conductivity is the proportionality factor in the Richards equation that relates the flux density to a unit potential gradient at a specific water content. Because the water content varies in the unsaturated zone, the unsaturated conductivity varies also.

Mathematical functions are used to represent the unsaturated conductivity data; these functions are typically estimated using the water retention functions and saturated conductivity. When measured unsaturated conductivity values are available, the conductivity and retention data can be fit to optimize both the retention and conductivity functions. Several functions are available, but the Mualem conductivity function is most commonly used (in conjunction with the van Genuchten retention function, assuming $m = 1 - 1/n$):

$$K = K_s \frac{\left\{1 - (\alpha h)^{n-1}\left[1 + (\alpha h)^n\right]^{-m}\right\}^2}{\left[1 + (\alpha h)^n\right]^{\ell m}}$$

The K_s value and the pore interaction term (ℓ) are the only requirements for this model. The parameter ℓ is typically assigned a value of 0.5.

Clastic Dike Samples

In March 1998, grab samples were collected from clastic dikes near the towns of Touchet and Lowden, WA (sites identified by Fecht et al. as No. 64 Touchet Road and No. 76 West Lowden). These samples were processed only for particle density and size distribution because of their small size and disturbed nature.

In September 1998, core samples were collected from a clastic dike and surrounding matrix at the Goose Egg site described by Fecht et al. (1998); this site is 6.3 km south-southwest of the ILAW Disposal Site. Two-foot long core liners were constructed from 3.0 in. ID PVC. One end of each liner was sharpened and placed on selected spots, either on a dike or the matrix. A sledge hammer was used to sink the liner into the sediment. The liners did not penetrate very easily and we could see broken, loose material on the top of the sample. The liners were brought back into the laboratory and sectioned into 6-in. lengths, starting with the sharpened end, which was deepest and least affected by the disturbance at the top of the liner. A total of seven undisturbed sections of these lined cores were identified as suitable for testing. All cores were taken from near surface (< 1 m) deposits within 10 m of Army Loop Road. Table 1 lists the sample numbers, depths, and diameters.

Methods

The core samples were tested with the multistep and steady-state methods, then sectioned for the tests of particle size distribution, particle density, and water retention using pressure plates and vapor adsorption. The cores were prepared for the multistep and steady-state tests according to the procedures described by Fayer et al. (1998)[3].

Procedures

Table 2 lists the procedures used to analyze the samples. Additional details for each procedure are discussed below. These additional details are almost exactly the same as those used by Fayer et al.

Particle Density. Two replicates of the particle density test were performed using the pycnometer method (Blake and Hartge 1986a). The Touchet and Lowden sample size was 10 g. For the Goose Egg samples, the entire core was homogenized following the bulk density test. Of this loose material, 8 to 28 g was used for the particle density test. The only deviation was for sample 4A. Because it was so heterogeneous, sample 4A was sub-sampled in three distinctly different regions. Each subsample was tested for particle density.

[3] Fayer MJ, AL Ward, JS Ritter, and RE Clayton, 1998. "Physical and hydraulic measurements of FY 1998 borehole cores," Letter Report to Mr. Fred Mann, Fluor Daniel Northwest, September 10, 1998.

Table 1. Clastic dike samples analyzed in fiscal year 1998.

Sample ID	Description of Sample	Core Internal Diameter in.	Location of Clastic Dike
1h	infill	na	Touchet
2h	infill	na	Touchet
3h	infill	na	Touchet
4h	infill	na	Touchet
5h	silt/clay skin	na	Touchet
6h	silt/clay skin	na	Touchet
7h	infill	na	Lowden
8h	matrix	na	Touchet
1	matrix, some dike/sand bands	3.0	Goose Egg Hill Site
2A	matrix	3.0	Goose Egg Hill Site
2B	matrix	3.0	Goose Egg Hill Site
3A	dike/matrix mix	3.0	Goose Egg Hill Site
3B	dike/matrix mix	3.0	Goose Egg Hill Site
4A	mostly dike	3.0	Goose Egg Hill Site
4B	mostly matrix, some dike	3.0	Goose Egg Hill Site

Table 2. Procedures for measuring physical and hydraulic properties.

Number	Title	Comment
PNL-MA-567, SA-2	Sieve Procedure	For materials > 50 μm effective diameter
PNL-MA-567, SA-3	Particle-Size Analysis	Hydrometer method for materials < 50 μm effective diameter
PNL-MA-567, SA-4	Constant Head Hydraulic Conductivity (HC)	Laboratory measurement for materials with HC> 10^{-6} cm/s
PNL-MA-567, SA-5	Falling Head–Saturated Hydraulic Conductivity (HC)	Laboratory measurement for materials with HC <10^{-6} cm/s
PNL-MA-567, SA-6	Water Retention Procedure	Laboratory method for core or bulk sample (saturation to air dry)
PNL-MA-567, SA-7	Water Content	Necessary for constant head hydraulic conductivity
PNL-MA-567, SA-8	Clod Density/Bulk Density	Necessary for constant head hydraulic Conductivity
PNL-MA-567, SA-9	Determining Particle Density	Necessary for constant head hydraulic conductivity
Klute (1986)	Water Retention: Laboratory Methods	Pressure plate and vapor adsorption methods
Klute and Dirksen (1986)	Hydraulic Conductivity and Diffusivity: Laboratory Methods	Steady-state flux control method for unsaturated conductivity
Eching and Hopmans (1993)	Unsaturated Hydraulic Properties	Multistep outflow method for unsaturated conductivity and water retention estimation

Particle Size Distribution. The PSD test was performed using the methods ASTM 1985 and Gee and Bauder (1986). The Touchet and Lowden sample size was 40 g. For the Goose Egg samples, the entire core was homogenized following the bulk density test. Of this loose material, 80 g was used for the particle size distribution test. The only deviation was for sample 4A. Because it was so heterogeneous, sample 4A was sub-sampled in three distinctly different regions (as mentioned previously). Each subsample was tested for particle density.

Bulk Density. A single measurement of bulk density was made for each intact Goose Egg core. Following the conductivity test, the sediment in the core was oven dried and weighed. Dividing this weight by the volume of the core yielded the bulk density, as per the method of Blake and Hartge (1986b).

Porosity. A single estimate of porosity was made using the bulk density of intact Goose Egg cores and the average particle density. The formula used was $\phi = 1 - \rho_b/\rho_s$ (Freeze and Cherry 1979).

Water Retention. Water retention data for the Goose Egg samples were measured using the pressure-plate extraction and vapor equilibrium methods described by Klute (1986). The tests were conducted on the subsample created after the bulk density core was homogenized. For sample 4A, separate tests were conducted for the three subsamples mentioned previously. Additional retention measurements were obtained during the unsaturated conductivity tests.

Saturated Hydraulic Conductivity. Saturated hydraulic conductivity for the Goose Egg cores was measured on the intact cores prior to the unsaturated conductivity tests using the method of Klute and Dirkson (1986). The measurement of saturated conductivity was conducted several times to verify that a steady value of conductivity was achieved.

Unsaturated Hydraulic Conductivity. The multistep and steady state methods were used to measure unsaturated conductivity of the Goose Egg cores. Both methods were performed on the same core using the same sensor locations. The multistep method, which is an improvement of the one-step method of Kool et al. (1985 a,b), provides θ-ψ pairs and cumulative outflow. These data were used in conjunction with the SFOPT program (a modified version of the MULSTP program of Eching and Hopmans 1993) to determine the optimal set of hydraulic parameters.

Because several tests must be performed on the same core, the following test sequence was established: saturated conductivity, multistep unsaturated conductivity, and steady state unsaturated conductivity. Following the saturated conductivity test, the cores were re-wetted to saturation and analyzed using the multistep method. After equilibrating the cores with zero pressure at the lower plate, three pressure increments were used that were equivalent to head values of 10.9, 71, and 315 cm. Following the multistep test, the cores were rewetted and tested using the steady-state method.

Results

When opened for the bulk density measurements, several cores had noticeable layering. The most dramatic layering occurred in sample 4A, in which it appeared that most of the sample was fine-textured dike material. Three sections of this core were sub-sampled for individual tests of particle density and size distribution, and water retention. These samples are referred to as 4A1, 4A2, and 4A3 in Tables 3, 4, 6, and 7.

Table 3 shows that particle density varies between 2.65 and 2.73 g/cm^3 for the various infill, clay skin, and matrix materials. There appears to be no distinction between infill, skin and matrix in the two locations studied. The particle densities of the three subsamples of 4A are identical.

Table 4 shows the results for both the sieve and hydrometer methods. In all samples, the gravel content was less than 1%. Figure 1 shows all of the data combined to highlight the degree of variability in particle size distribution. Included in Figure 1 are the distributions for dune sand from the southern edge of the ILAW site and sandy gravel from the Grout spoils pile. The clay skins and dike material have the finest particle size distribution. The infill material has a predominance of sand particles between 100 and 200 μm diameter, as does dune sand. Almost all of the infill material particles sizes are less than 500 μm, whereas about 20% of the dune sand particles are greater than 500 μm. The particle size distributions of the subsamples within 4A showed sand contents varying from 42 to 90%. These differences help to explain the water retention differences discussed below.

Table 5 shows that the bulk density ranged from 1.46 to 1.57 g/cm^3. Table 5 also shows the porosity data, which ranged from 0.424 to 0.464. These ranges are smaller than the variations observed by Fayer et al. for the FY 1998 ILAW borehole samples.

Table 6 shows the pressure plate data for four pressures. As expected, samples that had dike material had higher water contents at any given pressure. Within 4A, water content varied between 0.04 and 0.155 cm^3/cm^3 at a matric potential of -530 cm, and 0.024 and 0.089 cm^3/cm^3 at a matric potential of -4080 cm. These differences are large and will make it challenging to represent the properties of the entire core with the properties measured at discrete locations.

Table 7 shows that the vapor adsorption data covered a range of matric potential from -11,600 cm to as dry as -1,460,000 cm. The associated water contents ranged from 0.08 to 0.004 g/g. Most of the measurements are in the very low potential range. There are very few measurements in the range from -10,000 to -100,000 cm.

Table 8 shows the saturated hydraulic conductivity values for the Goose Egg Hill cores range from 1.8 x 10^{-4} to 5.4 x 10^{-3} cm/s. The matrix samples generally had the highest values. The results in Table 8 are consistent with other measurements. For the matrix at their dike sites, Fecht et al. measured K_s values that mostly ranged from 1 to 4 x 10^{-3} cm/s. The one sample that was different had a K_s value of 2 x 10^{-5} cm/s. This particular sample was measured with a different technique (i.e., the unsaturated flow apparatus, or UFA). For samples with various amounts of dike material and clays skins, Fecht et al. measured K_s values ranging from 5 x 10^{-5}

to 9 x 10^{-4} cm/s. The values in Table 8 fall within this range. Most of the values also fall within the lower portion of the range of values reported by Fayer et al. for the FY 1998 ILAW borehole samples. The lowest value in Table 8 (1.8 x 10^{-4}) is only slightly lower than the lowest ILAW borehole value (2.6 x 10^{-4}).

Table 9 shows the parameter estimates and fitting statistics determined using the SFOPT program with data from the multistep test. The parameter α varied from 0.0092 to 0.0839, a factor of about 10, and the parameter n ranged from 1.33 to 2.49. These ranges seemed small given the presence of fine-grained zones in some samples, but the statistics indicated reasonable fits to the data.

Some additional fitting tests were performed. To demonstrate the impact of the location of the tensiometer, sample 2A was refitted using the upper rather than lower tensiometer data. Of all the samples, sample 2A had the greatest differences in tension (about 40 cm) between the two tensiometer locations. The refitting reduced α by half (to 0.0342 cm^{-1}) and increased n by 33% (to 2.63). The R^2 was actually improved (from 0.747 to 0.894) and the mass error was reduced (from 1.51 to 0.59%). Outflow data represent the response of the entire sample, whereas the matric potential data are derived from a sample volume that could almost be considered a point. An assumption of the fitting process is that the material is homogeneous. With clastic dikes, the samples are not homogeneous, so point measurements are more likely to deviate from the expected values. The results from refitting sample 2A using the upper tensiometer data illustrate the parameter differences that could be encountered by using tension measurements elsewhere in the column. The matric potential sets from the other samples were much closer in value, so the differences in fitting results (between using the upper versus lower tensiometer data) should not be so large.

An additional fitting exercise was performed to demonstrate the impact of weighting the data. In this exercise, the matric potential and water retention weights were progressively reduced from 1.0 to 0.0 for sample 2A using the upper and lower tensiometer data. Figure 2 shows the sensitivity of the parameter estimates to the weighting used. Because tension is a point measurement, we may want to consider reducing the weight given to such data. One solution may be to weight the tension data according to the fraction of the sample volume that it measures.

The same fitting exercise using variable weighting was also performed for sample 3A using just the lower tensiometer data. The results were similar for most weights. The only exception was a weight of 0.0, which caused the program to terminate without a solution. In this case, the outflow data were not sufficient to allow the program to find an optimal solution.

Table 10 shows the θ-ψ-K triplets that were generated using the steady state method. All of the measurements are at matric potentials above -54 cm. Even so, unsaturated conductivity values were 1 to 2 orders of magnitude less than the saturated values. Because the potentials were so high, the water contents were also relatively high.

Summary

Samples were collected from clastic dike sites in the Columbia Basin in September 1998 and analyzed for physical and hydraulic properties. Eight disturbed samples were obtained from two sites in the towns of Touchet and Lowden, Washington. Seven undisturbed cores were obtained from a site near Goose Egg Hill, which is located 6.3 km SW of the ILAW site. Testing included particle density, particle size distribution, bulk density, water retention, and saturated and unsaturated conductivity. Saturated conductivity values were similar to values reported by Fecht et al. for other clastic dike samples. The samples exhibited some variability but not as much as reported by Fayer et al. for the ILAW borehole samples. The impacts of tensiometer location and data weighting were demonstrated.

Figure 2. Effect of data weighting on prediction of parameters α and n.

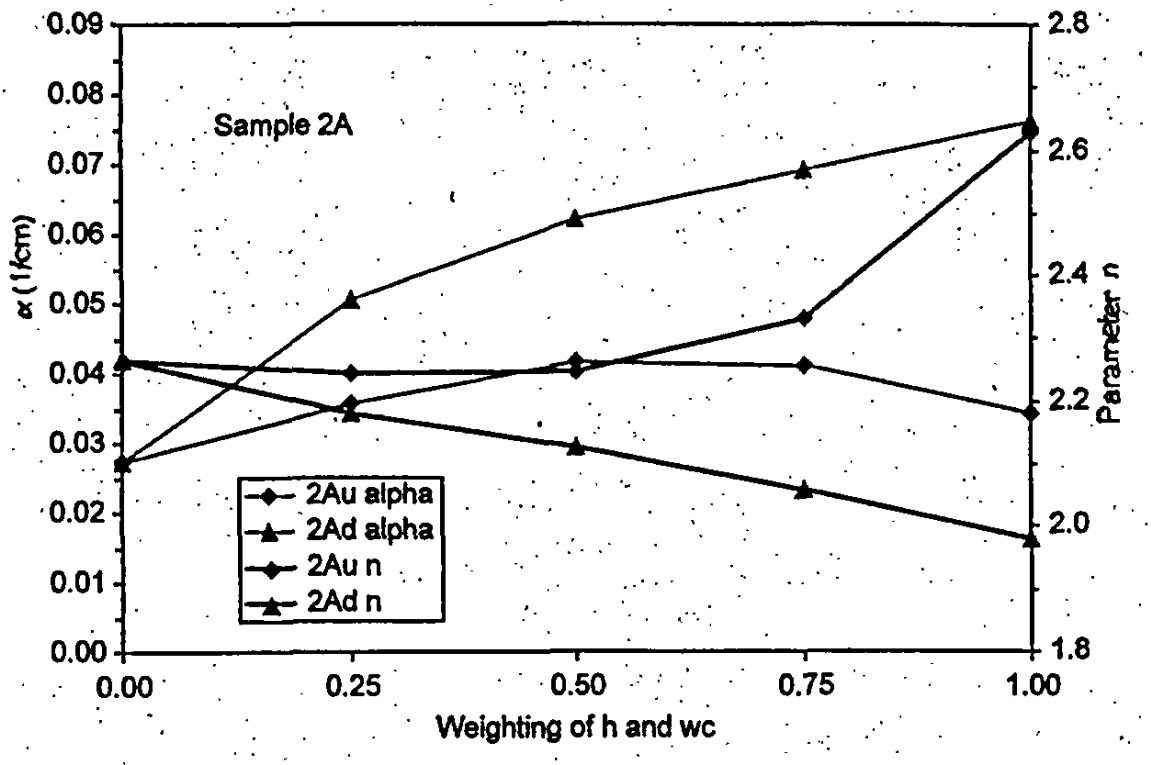

Table 3. Particle density

Sample	Particle Density rep 1 (g/cm^3)	Particle Density rep 2 (g/cm^3)	Average Particle Density, g/cm^3
1h	2.668	na	2.67
2h	2.677	na	2.68
3h	2.708	na	2.71
4h	2.698	na	2.70
5h	2.695	na	2.70
6h	2.651	na	2.65
7h	2.719	na	2.72
8h	2.681	na	2.68
1	2.729	2.734	2.73
2A	2.707	2.709	2.71
2B	2.713	2.709	2.71
3A	2.720	2.720	2.72
3B	2.722	2.722	2.72
4A1	2.717	2.730	2.72
4A2	2.720	2.727	2.72
4A3	2.720	2.727	2.72
4B	2.713	2.733	2.72

Table 4. Particle size distribution

Sample 1h		Sample 2h		Sample 3h		Sample 4h	
Particle Diameter (µm)	% Less Than Diameter	Particle Diameter (µm)	% Less Than Diameter	Particle Diameter (µm)	% Less Than Diameter	Particle Diameter (µm)	% Less Than Diameter
2000	100.0	2000	100.0	2000	100.0	2000	100.0
1000	100.0	1000	100.0	1000	100.0	1000	100.0
500	100.0	500	99.9	500	100.0	500	100.0
250	99.9	250	99.9	250	92.3	250	99.9
106	87.5	106	98.3	106	44.7	106	85.6
75	66.5	75	91.7	75	34.7	75	60.6
53	40.3	53	58.2	53	22.8	53	34.0
52.2	37.5	49.0	60.0	54.1	17.5	52.7	30.0
31.0	25.0	30.8	27.5	31.6	12.5	31.1	20.0
17.3	17.5	17.4	15.0	17.4	10.0	17.3	12.5
10.0	15.0	10.1	12.5	10.1	7.5	10.1	10.0
7.1	12.5	7.2	10.0	7.1	7.5	7.1	10.0
5.8	12.5	5.8	10.0	5.9	5.0	5.8	10.0
5.1	12.5	5.1	10.0	5.1	5.0	5.0	10.0
1.5	7.5	1.5	7.5	1.5	5.0	1.5	7.5

Sample 5h		Sample 6h		Sample 7h		Sample 8h	
Particle Diameter (µm)	% Less Than Diameter	Particle Diameter (µm)	% Less Than Diameter	Particle Diameter (µm)	% Less Than Diameter	Particle Diameter (µm)	% Less Than Diameter
2000	99.9	2000	100.0	2000	99.8	2000	100.0
1000	99.9	1000	100.0	1000	98.3	1000	99.9
500	99.9	500	100.0	500	90.3	500	99.7
250	99.9	250	100.0	250	42.3	250	99.4
106	98.0	106	99.7	106	18.0	106	93.7
75	94.3	75	99.4	75	15.7	75	81.4
53	84.9	53	97.8	53	13.3	53	48.7
46.6	75.0	44.2	95.0	54.5	12.5	50.6	47.5
27.9	62.5	26.4	85.0	31.5	12.5	31.1	22.5
15.9	47.5	15.3	67.5	17.4	7.5	17.5	10.0
9.6	32.5	9.2	52.5	10.1	7.5	10.2	7.5
6.8	27.5	6.7	42.5	7.1	6.2	7.2	7.5
5.6	25.0	5.5	37.5	5.8	5.0	5.9	7.5
4.9	22.5	4.8	35.0	5.1	5.0	5.1	7.5
1.5	10.0	1.4	17.5	1.5	5.0	1.5	5.0

Table 4. (cont.) Particle size distribution

Sample 1		Sample 2A		Sample 2B		Sample 3A	
Particle Diameter (µm)	% Less Than Diameter	Particle Diameter (µm)	% Less Than Diameter	Particle Diameter (µm)	% Less Than Diameter	Particle Diameter (µm)	% Less Than Diameter
2000	99.7	2000	100.0	2000	100.0	2000	100.0
1000	98.3	1000	100.0	1000	100.0	1000	100.0
500	93.2	500	99.9	500	99.9	500	99.6
250	83.5	250	95.7	250	96.1	250	89.8
106	38.9	106	17.5	106	12.0	106	35.1
75	30.8	75	7.3	75	5.9	75	18.4
53	25.6	53	4.5	53	4.2	53	10.5
51.3	24.8	56.7	5.6	56.6	6.0	55.1	11.3
30.7	17.9	32.9	4.8	32.8	5.0	32.6	5.6
17.2	13.8	18.0	4.4	18.0	4.0	18.0	4.4
10.1	10.6	10.4	4.0	10.4	3.5	10.4	4.0
7.2	8.8	7.4	3.8	7.4	3.5	7.4	3.5
5.9	8.8	6.0	3.8	6.0	3.5	6.0	3.1
5.1	8.5	5.2	3.5	5.2	2.8	5.2	2.8
1.5	4.8	1.5	3.5	1.5	2.5	1.5	2.5

Sample 3B		Sample 4A1		Sample 4A2		Sample 4A3	
Particle Diameter (µm)	% Less Than Diameter	Particle Diameter (µm)	% Less Than Diameter	Particle Diameter (µm)	% Less Than Diameter	Particle Diameter (µm)	% Less Than Diameter
2000	99.7	2000	100.0	2000	99.9	2000	99.8
1000	99.4	1000	99.9	1000	99.8	1000	99.6
500	98.6	500	99.8	500	99.7	500	99.4
250	90.4	250	93.6	250	98.2	250	97.1
106	44.4	106	13.9	106	71.5	106	60.3
75	25.6	75	9.6	75	63.0	75	50.6
53	18.8	53	7.4	53	56.1	53	42.8
53.2	18.8	56.0	7.5	45.2	47.0	46.9	41.3
31.8	11.3	32.4	6.9	28.3	34.1	28.7	31.3
17.7	7.5	17.9	5.6	16.2	25.7	16.5	22.5
10.3	6.5	10.3	4.8	9.6	21.3	9.8	16.5
7.3	5.0	7.3	4.0	nd	nd	7.0	15.0
6.0	5.0	6.0	3.8	5.7	13.8	5.8	12.5
5.2	4.8	5.2	3.8	5.0	13.8	5.0	12.3
1.5	3.5	1.5	3.1	1.5	7.5	1.5	7.5

Table 4. (cont.) Particle size distribution

Sample 4B	
Particle Diameter (μm)	% Less Than Diameter
2000	100.0
1000	99.8
500	99.1
250	64.8
106	8.1
75	6.0
53	4.9
56.3	6.3
32.8	4.4
18.0	3.8
10.4	3.1
7.4	3.1
6.0	2.8
5.2	2.8
1.5	2.5

Figure 1. Summary of particle size distributions for all samples, along with dune sand from the ILAW site and sandy gravel taken from the Grout Spoils pile.

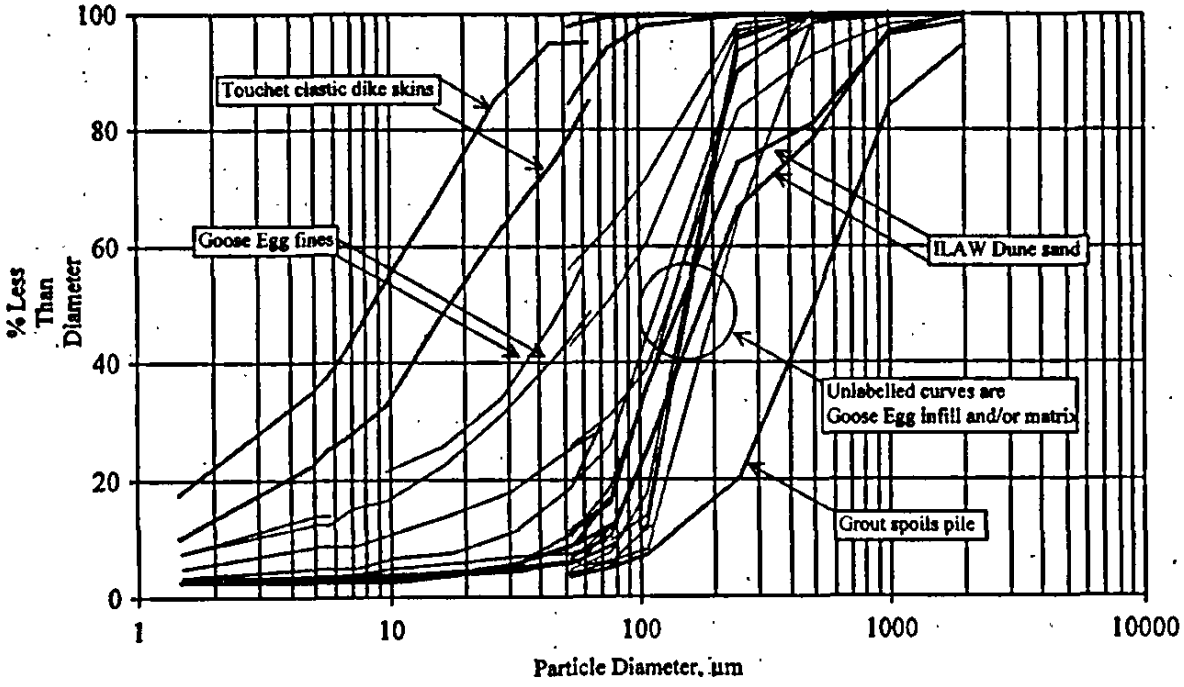

Table 5. Core volume, bulk density, and porosity data for the core samples.

Sample	Core Volume (cm^3)	Bulk Density (g/cm^3)	Porosity (cm^3/cm^3)
1	693	1.57	0.424
2A	684	1.50	0.446
2B	693	1.51	0.443
3A	689	1.46	0.464
3B	698	1.52	0.443
4A	698	1.49	0.454
4B	684	1.57	0.425

Table 6. Water retention data from the pressure plate technique for the core samples.

1		2A		2B		3A	
Matric Potential -cm	Water Content g/g	Matric Potential -cm	Water Content g/g	Matric Potential -cm	Water Content g/g	Matric Potential -cm	Water Content g/g
530	0.1001	530	0.0233	530	0.0339	530	0.0363
1010	0.1088	1010	0.0210	1010	0.0311	1010	0.0322
2040	0.0701	2040	0.0216	2040	0.0243	2040	0.0288
4080	0.0549	4080	0.0099	4080	0.0209	4080	0.0219

3B		4A1		4A2		4A3	
Matric Potential -cm	Water Content g/g	Matric Potential -cm	Water Content g/g	Matric Potential -cm	Water Content g/g	Matric Potential -cm	Water Content g/g
530	0.0678	530	0.0401	530	0.155	530	0.133
1010	0.0740	1010	0.0363	1010	0.149	1010	0.116
2040	0.0585	2040	0.0302	2040	0.125	2040	0.0901
4080	0.0450	4080	0.0242	4080	0.0887	4080	0.0722

4B	
Matric Potential -cm	Water Content g/g
530	0.0298
1010	0.0258
2040	0.0212
4080	0.0162

Table 7. Water retention data from the vapor adsorption technique for the core samples (measurements at potentials above -10,000 cm are uncertain and should be used with caution).

1		2A		2B		3A	
Matric Potential -cm	Water Content g/g	Matric Potential -cm	Water Content g/g	Matric Potential -cm	Water Content g/g	Matric Potential -cm	Water Content g/g
28182	0.033	258592	0.018	11648	0.022	121667	0.012
693204	0.012	262464	0.0073	22040	0.017	516971	0.007
1433126	0.009	533191	0.0071	286323	0.008	1018703	0.006
		891172	0.0059	1446643	0.004	1444671	0.005
		1442563	0.0045				

3B		4A1		4A2		4A3	
Matric Potential -cm	Water Content g/g	Matric Potential -cm	Water Content g/g	Matric Potential -cm	Water Content g/g	Matric Potential -cm	Water Content g/g
98149	0.016	361735	0.010	36699	0.041	19639	0.041
209007	0.011	1233979	0.005	56058	0.036	25367	0.039
326217	0.008	1367281	0.005	992535	0.015	1050295	0.012
1392767	0.005	1459642	0.004	1103810	0.014	1431458	0.010
1450243	0.005			1424506	0.013		

4B	
Matric Potential -cm	Water Content g/g
1395754	0.004
1466263	0.004
1428052	0.004

Table 8. Saturated hydraulic conductivity of the core samples.

Sample	Saturated Hydraulic Conductivity (cm/s)			Average Saturated Hydraulic Conductivity (cm/s)	Method
	Rep 1	Rep 2	Rep 3		
1	5.97E-04	5.97E-04	5.97E-04	5.97E-04	Constant head
2A	4.77E-03	4.97E-03	4.37E-03	4.70E-03	Constant head
2B	3.38E-03	3.06E-03	2.98E-03	3.14E-03	Constant head
3A	3.29E-03	3.58E-03	3.37E-03	3.41E-03	Constant head
3B	1.14E-03	1.14E-03	1.14E-03	1.14E-03	Constant head
4A	1.67E-04	1.96E-04	1.89E-04	1.84E-04	Constant head
4B	5.56E-03	5.40E-03	5.32E-03	5.43E-03	Constant head

Table 9. Parameters and statistics for the van Genuchten function fitted to data from the multistep method using SFOPT (θ_s and K_s were held constant at their measured values; θ_r was estimated for a ψ value of -15,300 cm from the pressure plate and vapor adsorption data; m=1-1/n; ℓ=0.5; matric potential values were from the lower tensiometer; all data were weighted by a factor of 1.0)

Sample	θ_s (cm^3/cm^3)	θ_r (cm^3/cm^3)	α (1/cm)	n (-)	R^2	Mass Balance Error, %
1	0.424	0.063	0.0839	1.33	0.878	2.37
2A	0.446	0.019	0.0762	1.98	0.747	1.51
2B	0.443	0.023	0.0741	1.84	0.815	1.47
3A	0.424	0.025	0.0143	2.49	0.985	0.67
3B	0.448	0.050	0.0593	1.54	0.860	1.48
4A	0.454	0.030	0.0092	1.97	0.968	0.79
4B	0.425	0.021	0.0823	2.09	0.836	1.60

Table 10. Water retention and unsaturated conductivity data for each sample during the steady state tests (nd = no data). Matric potential and water content values represent the average of sensors at two depths (approx. 4 and 11 cm) in the sample.

Sample	Matric Potential -cm	Water Content cm^3/cm^3	Unsaturated Hydraulic Conductivity cm/s
1	15.5	0.267	5.4E-5
1	40.2	0.250	2.9E-6
2a	25.6	0.259	2.0E-03
2a	45.3	0.156	1.3E-4
2b	33.9	0.354	1.0E-4
2b	34.2	0.352	1.0E-4
2b	52.6	0.331	3.7E-5
3a	33.3	0.220	2.7E-4
3a	53.9	0.207	8.1E-5
3a	53.3	nd	3.9E-5
3b	13.6	nd	1.5E-5
3b	48.0	0.293	1.4E-5
4a	19.5	0.365	8.9E-6
4a	22.2	nd	9.3E-6
4b	17.5	0.249	4.9E-5
4b	35.6	0.196	2.9E-5

References

American Society for Testing and Materials. 1985. "Standard Test Method for Particle-size Analysis of Soils. D 422-63 (1972)." 1985 Annual Book of ASTM Standards 04.08:117- 127. American Society for Testing and Materials, PA.

Blake GR, and KH Hartge. 1986a. "Particle Density." In Methods of Soil Analysis, Part 1, ed. A. Klute, pp. 377-382. American Society of Agronomy, Madison, WI.

Blake GR, and KH Hartge. 1986b. "Bulk Density." In Methods of Soil Analysis, Part 1, ed. A. Klute, pp. 363-375. American Society of Agronomy, Madison, WI.

Eching SO, and JW Hopmans, 1993. "Optimization of hydraulic functions from transient outflow and soil water pressure data," Soil Sci. Soc. Am. J. 57:1167-1175.

Freeze RA and JA Cherry, 1979. *Groundwater.* Prentice-Hall, Inc., Englewood Cliffs, NJ.

Gee GW and JW Bauder, 1986. "Particle-Size Analysis." In Methods of Soil Analysis, Part 1, ed. A. Klute, pp. 383-409. American Society of Agronomy, Madison, WI.

Khaleel R, and EJ Freeman, 1995. "Variability and scaling of hydraulic properties for 200 Area soils, Hanford Site, WHC-EP-0883, Westinghouse Hanford Company, Richland, Washington.

Klute A, 1986. " Water Retention: Laboratory Methods," In Methods of Soil Analysis, Part 1, ed A. Klute, pp. 635-662. American Society of Agronomy, Madison, Wisconsin.

Klute A and C Dirksen, 1986. "Hydraulic conductivity and diffusivity: Laboratory methods," In Methods of Soil Analysis, Part 1, ed A. Klute, pp. 687-734. American Society of Agronomy, Madison, Wisconsin.

Kool JB, JC Parker, and MT van Genuchten, 1985a. "Determining soil hydraulic properties from one-step outflow experiments by parameter estimation, I, Theory and numerical studies," Soil Sci. Soc. Am. J. 49:1348-1354.

Kool JB, JC Parker, and MT van Genuchten, 1985b. "Determining soil hydraulic properties from one-step outflow experiments by parameter estimation, I, Experimental studies," Soil Sci. Soc. Am. J. 49:1354-1359.

This page intentionally left blank.

APPENDIX G

QUALITY ASSURANCE/QUALITY CONTROL CONSIDERATIONS

This page intentionally left blank.

QUALITY ASSURANCE/QUALITY CONTROL (QA/QC) CONSIDERATIONS

This data package is based on data reported in Appendices A through F or taken from peer-reviewed, open literature. Data reported in Appendices A through C, E and F were collected by Pacific Northwest National Laboratories (PNNL), following applicable PNNL QA/QC procedures. Data reported in Appendix D were collected by Westinghouse Hanford Company Geotechnical Engineering Laboratory (GEL), following applicable GEL QA/QC procedures.

For the analysis of data collected in the laboratory and field, as well as those based on literature, a peer review procedure was established and followed. The peer review members were selected based on their experience and knowledge of specific subject areas. The internal peer review was provided per Fluor Government Group's internal procedures. The Hanford Site peer review was provided by Michael Fayer, Fred Zhang, and Steve Simmons of PNNL. An external peer reviewer, Professor L. W. Gelhar, Massachusetts Institute of Technology, Cambridge, MA, reviewed the 1999 far-field hydrology data package.

This page intentionally left blank.